Interaction of Antenna Systems with Human Body

By

Oluwaseun Adeniyi OJERINDE

Doctoral Thesis

Submitted in partial fulfilment of the requirements for the award of

Doctor of Philosophy of Loughborough University

2014

Abstract

The research investigates the influence on the human body on a communication system. To understand this, the effect of hands free kit (HFK) on energy absorption in the body was investigated when operating a smart phone at 2G. Findings on the research are given in the thesis report. Also, the influence of the way in which a phone is held on a phone's received power was investigated. The result was compared to that obtained using a hand phantom acquired from SPEAG. This was to check if the hand phantom best represents the human hand when using it in experiments. The setup for the experiment was in an anechoic chamber at Loughborough University. The mobile phone transmitted in the 2G system. In further experiments carried out on the body, two antennas were attached to the body in six different orientations to receive power from a source creating a Single Input Multiple Output (SIMO) system. The antennas used were monopoles mounted on a circular ground plane. These antennas were designed and constructed with the influence of the body taken into consideration. The use of diversity techniques to improve transmission to an on-body system is investigated with the antennas on the body. For each alignment, the transmission to the on-body was compared with the transmission to the corresponding off-body (free space). Experiments for this work were carried out in three environments.

This thesis is dedicated to my late mother Dr. (Mrs) Odusola Dibu-Ojerinde

and all those in pursuit of knowledge.

Acknowledgements

Publications

- ➢ M. Khattak, R. Edwards, and O. Ojerinde, "A study of perturbations in linear and circular polarized antennas in close proximity to the human body and dielectric liquid filled rectangular and a cylindrical phantom," in *Loughborough Antenna & Propagation Conference*, 2010, November, pp. 409–412.

- ➢ O. Ojerinde, C. Panagamuwa, and R. M. Edwards, "Effect of hands free kit on SAR when using a Smart phone at 1800MHz," *European Microwave Conference (EuMC)*, October, pp. 721–724, 2011.

- ➢ O. Ojerinde, C. J. Panagamuwa, W. G. Whittow, and R. M. Edwards, "Comparison between CTIA hand phantom and different human hands for OTA power measurements," *Proceedings of the 2012 IEEE International Symposium on Antennas and Propagation*, pp. 1–2, Jul. 2012.

LAPC paper in progress

- • Effects of the body on multiple antennas using selection combing.

Acronyms

AC	Alternating Current
AWGN	Additive White Gaussian Noise
BAN	Body Area Network
BER	Bit Error Rate
CAD	Computer Aided Design
CMCR	Centre for Mobile Communications Research
CTIA	Cellular Telecommunications Industry Association
DAE	Data Acquisition Electronics
DAM	Dynamic Antenna Matching
DASY	Dosimetric and Assessment Systems
DC	Direct Current
DCS	Digital Cellular Service
DGBE	Diethylenglycol-monobuthyl Ether
DUT	Device Under Test
EGC	Equal Gain Combining
EM	ElectroMagnetic
EMF	ElectroMagnetic Field
FCC	Federal Communications Commission
FDTD	Finite-Difference Time-Domain
FM	Frequency Modulation
GPS	Global Positioning System
GSC	Generalized Selection Combining
GSM	Groupe Spécial Mobile
HF	High Frequency
HFK	Hands Free Kit
HP	Hewlett-Packard
ICCIT	International Conference on Computer and Information Technology
ICEAA	International Conference on Electromagnetics in Advanced Applications
ICES	International Committee on Electromagnetic Safety
ICT	Information and Communications Technology

IEC	International Electrotechinal Commission
IEE	Institution of Electrical Engineers
IEEE	Institute of Electrical and Electronics Engineers
IET	Institution of Engineering and Technology
IFA	Inverted F Antenna
ISI	Inter Symbol Interference
ISM	Industrial Scientific and Medical
ITU	International Telecommunication Union
LAN	Local Area Network
LAPC	Loughborough Antenna Propagation Conference
LS	Left Shoulder
LW	Left Waist
MGF	Moment Generating Function
MIL	Measurement In the Laboratory
MIMO	Multiple Input Multiple Output
MIO	Measurement In the Office
MISO	Multiple Input Single Output
MOC	Measurement On the Corridor
MRC	Maximal Ratio Combining
MRI	Magnetic Resonance Imaging
MTHR	Mobile Technology and Health Research
OFDM	Orthogonal Frequency-Division Multiplexing
OTA	Over The Air
PAN	Personal Area Network
PCB	Printed Circuit Board
PDA	Personal Digital Assistant
PEC	Perfectly Electrically Conducting
PIFA	Printed Inverted F Antenna
PMMA	Polymetyl Methacrylate
RF	Radio Frequency
RH	Rohacell
RS	Right Shoulder
RW	Right Waist

SAM	Specific Anthropomorphic Mannequin
SAR	Specific Absorption Rate
SC	Selection Combining
SCC	Standard Coordinating Committee
SDA	Serial Data Analyser
SHO	SAM Hand OTA
SIM	Subscriber Identity Module
SIMO	Single Input Multiple Output
SISO	Single Input Single Output
SMT	Surface Mount Technology
SNR	Signal to Noise Ratio
SP	Smart Phone
SPEAG	Schmid & Partner Engineering AG
TRP	Total Radiated Power
TSL	Tissue Simulating Liquids
UWB	Ultra Wide Band
VTC	Vehicular Technology Conference
VSWR	Voltage Standing Wave Ratio

List of Variables

r^i internal resistance per unit length

Z_c impedance

R_c resistance

X_c reactance

ρ mass density

σ conductivity

E_{int} rms electric field strength

ΔT temperature rise

Δt exposure duration

h heat capacity

λ wavelength

c speed of light

f frequency

D maximum dimension on the antenna

$|\mathrm{S}_{11}|$ reflection coefficient

Table of Contents

List of Figures

List of Tables

1 Introduction

1.1 Introduction

Building upon the work of the Centre for Mobile Communications Research at Loughborough University, this thesis considers four important impacts of humans on current mobile phone technology for 2G, 3G and 4G Systems. In brief, these are the ways the body interacts with radio frequency radiation from mobile handsets; the effects the human body has upon hands free kits when used close to humans; the levels of radio frequency radiation in the hands of users and the improvement of the mobile channel using selection combining in free space and on the human body.

Although there is a large body of research on antennas in general [1] the majority of this has been for antennas in free space. Martin Cooper from Motorola, USA demonstrated the use of the very first cellular telephone in 1973 [2] and since that date the study of antennas close to humans has now began to dominate.

The main difference between antennas in free space and antennas close to humans is that in use mobile communications devices require a transceiver in the hand, which at popular mobile communications frequencies mean that humans close to antennas cause a near-field effect. Electromagnetic (EM) fields have the property that at one distance from the antenna certain characteristics will dominate whilst at another distance a different set of characteristics will dominate.

Engineers separate field distance into three ranges, namely a far-field region that begins at $\frac{2D^2}{\lambda}$ out to infinity. Here D is the maximum overall dimension of the source antenna and λ is the wavelength. It can be seen that D (one size of the antenna) dominates the start of the region.

Within about a wavelength of the antenna is the near-field region and between one and approximately two wavelengths is the transition zone which is between the near-field and the much more predictable far-field.

The near-field can be further divided into a reactive region that is defined as from the antenna to $\frac{\lambda}{2\pi}$ or 0.159 wavelengths and the radiative near-field region. Note that the most popular mobile communications frequencies are between about 1GHz = 30cm wavelength and 2.45GHz = 12.2 cm in wavelength.

Study of antennas in the near-field is much more complicated than the study of antennas in the far-field. For example in the far-field, polarity [3] can be horizontal, vertical, circular or elliptical but in the near-field all four can exist at once [4].

In the reactive near-field the relationships between the Electric and Magnetic fields may be too complicated to predict analytically and therefore have to be measured whilst in the far-field as they are easily predictable from the source. The reactive near-field has a reactive component and couples strongly with humans.

Although the interactions between humans and mobile phones are common they still provide a very challenging set of research questions for radio engineers.

Almost everyone, in the western world at least, owns/uses a mobile phone [5]. With the inception of the Smart phone; 3G [6] and 4G [7] communication networks, making a traditional voice call is no longer the primary function of the handset. Accessing multimedia content now holds that spot [8].

Firstly, the interaction between the mobile phone and the user is investigated through the use of wired hands free kits. This topic has caused controversy in the past because of suggestions that using a wired hands free kit could actually *increase the radiation absorbed in the head* [9] when compared to that absorbed when the phone is held directly to the side of the head. The experiments concentrate on the measurement of the specific absorption rate (SAR) in body phantoms. In this regard, SAR quantifies the time rate at which RF energy is absorbed in a unit mass of tissue. The novelty of this work arises from the use of a Smart phone and its associated modes of use.

Secondly, the effect of the user on the mobile phone's antenna performance is investigated. The impact the user's hand has on the antenna performance is a critical aspect that must be considered when designing a mobile phone. In this work, volunteers have been recruited to test how real hands impact on the antenna's transmission capabilities. Variations caused by different hand sizes and locations, left and right hand

combinations and finger jewellery have also been considered. Results are compared to a hand phantom developed for industry standard over the air testing. The novelty of the work arises from the use of real hands through a volunteer based study, the likes of which has not been reported in the literature.

In the final part of the study, the thesis addresses the issue of improving the mobile communication system performance. Well established diversity techniques have been presented in literature for improving signal to noise ratios without boosting transmit powers. The work presented in this thesis explores the possibility of using the ample space available on the user's body to implement diversity gain.

Comprehensive literature reviews pertaining to the topics of investigation will be presented in their respective chapters.

1.2   Aims and Objectives

The aim of this research was to understand the interaction of the human body with antenna systems for mobile communication. The research was focused to investigate the influence of antenna systems in close proximity to the body. This work also aimed to propose how antenna systems and the human body can co-exist without diminishing the performance of a mobile communication system.

For these aims to be achieved, the following objectives were defined.

Perform analysis of body simulating liquid components.

Design mixtures of liquid components to simulate the body.

Manufacture a range of tissue simulating liquids for different frequencies.

Carry out review of SAR measurement techniques and associated equipment.

Make measurements of SAR in head while using smart phone in front of the face with HFK connected to the ear using the DASY4.

Test the effect of the hand on a mobile phone with its antenna at the top back region of the case. Make measurements of power received in a mobile phone antenna system when phone is held in the hand.

Compare received power from various hand sizes with the hand phantom developed by CTIA.

Simulate, design and manufacture of circular ground plane monopole antenna for use on-body.

Carry out measurement of multiple antenna system on-body (SIMO).

Compare the results on/off-body in various environments.

Redefine the received channel matrix to isolate the value of the body effect from the channel matrix.

Part of the goals of the research was to manufacture tissue simulating liquid for the test of SAR. Although calculations were made for the mixture of the tissue simulating liquid due to time constraint, it was bought of the shell from a manufacturer. Also one of the set goals of this research was to redefine the received channel matrix. This was to isolate the value of the body effect form the channel matrix of the received signal. This was not achieved due to time and has been recommended for future work. Other objectives stated in this thesis were achieved. The thesis outline presented in the section 1.4 shows the work done to achieve the outlined work.

1.3   Methodology

Due to the nature of the subject under investigation, a major part of this thesis deals with experimental work and its full analysis. Where simulations have been carried out, the Finite Difference Time Domain (FDTD) electromagnetic simulation software EMPIRE XCcel has been used. In numerical analysis of antennas, three main analysis methods are used to build simulators; method of moment (MOM), finite-difference time-domain (FDTD) and finite element method (FEM). The MOM is the oldest antenna analysis technique. It is based on the fundamental of Maxwell's equation. The

MOM is mainly used for metallic antennas and large objects. It is highly efficient for homogenous components. The FDTD uses the Maxwell's equation in the time domain. It can handle anisotropy and inhomogeneous component. It is a powerful and popular numerical analysis method because of its simplicity in formulation, implementation and grid generation. The FEM is more complicated than the FDTD. It requires more sophisticated computation. The FEM is less popular because of its necessity for complicated computation. The choice of Empire XCcel for the model of the antenna was based on its computational ability. With the program which is FDTD based, the antenna constructed could be optimized over a range while running the simulation.

Where large sets of data have been collected, Matlab and Microsoft Excel have been used to perform the analysis. Antennas and all their other support rigs were built by the school's electrical and mechanical workshops. All experiments were carried out in the Centre for Mobile Communications Research laboratories and offices.

1.4   Thesis outline

The thesis is presented in six chapters including the introduction and overall conclusions.

In Chapter 2, a background study on SAR is carried out. Guidelines on the amount of radiation the human body can be exposed to are explained. Also, different methods of measuring SAR are explored. The Dosimetric Assessment System (DASY) system that is mainly used in the work is explained in detail along with the possible phantom shapes used with it. The tissue simulating liquid for different frequencies is explained and recipes for creating these tissue simulating liquids are stated in this chapter. This chapter also gives an insight on SAR theory and works that have been carried out around SAR.

Chapter 3 is about the effect of hands free kit (HFK) on SAR when using a Smart phone in front of the face. It commences with a literature review of the state of the art. Using two different types of head phantoms, the twin phantom and Loughborough SAM, this chapter investigates if the HFK increases or decreases the SAR from the Smart phone. The work is carried out in the GSM 1800 communications band. It looks into different

HFK wire positioning and how it affects the SAR level from the Smart phone. This work is important to the growing Smart phone industry as multiple functions are carried out with the phone in front of the face.

Chapter 4 investigates the effect of the index finger of the hand holding a mobile phone on its ability to transmit. The chapter commences with a literature review of the state of the art. Nearly 33 volunteers were recruited to hold a Nokia 6220c mobile phone whilst it was programmed to radiate the maximum permissible power. With the hand positioned in predetermined locations, the power received at a secondary antenna probe was recorded. The chapter presents the captured data and its analysis. The chapter attempts to correlate variables such as hand position and size, the use of the left or right hand, and finger jewellery to the received power at the probe antenna. Finally, the volunteers' data is compared to the industry standard lossy hand phantom designed for use in measurements of this type.

Chapter 5 gives details on the building of a monopole antenna on a circular ground plane for on-body measurements. Diversity techniques when using multiple antennas is discussed. Selection combining is used to investigate the interaction of on-body antenna when receiving signal from a transmitter. Six combinations of waist and shoulder alignments are used in this experiment and the corresponding on-body and off-body measurements are taken. The experiments are carried out in an office space, corridor and the CMCR laboratory. In this experiment, power received by the antenna on the body is measured. Data collected from the experiment is analysed using Matlab to understand the influence of the body and the position of the antenna on received power.

Chapter 6 completes the thesis by drawing overall conclusions and presenting avenues for further research.

Reference

[1]   C. A. Balanis, *Antenna Theory*, 3rd ed. Hoboken, New Jersey: John Wileys & Sons, 2005.

[2]   Newstream/Arraycomm, "Martin Cooper - History of Cell Phone." [Online]. Available: http://inventors.about.com/cs/inventorsalphabet/a/martin_cooper.htm.

[3]   C. A. Balanis, "Antenna Theory," Hoboken, New Jersey: John Wileys & Sons, 2005, pp. 34–38.

[4]   Occupation Safety and Health Administration, "Electromagnetic Radiation Field Memo." 1990.

[5]   International Telecommunications Division, "The world in 2013: ICT facts and figures," in *International Telecommunication Union*, 2013.

[6]   International Telecommunications Division, "The world in 2010: ICT facts and figures," in *ITU Telecom World*, 2010.

[7]   K.-H. Kim, "Key technologies for the next generation wireless communications," *Proceedings of the 4th international conference on Hardware/software codesign and system synthesis - CODES+ISSS '06*, p. 266, 2006.

[8]   "Communications Market Report 2013," *Mobile Operators Association*, 2013. [Online]. Available: http://www.mobilemastinfo.com/stats-and-facts/#mce_temp_url#.

[9]   "Which?," *Special Report: Mobile Phone Risks*, pp. 11–17, 2000.

2   SAR Measurement

2.1   Introduction

The explosion in mobile phone use by the general public over the last 20 or so years has resulted in small RF antennas coming into close contact with a user in a way that has never been seen before. The body has significant effects on the properties of antennas used close to bodies, acting to both increase losses (thereby changing the Q of an antenna [1]) and changing the resonant frequency/frequencies at which a free space version of the antenna would normally operate.

There have been many great measurement campaigns involving on-body antennas with human volunteers [2–5]. These have used complex systems with varied equipment.

A different approach has been used to research the effect of antennas or rather the radio frequency radiation they emit on humans. The logic is that since there is no standard human, a standard phantom [6] should be used and the effect of radio frequency radiation on a phantom is now used as a benchmark.

Phantoms allow experiments involving radiation from mobile phone antennas to be repeatable. Conversely, phantoms also allow representative effects of on mobile phone antennas to be measured accurately.

This chapter then is an introduction to the techniques for measuring fields from mobile handset antennas and the way in which phantoms can be used to measure the effects that humans have on antennas close to the body. It gives an overview of techniques used to take measurements in the near-field region of antennas close to the body.

It is worth mentioning here that the energy produced by mobile phones is non-ionising. This means that the microwave energy emitted does not have enough energy to remove electrons from molecules no matter the power level. However radiation from mobile phones can move atoms in a molecule around and cause them to vibrate. If the power were high enough such energy could cause heating and is commonly used in applications that involve heating food (microwave ovens). The standard therefore seeks

to keep radiated power levels well below the point at which heating is known to cause damaging effects on health.

In this thesis and in this chapter in particular the unit of specific absorption rate (SAR) is used. It turns out that the size of living organisms greatly affects energy absorption [7]. For example a small child and an adult exposed to the same electric field would have different field density inside their bodies. SAR is measured either in W/kg or mW/g and is a measure of the average energy turned into heat in a region divided by the weight of the material in that region. The equation for SAR is given in equation 2.2. However, it is important to note that if the SAR values measured from an antenna are too high then that antenna cannot be used close to the body.

2.2   SAR measuring systems

In [8], three ways of measuring SAR were discussed. These methods are:

- Electric-field probes
- Temperature probes
- Calorimetric determination of whole body SAR.

A probe is a device used for measuring a field in a medium. Probes for RF measurement typically have: an electrically small sensor for detecting the field; a means of converting the RF signal to a proportional DC or slowly varying AC signal and a balanced high-impedance resistive transmission line to amplify the rectified signal [8]. The high impedance line is needed to prevent current being drawn from the system.

2.3   Electric-field probe

The E-field probe is made of three orthogonally positioned dipole antennas. The antennas are orthogonal in order to allow measurement of all polarisations on the incident field [9]. Although not co-located, the three antennas in the probe look essentially like a point which is important when measuring total field if the components of the field are divergent. The detector is typically placed in the gap separating the

antenna arms. The E-field probe has the ability to measure accurately field strengths from about 1 V/m to 1000 V/m (rms). A schematic diagram on the E-field probe is shown figure 2-1.
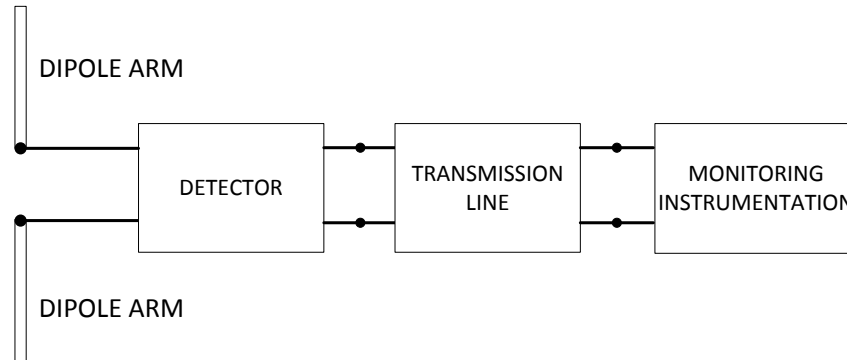
Figure 2-1: Schematic diagram of a simplified E-field probe [9]

The E-field probe is used to measure the E-field within body tissue simulating materials such as liquids [10] or gels [11]. It is more sensitive than thermal probes. It can be used to measure SAR as low as 1µW/kg [12]. A distinctive feature of the E-field probe is its sensitivity and the range over which it can be operated in relation to mobile communications frequencies (10MHz to over 3GHz) [12]. Note that both the probe and the tissue simulating liquids are not generally broadband and several sets are needed.

The transmission line connects the detector which is often a diode to the monitoring instrumentation. The transmission line has an internal resistance per unit length r^i for each conductor and a capacitance per unit length c. The resistance per unit length is much greater than the inductive reactance per unit length $(2r^i \gg \omega l)$ [9]. The characteristic impedance of the line is approximately

$$Z_c(\omega) = R_c + jX_c \approx \sqrt{\frac{r^i}{\omega c}}(1 - j)$$

2-1

In which Z_c is impedance;

R_c is resistance; and

X_c is reactance.

The high resistance per unit length in the impedance of the transmission line produces three beneficial effects:

i.   Reduction of direct reception of the incident fields by the line.

ii.   Reduction of scattering of the incident field by the line.

iii.   Introduction of a low-pass filter to the measurement system [13].

When taking SAR measurements close to the surface of the phantom, they can be affected by the change in the dielectric component in the probe region. This is referred to as boundary effect. Errors due to boundary effects can be reduced to less than 2% if the distance between the probe tip and phantom shell is greater than half the probe diameter [8]. The probe diameter is 1.6 cm.

The SAR is calculated using the equation below.

$$SAR = \frac{\sigma}{\rho} E_{int}^2 \quad W/kg$$

2-2

ρ is the mass density (kg/m^3)

σ is the conductivity (S/m)

E_{int} is the rms electric field strength in V/m at the point in the phantom, with the subscript "int" used to emphasize the fact that the field inside the body is not the same as the external field strength surrounding the exposed object.

The electrical conductivity of simulated tissue at different frequencies is shown in table 2-1.

Tissue type	Frequency(MHz)			
	10	100	1000	2450
Muscle	0.7[a]	0.9[a]	1.3[a]	2.2[a]
Brain	-	0.47[b]	0.75[a], 1.2[b]	1.2[a]
Fat and bone	-	0.008	0.07[a], 0.12[b]	0.18[a]

Table 2-1: Electrical conductivity of simulated tissues at RF frequencies [8]

[a]Polyethylene powder and X 150 gelling used for muscle and brain simulant

[b]HEC gelling agent without polyethylene powder used for muscle and brain simulant

For the corresponding biological tissue, table 2-2 states the conductivity at different frequencies.

Tissue type	Frequency(MHz)			
	10	100	1000	3000
Muscle	0.645	0.731	1.006	2.237
Bone (grey matter)	0.290	0.560	0.990	2.220
Brain (white matter)	0.160	0.320	0.620	1.510
Fat	0.029	0.037	0.054	0.130
Bone (cancellous)	0.122	0.172	0.364	1.006
Bone (cortical)	0.043	0.064	0.155	0.506

Table 2-2: Electrical conductivity of biological tissues at RF frequencies[8]

To get accurate SAR measurements, the probe has to be calibrated carefully in the simulant being used to represent biological tissue. The electric-field probe is widely accepted in research and industry for measuring SAR in the body. In [14], a SAR measuring system designed by APREL was used for measuring SAR during antenna development. In [15–17] a SAR measuring system called DASY4 (Dosimetric Assessment System 4) designed by SPEAG [18] was used to measure SAR in various parts of a body phantom using an electric-field probe. This system was used to conduct most of the SAR measurements in this thesis, and so more details of the DASY4 will be presented in Section 2.3.

2.4   Temperature probes

The temperature probe measures the radiation induced temperature rise ($\Delta T/\Delta t$) in a specific location in the phantom's tissue simulating material. SAR in the specific location which is proportional to temperature rise can be determined using equation 2-3. When the temperature rise in the irradiated tissue simulating material under test is not linear, other factors like heat loss or gain by thermal conduction and

 convection become increasingly more important. In order to prevent this non linearity, the temperature probe should be setup in an environment with relatively small change in ambient temperature. In [19], a list of requirements for a temperature probe are listed to ensure an accurate SAR measurement. These are:

- Small size

- Nonconductive material

- Low noise level

- Short reaction time

To obtain SAR with a temperature probe, the probe output is recorded before and during irradiation and the irradiation–induced rate of temperature rise is either graphically determined or found through the use of a slope-determining algorithm. A graphical plot of the temperature rise and the RF power is useful in verifying the linearity of the slope. SAR is calculated from temperature rise using the formula

$$SAR = \frac{\Delta T \times h}{\Delta t}$$ 2-3

ΔT (in Celsius) is the temperature rise measured with the thermal sensor

Δt (in seconds) is the exposure duration

h is the tissue specific heat capacity in J/kg°C. Typical values for specific heat capacities of different materials are shown in table 2-3.

Tissue	Specific Heat capacity (kJ/kg°C)	Mass density (kg/m^3)
Muscle simulant[a]	3.70	1000
Brain simulant[a]	3.40	980
Adipose tissue (fat) simulant[b]	1.10	1400
Muscle in vitro	3.50	1100
Brain in vitro	3.50	1100
Adipose tissue in vitro	1.20-1.60	1050
Bone	1.25-3.00	1250-1800

Table 2-3: Specific heat capacity and mass density of tissue-equivalent (phantom) material

and actual biological tissues[8]

[a] Data for tissue formulated for use at 2450MHz

[b] Simulated fat material has dielectric properties that are almost identical to living bone.

The temperature probe method has many sources of errors. For example it is very difficult to obtain repeatable results. To reduce the possible error when measuring SAR, a fibre optic thermometer was used in [20]. A block phantom was used in the work and the experiment was conducted at 2.4GHz and 2.45GHz. The measurements were also compared with those obtained with an electric-field probe. It was observed that the error margin for the thermal probe was less than 2% of the 1g SAR and 10g SAR. To check the SAR effect in the head using a thermal probe, in [21] a solid phantom of the head was built with tissue equivalent solids. The head was exposed to radiation at a frequency of 900MHz in an anechoic chamber. The thermal changes were captured using a thermographic camera and the SAR calculated from equation 2-3.

2.5   Calorimetric determination of whole-body-average SAR

The calorimetric method can be used to measure average SAR for the whole body. The method relies on calculating how a body absorbs and releases heat energy in a known controlled environment [19]. These processes of absorption and energy release in the body are called endothermic and exothermic reactions respectively. The main device used is the calorimeter and the most common type is the gradient layer calorimeter [22]. A calorimeter is a device for measuring the amount of heat involved in a chemical reaction or other processes. The generic form is a thermometer attached to a vessel of some sort.

For calorimetric SAR measurement in the laboratory, the test object is initially kept at room temperature along with the calorimeter. Then the test object is irradiated for a particular amount of time and afterwards placed in the calorimeter. The temperature is periodically monitored until all radiation induced heat energy is out of the object and its temperature is back to the initially measured temperature. This duration of the process is dependent on the size and mass of the object.

Accuracy of the calorimetric method depends on overall accuracy of the system. Errors in results depend on the modelling of the test object and amount of irradiation-induced heat that was not measured from the test subject.

The calorimetric method was used to determine the whole body SAR for mice in [23]. As a result of trying to create an ideal environment for the SAR measurement, the setup time for the experiment in [23] was close to eight hours. A twin-well calorimeter was used in [24] to measure the whole body SAR of a small phantom. The heat transfer medium for the experiment was air, water and silicon oil. The phantom was exposed to radiation at 2.45GHz for durations of 10 seconds and 50 seconds. The experiment showed that at 10 seconds, the effect of the heating medium on maximum temperature was not felt immediately but at 50 seconds, there was a change. Also it showed that water takes a longer time to measure the whole body SAR but it has the lowest error margin compared to simulation. In [23] and [24], calorimetric method was used to determine the whole body SAR effect after exposure to MRI scanner.

2.6   Dosimetric Assessment System 4 (DASY4)

The system available for SAR measurement at Loughborough University was supplied by Schmid & Partner Engineering AG (SPEAG) of Switzerland. Dosimetry is the science of quantifying the three dimensional distribution of EMF inside tissues and organs [19]. When properly calibrated the DASY4 fully complies with the OET65 C (01-01) [27], IEEE 1528 [28] and EN50361 [29] SAR measurement requirements. It is a robot based system that enables automated electric field scanning in tissue simulating liquid. The DASY4 system consists of the following:

- DASY4 measurement server: The server performs data evaluation for field measurement and surface detection. It also controls robot movement and handles safe operation.
- Data Acquisition Electronics (DAE): Data acquired via the probe is relayed to the measurement server through the DAE.
- Probe: The probe is connected to the DAE. The probe tip samples the mapped out region in a phantom for SAR detection. The probe has an optical surface detecting systems which enables its accurate positioning [12]. The probe is a two-layer construction. The inner core which holds the ceramic substrate is made of synthetic microwave material (STYCAST 0005) and the tip of the outer shell is made of the same material. The main outer layer is made of polymetyl

methacrylate (PMMA) tubing. The probe's optical sensor is designed to signal if excessive force is applied by the robot. This is done by sending a message to the robot to stop immediately [12].

- SAM twin phantom: A phantom is a device that simulates the size, contours and electrical characteristics of human tissue at normal body temperature. It is composed of a mannequin (solid shell) and a tissue-equivalent liquid synthetic material solution.

Traditional mannequins are rich in features representing eyes, nose, etc. which makes them visually humanlike. The consequence of this complexity is increased uncertainty in the positioning of a test unit against the outer surface of this mannequin and locating the bottom of the simulated tissue with a probe.

The shape and size of the head phantom is derived from a study of head dimensions of US military personnel [30]. The parameters of the head are defined in [8] and is called the Specific Anthropomorphic Mannequin (SAM). The SAM head is sagittally bisected and laid on its side. The shape is then extruded by about 10cm to ensure there is sufficient volume to hold the tissue simulating liquid. The DASY4 twin phantom has both the left and right side of the head as well as a flat section, which is normally used to represent the trunk. The SAM twin phantom is made from 2mm thick fibreglass. The picture of the SAM twin phantom is shown in figure 2-2 and figure 2-3.

Figure 2-2: Picture of the SAM twin phantom
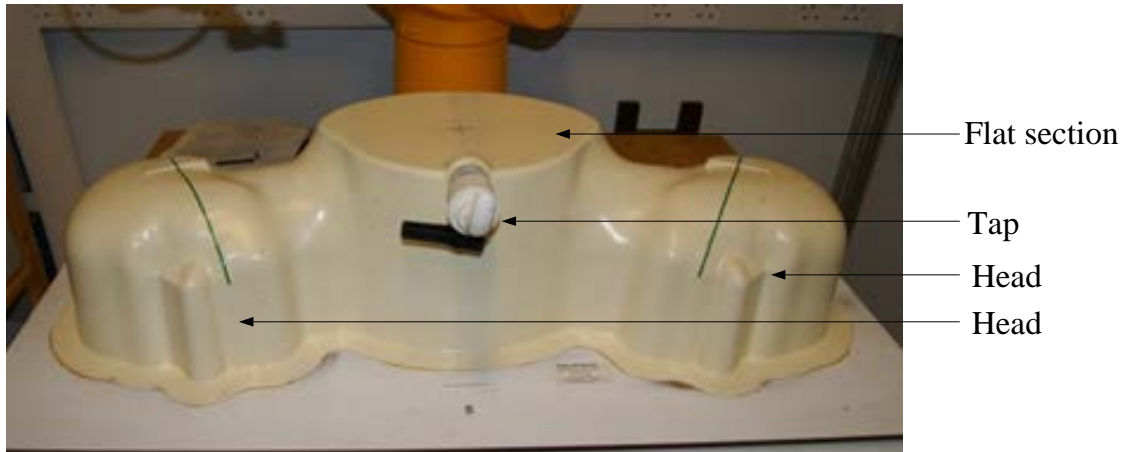
Figure 2-3: Pictures of the SAM twin phantom

- Robot: The DASY4 system uses the RX60BL high precision robot. The robot has features important for SAR measurements, which require high precision and high reliability. In normal operation the DAE and probe are mounted on the robot. The robot arm has six axes of rotation. The robot arm can position the probe with a repeatability of ±0.02mm [12].

The DASY4 system is shown as a schematic diagram in figure 2-4. The system server and the robotic setup are shown in figure 2-5 and figure 2-6 respectively.
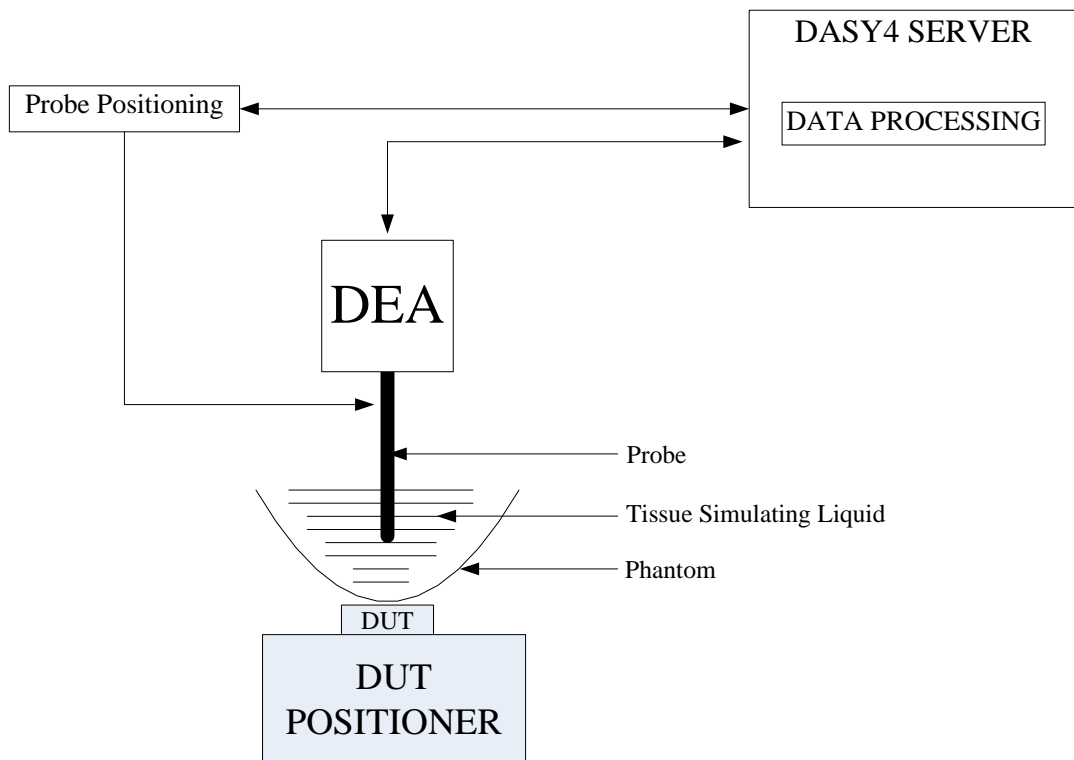
Figure 2-4: Schematic of the DASY4 system

Figure 2-5: DASY4 Robot controller
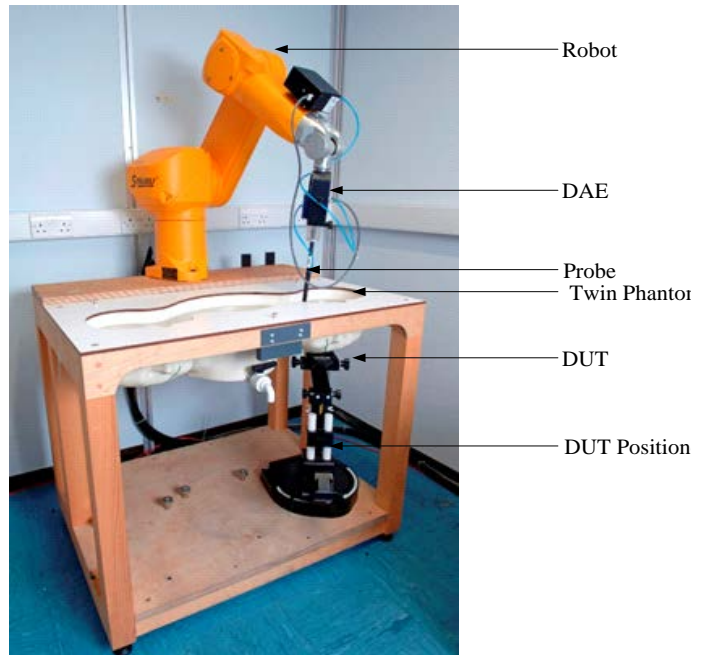
Figure 2-6: DASY4 system

The experiments in Table 2-4 show the works carried out in this thesis using the DASY4 system in Loughborough University. More details on experiments can be seen in Chapter 3.

Measurement with the DASY4	Experimental set up	Results
SAR measurement in the flat section due to Smart phone position	Figure 3-8	Figure 3-12
SAR measurement in the left head of the twin phantom due to a hands free kit	Figure 3-11	Figure 3-15
SAR measurement in the LouSAM head phantom due to Smart phone in front of the face	Figure 3-9	Figure 3-14
SAR measurement in the left head of the twin phantom due to Smart phone in talk position	Figure 3-7	Figure 3-12

Table 2-4: Experiments carried out in the thesis using DASY4

2.7   Flat section of the twin phantom for SAR measurement

The flat section of the twin phantom has been used extensively during this research. It should be noted that there is no ideal phantom shape to represent any part of a human. Phantoms used in this way are standard rather than models. The flat section can therefore be seen as a representative of the type of effect a typical lossy load would have on a phone antenna. The flat section of the phantom is used in the calibration of the system and for validation of results from the system [12].

In [31], the effects of straight metallic jewellery on the face with PDA phones was investigated. For validation of the results, experiments were conducted using the flat section of the twin phantom. In [32] SAR in the head when wearing circular earrings was researched at 1800MHz using a Finite-Difference Time Domain (FDTD) code. The results were validated using the flat section of the twin phantom with the DASY4 measurement system. For the testing of wireless devices used in the home and office environment discussed in [33] all the sections of the twin phantom were used.

2.8   Tissue Simulating Liquid

Whilst it is possible to infer the electric fields inside human-like structures from the type and strength of electric fields outside of human-like structures, it is more convincing to measure inside. However, measurement of electric field requires a probe and it is not normally possible to use a probe inside a living subject. For example it would not be possible to measure inside a human head since the brain is in the way. Therefore phantoms filled with tissue simulating liquids are used to represent parts of the human body. The probe can be operated unimpaired in the liquid. There are different liquid recipes of tissue simulating liquid for different parts of the body. Commonly, there is the head simulating liquid and muscle simulating liquid. Also because human tissue is dispersive, tissue simulating liquids (TSL) have recipes that are frequency dependent. This TSL is predominantly made up of water, sugar and salt [34]. If the liquid is to have a shelf life, anti-fungal agents can also be used. In [18], the simulating liquid recipe consist of the following in various proportions:

- Water: Deionized water

- Sugar: refined white sugar. To reduce relative permittivity.

- Salt: pure NaCl. To increase conductivity.

- Cellulose: Hydroxyethyl-cellulose. To increase viscosity and keep sugar in solution.

- Preservatives: Preventol D-7 Bayer AG.

- DGBE: Diethylenglycol-monobuthyl ether (DGBE). To reduce relative permittivity.

Table 2-5 shows the percentage of each ingredient in the recipe for the head and body simulating liquid at different frequencies. When making the simulating liquid, the liquid should be kept hot but below boiling point.

Ingredients (% by weight)	Frequency(MHz)					
	900		1800		2450	
Tissue Type	Head	Body	Head	Body	Head	Body
Water	40.29	50.75	55.24	70.17	55.00	68.64
Sugar	57.90	48.21	-	-	-	-
Cellulose	0.24	-	-	-	-	-
Salt	1.38	0.94	0.31	0.39	-	-
Preventol	0.18	0.10	-	-	-	-
DGBE	-	-	44.45	29.44	45.00	31.37

Table 2-5: Recipe for making tissue simulating liquid

The SAM twin phantom requires 25 litres of simulating liquid to fill it up. The recipe and right measure for preparing the simulating liquid at various frequencies is shown in table 2-6.

Ingredients (weight (g))	Frequency(MHz)					
	900		1800		2450	
Tissue Type	Head	Body	Head	Body	Head	Body
Water	12893	15327	13644	17501	13585	17091
Sugar	18528	14559	-	-	-	-
Cellulose	77	-	-	-	-	-
Salt	442	284	77	97	-	-
Preventol	58	3	-	-	-	-
DGBE	-	-	10979	7286	11115	7811

Table 2-6: Recipe for preparing 25 litres of tissue simulating liquid at different frequencies for the head and body

2.9   Environmental Condition for SAR measurement

To minimise error during SAR measurement, [28] states the conditions to be checked. The noise level when the device under test (DUT) is off, the reflection from cables, DUT and other reflectors should be checked when the DUT is transmitting. Also the environmental temperature where the test is being carried out should be kept within 18 °C - 25 °C.

2.10 Custom Phantoms

In addition to the phantom provided with the DASY4 [18], three other phantoms were also used in this work. They were a rectangular [35] and cylindrical [35] phantom used within the research group and a modified SAM head phantom [36], [37] called simply the Loughborough phantom (to be referred to as the LouSAM from here on in). These phantoms used comply with IEEE standards as stated in [28]. Solid phantoms in block and cylindrical shapes may be used to represent various parts of the body. In [35], a block and cylindrical phantom was used to check the effect of the body on the return

loss of an antenna when it is in proximity to the body. There are cases where a solid phantom is used to represent a part of the body. In [20], [21] a solid block phantom was used to evaluate the SAR via thermal and electric field probes.

In order to investigate SAR in the facial area, the LouSAM was developed from a standard full-head SAM phantom. This phantom is normally intended for radiation pattern and efficiency measurements; the head is completely filled with tissue simulating liquid through an opening at the top of the head. The LouSAM head is an open back head phantom that gives access to the eyes, forehead and cheeks allowing SAR measurements for radiation sources in front of the face. Initially, an investigation was carried out to ascertain how much of the back of the head could be removed in order to maximise accessibility without impacting on accuracy [36]. Figure 2-7 shows the area of the SAM head cut off for the E-probe to have access to the eyes, forehead and cheeks. It was concluded that 60mm of the back of the SAM head can be chopped off to evaluate SAR in front of the face. A picture of different views of the LouSAM is shown in figure 2-8. In [37], experiments were carried out with a DASY4 system to verify the initial analysis done in [36].
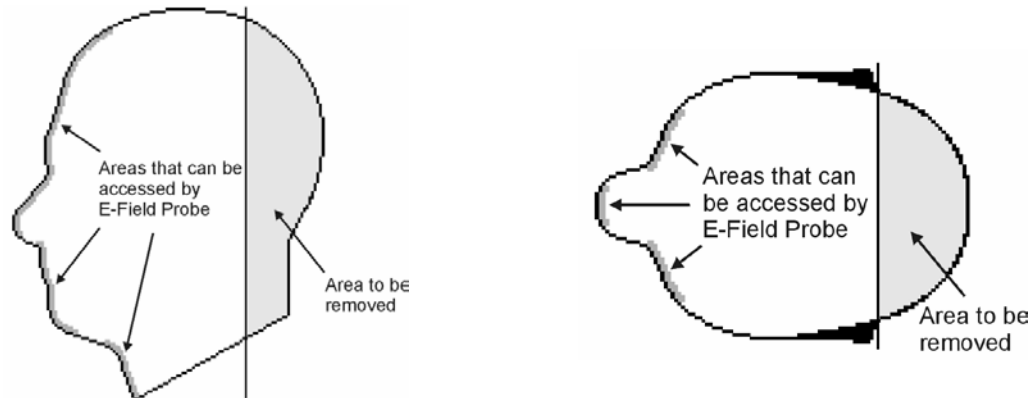
Figure 2-7: Side and top view of the SAM head showing area to be removed and the
areas that can be accessed by the probe [36]

(a) Front view   (b) Side view   (c) Back view

Figure 2-8: Modified SAM head phantom (Loughborough SAM head) [37]

2.11 Conclusion

This chapter has presented several common methods for the measurement of SAR. Methods using electric field probes have been shown to be highly repeatable and currently provide the main method for compliance testing. The properties, recipes and storage conditions for tissue simulating liquids at various frequency ranges were also presented. Industry standard and custom built phantoms used for measuring SAR were reviewed.

In this research extensive use was made of the DASY4 system. The flat section and the left head of the twin phantom in particular are used in experiments relating to hands free kits discussed in chapter 3.

The chapter has described different methods of measuring SAR. It has chosen the DASY4 system is a reliable and recognised system in the research environment for analysing SAR.

Reference

[1]   J. Toftgard, S. N. Hornsleth, and J. B. Andersen, "Effects on portable antennas of the presence of a person," *IEEE Transactions on Antennas and Propagation*, vol. 41, no. 6, 1993.

[2]   S. L. Cotton and W. G. Scanlon, "An experimental investigation into the influence of user state and environment on fading characteristics in wireless body area networks at 2.45GHz," *IEEE Transactions on Wireless Communications*, vol. 8, no. 1, pp. 6–12, Jan. 2009.

[3]   A. Sani, S. Member, Y. Zhao, Y. Hao, and S. Member, "An Efficient FDTD Algorithm Based on the Equivalence Principle for Analyzing Onbody Antenna Performance," vol. 57, no. 4, pp. 1006–1014, 2009.

[4]   X. Wu, Y. Nechayev, and P. Hall, "Antenna Design and Channel Measurements for On-Body Communications at 60GHz," *2011 XXXth URSI General Assembly and Scientific Symposium*, pp. 1–4, Aug. 2011.

[5]   A. A. Serra, P. Nepa, G. Manara, and P. S. Hall, "Experimental investigation of diversity techniques for on-body communication systems," *IET Seminar on Antennas and Propagation for Body-Centric Wireless Communications*, pp. 63–66, 2007.

[6]   IEC62209-2, "Human exposure to radio frequency fields from hand-held and body-mounted wireless communication devices- Human models, instrumentation, and procedures," *International Electrotechnical Commission*, 2010.

[7]   C. H. Durney, H. Massoudi, and M. F. Lskander, "RADIOFREQUENCY RADIATION DOSIMETRY," *Armstrong Laboratory (AFMC) Occupational and Environment Directorate Radiofrequency Radiation Division*, 1996.

[8]   "IEEE Recommended Practice for Measurements and Computations of Radio Frequency Electromagnetic Fields With Respect to Human Exposure to Such Fields,100kHz-300GHz," *IEEE Std C95.3-2002 (Revision of IEEE Std C95.3-1991)*, pp. i–126, 2002.

[9]   H. Bassen and G. Smith, "Electric field probes--A review," *IEEE Transactions on Antennas and Propagation*, vol. AP-31, no. 5, 1983.

[10]   H. I. Bassen, R. Health, and D. Administration, "Electric Field Probes for Cellular Phone Dosimetry," *19th International Conference- IEEE/EMBS*, vol. 2492, no. C, pp. 2492–2495, 1997.

[11]   H. Tamura, Y. Ishikawa, T. Kobayashi, and T. Nojima, "A dry phantom material composed of ceramic and graphite powder," *IEEE Transactions on Electromagnetic Compatibility*, vol. 39, no. 2, pp. 132–137, May 1997.

[12]   T. Schmid, O. Egger, and N. Kuster, "Automated E-field scanning system for dosimetric assessments," *IEEE Transactions on Microwave Theory and Techniques*, vol. 44, no. 1, pp. 105–113, 1996.

[13]   G. Smith, "Analysis of miniature electric field probes with resistive transmission lines," *Theory and Techniques, IEEE Transactions on*, pp. 1213–1224, 1981.

[14]   J. Wojcik and P. Cardinal, "New advanced methodology for near field measurements for SAR and antenna development," *Electromagnetic Compatibility, 1999*, pp. 3–7, 1999.

[15]   S. Kühn, E. Cabot, A. Christ, M. Capstick, and N. Kuster, "Assessment of the radio-frequency electromagnetic fields induced in the human body from mobile phones used with hands-free kits.," *Physics in medicine and biology*, vol. 54, no. 18, pp. 5493–508, Sep. 2009.

[16]   O. Ojerinde, C. . Panagamuwa, and R. M. Edwards, "Effect of hands free kit on SAR when using a Smart phone at 1800MHz," *European Microwave Conference (EuMC)*, no. October, pp. 721–724, 2011.

[17]   T. Iyama and R. Yamaguchi, "Novel specific absorption rate (SAR) measurement system using flat-plane solid phantom," *Propagation and EM*, pp. 638–641, 2003.

[18]   Schmid and Partner Engineering AG, "DASY4 Manual."

[19]   F. S. Barnes and B. Greenebaum, *Bioengineering and Biophysical Aspects of Electromagnectic Field*. 2007.

[20]   Y. Okano, "The comparison measurement for SAR by thermal evaluation and the electric field probe," *International Zurich Symposium on EMC Zurich 2007*, pp. 147–150, 2007.

[21]   Y. Okano, K. Ito, I. Ida, and M. Takahashi, "The SAR Evaluation Method by a Combination of Thermographic Experiments and Biological Tissue-Equivalaent Phantoms," *Microwave Theory and Techniques*, vol. 48, no. 11, pp. 2094–2103, 2000.

[22]   T. H. Benzinger and C. Kitzinger, "Direct Calorimetry by Means of the Gradient Principle," *Review of Scientific Instruments*, vol. 20, no. 12, p. 849, 1949.

[23]   S. Allen and W. Hurt, "Calorimetric measurements of microwave energy absorption by mice after simultaneous exposure of 18 animals," *Radio Science*, vol. 14, pp. 1–4, 1979.

[24]   T. Akiyama and K. Wake, "Whole-body averaged SAR measurements for small phantom by calorimetric method," *Internation Symposium on Antennas and Propagation*, no. 1, pp. 692–695, 2012.

[25]   W. Kainz, F. Fidler, J. Bobgan, G. Schaefers, R. Luechinger, N. Szeverenyi, and S. Wedan, "Variation of whole body averaged phantom specific absorption rate

(SAR) in seven different 1.5 T MR systems," *2008 Asia-Pacific Symposium on Electromagnetic Compatibility and 19th International Zurich Symposium on Electromagnetic Compatibility*, no. May, pp. 220–223, May 2008.

[26] K. R. Gorny, M. a Bernstein, J. P. Felmlee, H. a Ward, K. P. McGee, D. M. Lanners, and K. H. Lee, "Calorimetric calibration of head coil SAR estimates displayed on a clinical MR scanner.," *Physics in medicine and biology*, vol. 53, no. 10, pp. 2565–76, May 2008.

[27] D. Means and K. Chan, "Evaluating compliance with FCC guidelines for human exposure to radiofrequency electromagnetic fields," *Supplement C (Edition 01-01) to OET Bulletin*, vol. 65, 2001.

[28] "Recommended Practice for Determining the Peak Spatial-Average Specific Absorption Rate (SAR) in the Human Head from Wireless Communications," *First and Second Drafts*, no. December, 2003.

[29] BS EN 50361, *Basic standard for the measurement of specific absorption rate related to human exposure to electromagnetic fields from mobile phones (300MHz - 3GHz).* 2001.

[30] C. Gordon, T. Churchill, and C. Clauser, "Anthropometric survey of US army personnel: methods and summary statistics 1988," *U.S. Army Natick Research Development and Engineering Center Natick Massachusetts Technical Report*, 1989.

[31] W. G. Whittow, C. J. Panagamuwa, R. M. Edwards, and J. C. Vardaxoglou, "On the effects of straight metallic jewellery on the specific absorption rates resulting from face-illuminating radio communication devices at popular cellular frequencies.," *Physics in medicine and biology*, vol. 53, no. 5, pp. 1167–82, Mar. 2008.

[32] W. Whittow, C. J. Panagamuwa, R. M. Edwards, and J. C. Vardaxoglou, "Specific absorption rates in the human head due to circular metallic earrings at 1800MHz," *Loughborough Antenna & Propagation Conference*, no. April, pp. 277–280, 2007.

[33] S. Kuhn, U. Lott, A. Kramer, and N. Kuster, "Assessment methods for demonstrating compliance with safety limits of wireless devices used in home and office environments," *IEEE Transactions on Elelctromagnetic Compatibility*, vol. 49, no. 3, pp. 519–525, 2007.

[34] D. Simunic and D. Saik, "Preparation of head tissue equivalent simulating liquid at mobile communications frequencies," *2003 IEEE International Symposium on Electromagnetic Compatibility, 2003. EMC '03.*, pp. 1237–1240, 2003.

[35] M. Khattak, R. Edwards, and O. Ojerinde, "A study of perturbations in linear and circular polarized antennas in close proximity to the human body and dielectric liquid filled rectangular and a cylindrical phantom," in *Loughborough Antenna & Propagation Conference*, 2010, no. November, pp. 409–412.

[36]   C. J. Panagamuwa, W. Whittow, J. C. Vardaxoglou, and P. McEvoy, "A study of the validation of RF energy Specific Absorption Rates for simulations of anatomically correct head FDTD simulations and truncated DASY4 standard equipment measurements," in *Proceedings of the EuCAP 2006.*, 2006, vol. 2006, no. October, pp. 2–6.

[37]   C. J. Panagamuwa, W. G. Whittow, R. M. Edwards, and J. . Vardaxoglou, "Experimental Verification of a Modified Specific Anthropomorphic Mannequin (SAM) head used for SAR measurement," in *Loughborough Antenna & Propagation Conference*, 2007, vol. 00, no. April, pp. 261–264.

3 Effects of Hands free kit on SAR when using a Smart Phone

3.1 Introduction

The telecommunication industry has a great influence on society. Since the development of mobile phones, there has been an unprecedented growth in subscribers. The mobile phone has grown from a luxury product to a necessity. According to the International Telecommunication Union, the number of mobile phone subscribers was estimated to reach 5.3billion in 2010 [1]. Over the years, the mobile phone has taken different shapes and sizes, from large heavy 'brick' like devices to compact light items that sit easily in the palm of a user. Mobile phones can be held in various ways, from side of the head for voice calls to in front of the face for texting, gaming and other multimedia applications. The conventional and most popular way of conducting a voice call is still at the side of the head. The power absorbed in the head when using mobile phone has been investigated thoroughly over the years [2–4]. As a result, the power absorbed in the head is now limited through internationally adopted standards [5–7] and is measured as the Specific Absorption Rate (SAR) in W/kg. The SAR limit in Europe is 2W/kg averaged over 10g of tissue while in America it is 1.6W/kg averaged over 1g of tissue.

In order to address increasing public concern over the effects of mobile phone radiation on health and to improve ease of use, mobile phone manufacturers developed Hands Free Kits (HFKs). The basic HFK links a small earpiece speaker and microphone to the mobile phone through a wired link. The microphone part of the HFK is located way down the wire. The wire length varies from one manufacturer to another. Although the inception of Bluetooth [8] led to the development of low power wireless headsets, wired HFKs were more widely used because they were included for free when purchasing a phone in most countries.

Apart from the basic making and receiving of calls, various functionalities have now been embedded in mobile phones. These functionalities include FM radio, music player, camera, wireless internet access and many more. With more processing power and other

enabling technologies, these functionalities gave rise to development of a multitude of different applications. This new type of phone was termed the "Smart phone". The Smart phone is a platform for multiple tasks on the phone. For instance, the user can listen to music while composing a text message. With touch-enabled large screens, holding a voice call whilst using other applications has become commonplace, especially with HFKs. In this scenario where the Smart phone is held in front of the eyes, the HFK position is different from the previously studied work.

In this chapter, the effect of the HFK on SAR inside the head when using Smart phone at 1800MHz is investigated. A detailed literature review of other work in this area of study is presented first.

3.2   Background study on the effects of HFKs on SAR

A number of studies have been carried out in the past to investigate the effects of phone and HFK on SAR in the head.

With the HFK, it has been suggested that the fields from the mobile phone may couple/induce current on the HFK wire and cause radiation at the earpiece. The consumer association *Which?* conducted an experiment to measure the radiation into the head as a result of using a HFK [9]. The experiment was carried out with two different HFKs. It discovered the HFKs tested acted like an antenna and tripled the radiation level in the head. The tests in [9] were carried out using a phantom head filled with tissue simulating liquid. In contrast, a similar study conducted by Sartest Limited [10] showed that the HFK had a large reduction in the SAR in the head compared to when the mobile phone is held to the ear. The experiments were carried out using five phones and seven HFKs at 900MHz and 1800MHz. It also concluded that for further reduction of SAR in the head, ferrite suppressors can be attached to the cables of the HFK. In [11], the effect of a HFK was investigated when a mobile phone was operating at 1800MHz. The phone's radiation efficiency and SAR levels were investigated using a finite difference time domain (FDTD) and an adult male body tissue model available from Remcom Inc. The mobile phone was represented by a perfectly electrically conducting (PEC) box and the HFK by a 1m PEC wire. The experimental setup is shown in Figure 3-1.
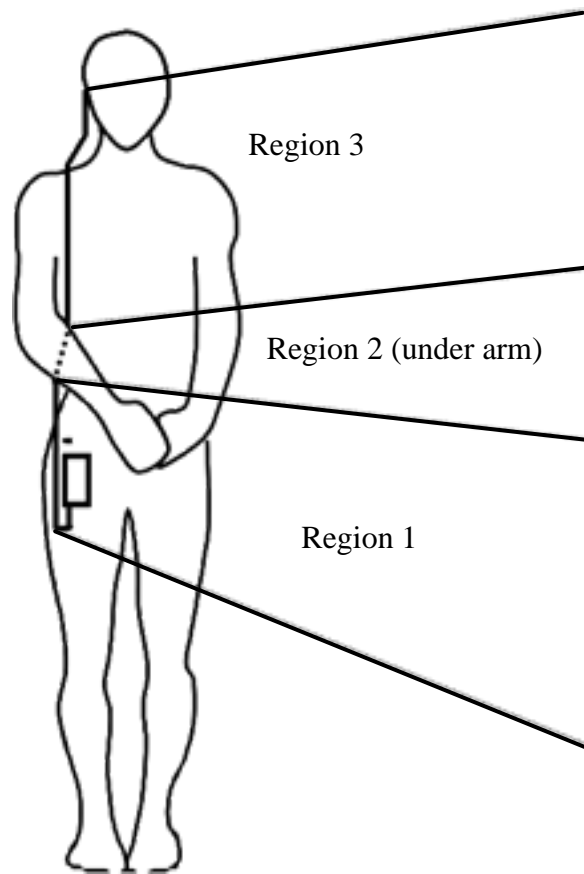
Figure 3-1: Layout of HFK and handset for SAR and radiation efficiency simulation[11]

The radiation efficiency of the system decreased when the HFK was connected to the phone attached to the waist. This also led to an increase in power absorbed by the body and an increase in the peak and average SAR values. The SAR value in the waist region increased as a result of the phone position but it was still within international guidelines. This shows that the HFK affects SAR level in the mobile phone. In [12], SAR associated with the use of a HFK with a mobile phone was tested. The experiment was carried out at 888MHz and 1750MHz. For this experiment, current probes were developed to work at each frequency. For the experiment, a typical block shaped phone and a flip-open phone was used. It was concluded that the HFK reduced the SAR in the head. It was also confirmed as stated in [10] that placing ferrite beads around the HFK further reduced the SAR. In [13] and [14], Porter *et al* performed a similar experiment to [12] with the use of seven mobile phones. For the SAR test, an IndexSAR SARA2 [15] suite was used. It was also concluded that the SAR level associated with the use of a HFK with mobile phones was substantially lower than when the phone is placed

directly at the ear. In [16], a full assessment of the effect of wired and wireless HFK on SAR in the head was carried out at 900MHz, 1800MHz and 1950MHz. The assessment was done both experimentally and mathematically. It was concluded that both wired and wireless HFK reduced the SAR effect in the head. However, SAR reduction with wired HFK depended on the transmit power of the mobile phone, coupling of cable with the phone and attenuation of current. With the wireless HFK, the SAR level was low and maintained a constant level.

An outline of steps to be carried out when assessing SAR in the head due to a HFK is given in the IEC international standard 62209-2 [7]. It emphasises the importance of the body when testing the HFK. The body attenuates energy in the cable as the cable couples with it. An example of the recommended setup was used to test a phone placed on the chest and connected to a HFK. Results showed that when the torso is filled with body simulating liquid, the SAR at the ear was 13dB lower than when the phone was tested directly at the side of the head [4].

3.3   Novelty of work with HFK

In all the works reviewed on the use of HFKs with mobile phones, it was only [9] that claimed a HFK increased the SAR in the head. Other works [10–14], [16] showed that the HFK reduced the SAR in the head. In the work presented in this chapter, a Smart phone will be used. Past studies have not included Smart phones.

The term *Smart phone* is used to describe the new generation of mobile phones. They are characterised by large touch screens and complex operating systems that enable the use of countless applications. They are able to make use of the higher data rates provided by 3G and even 4G mobile communication systems. Anecdotal evidence now suggests Smart phones are used more for apps/games and surfing the internet, rather than actually making a voice call with the phone held at the side of the head. Advanced processor technology now allows a voice call to be held while the user interacts with an application or surf the internet. Therefore, the Smart phone is more likely to be found in front of the face and when used with a HFK represents a different scenario to those investigated in the past. For one, the HFK cable is more likely to be *bunched up* due to the shorter distance to the ear. For ease of use, the operator may bunch up the cable and

hold it in the same hand as his phone, thus placing more of the wire closer to the body of the Smart phone. With the use of two different SAR measurement systems, these scenarios will be investigated further.

3.4   Theoretical analysis of the HFK wire coiling

For the test of the effect of HFK on the smart phone, the HFK is coiled and positioned in different positions for some of the scenarios. In this scenarios, the coiling of the HFK wire can be likened to the coils of an inductor. Since the HFK cable is made of conducting wires, the coiling can be prefered to acting as an inductor. An inductor is an energy storing device which stores energy in the form of magnetic field in and around the coil. When the HFK iis connected to the smart phone, the HFK is a channel for redistribution of power in the antenna system of the smart phone. The coiling of the HFK makes it act like an inductor. The energy stored in this HFK is dissipated as heat and absorbed by the body hence leading to SAR. The inductor formed by the coiling the HFK has a core made from air.

Figure 3-2: Electronic symbol for inductor

If the current flowing through an inductor is I, the voltage V_L acros s the inductor is proportional to the time rate of change of I i.e $\frac{dI}{dt}$

$$V_L = L\frac{dI}{dt}$$ 3-1

L is inductance. Inductance depends on the number of coils, configuration of coil and the material filling the coils of an inductor.

In this work, the distribution of energy in the HFK is similar to that of a coil. But emphasis is on the rate of absorption of energy by the body when the coils formed by the HFK are positioned around the face when using a smart phone.

3.5 Experimental setup for measuring SAR in the head due to a HFK when using a Smart phone

The School of Electronic, Electrical and Systems Engineering at Loughborough University has a dedicated SAR measurement facility housing a DASY4 [17]. The standard twin phantom of the DASY 4 is complimented by a custom built rear-entry Specific Anthropomorphic Mannequin (SAM) head, called the Loughborough SAM phantom (LouSAM). The design and verification of the LouSAM phantom is given in [18] and [19]. Figure 3-3 shows the part of the SAM head truncated to create the LouSAM. This phantom is used to measure the SAR in the face when a Smart phone is in front of the face. The twin phantom can only be used to measure the SAR in the side of the head, concentrating mainly around the ear. The experiment was carried out at 1800MHz. The phantoms were filled with head simulating liquid (HSL1800). The dielectric properties of the head simulating liquid at 1800MHz are permittivity (ε_r) 40 and conductivity (σ) 1.40 S/m.
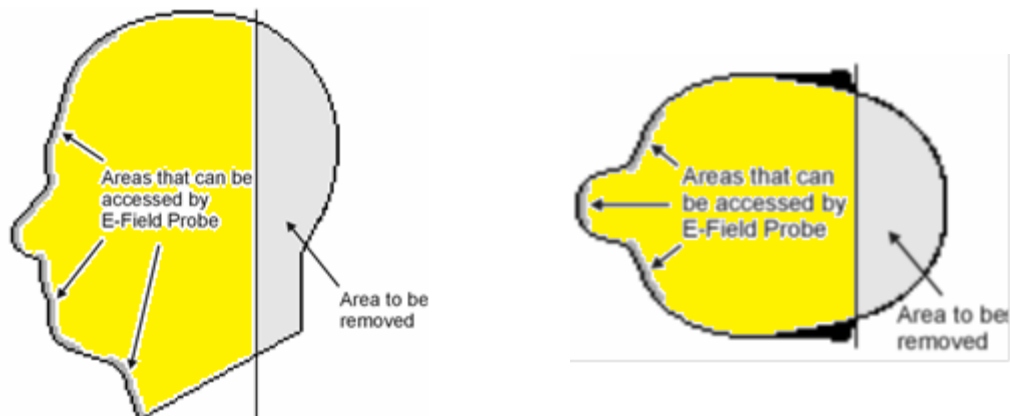
Figure 3-3: Side and top view of the SAM head showing area to be removed and the areas that can be accessed by the probe [18].

At the time of conducting the experiments, the base station simulator available only allowed testing at GSM 900 and GSM 1800. It was impossible to perform experiments

at 3G. Although a 3G smart phone was chosen for these studies, experiments were carried out using GSM 1800 standard. The uplink frequency was 1710 MHz which is only 210 MHz from the 3G uplink frequency. The difference in wavelength between these operating frequencies is only 19.19 mm. The loop size is not standardized and can vary from manufacturer to another. If the loop size however has an effect when transmitting at GSM 1800, it can be inferred a slightly different loop size will have an effect when operating at 3G.

The Smart phone used for this experiment is the Samsung SGH-i600 along with its factory made HFK. The HFK cable comprises of 5 wires. The wires are covered with a copper shield and protected with insulation covering. A picture of the phone is shown in figure 3-4. The maximum SAR value for the Samsung SGH-i600 was 0.776W/kg measured at the side of the head in the normal talk position [20]. This Smart phone was chosen based on availability at the time of experiment. The work with this Smart phone is depicts how the Smart phone is used in front of the face. The Smart phone is kept in the required position with a phone positioner. An Anritsu SIM card was used in the Smart phone. To initiate a call to the Smart phone, an Agilent 8922M base station simulator was used with a dipole antenna working at 1800MHz. The setup for the experiment is shown in figure 3-5.

Figure 3-4: Samsung SGH-i600 Smart phone used in the experiment
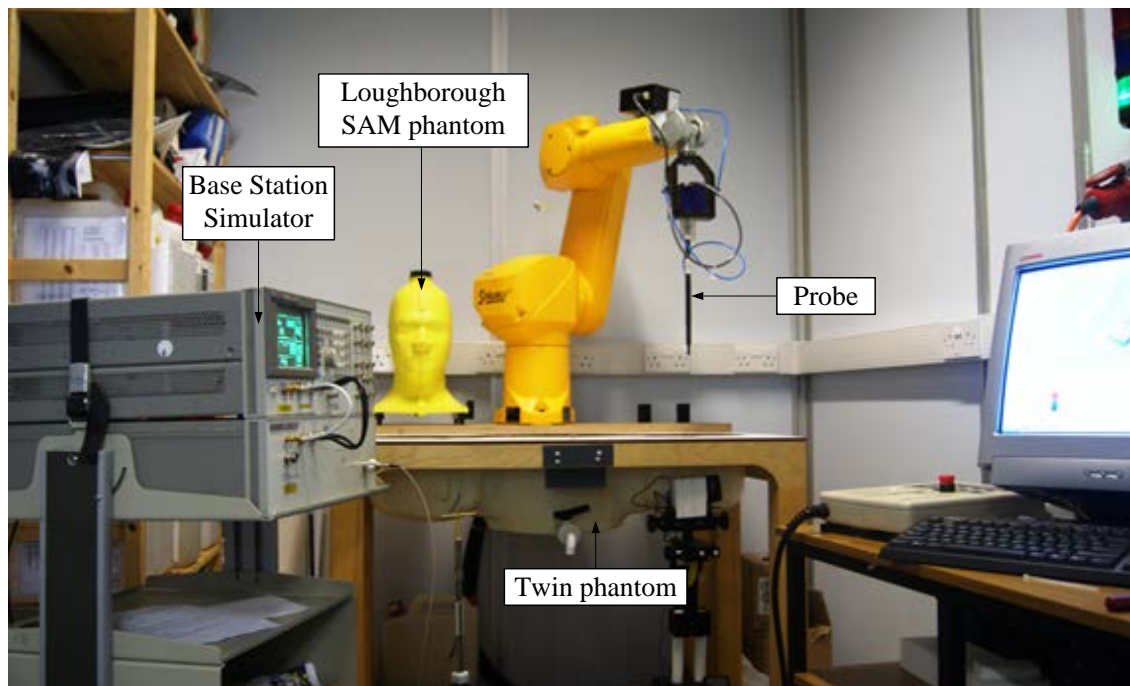
Figure 3-5: Experimental setup for the SAR measurement

The equipment described is shown in figure 3-5 and it will be used to perform a series of experiments in the upcoming sections to investigate the influence of the HFK on SAR from a Smart phone.

3.6   SAR in the head due to a Smart phone held in front of the face

This experiment is carried out to measure the SAR in the head when the Smart phone is in front of the face. A worst case scenario is chosen. This scenario is when the phone is very close to the face with no space between the nose and the Smart phone. For this experiment, the LouSAM head phantom is used with HSL1800. The setup of the experiment is shown in figure 3-6. A full facial area scan is first performed to locate the area of maximum SAR, followed by a volume scan to calculate the 1g and 10g SAR. Figure 3-7 shows the SAR heat map produced by a scan of the face region.
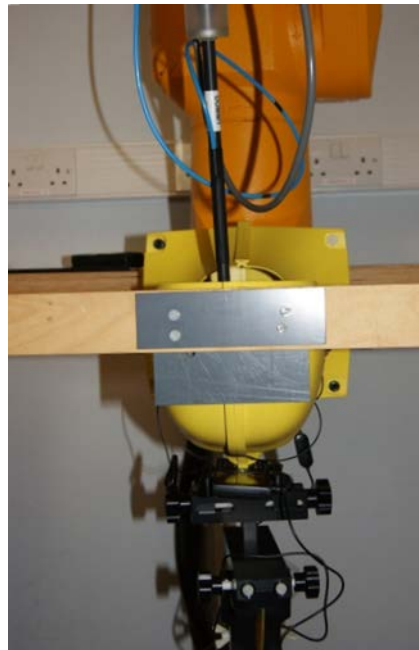
Figure 3-6: LouSAM head phantom with Smart phone in front of the face
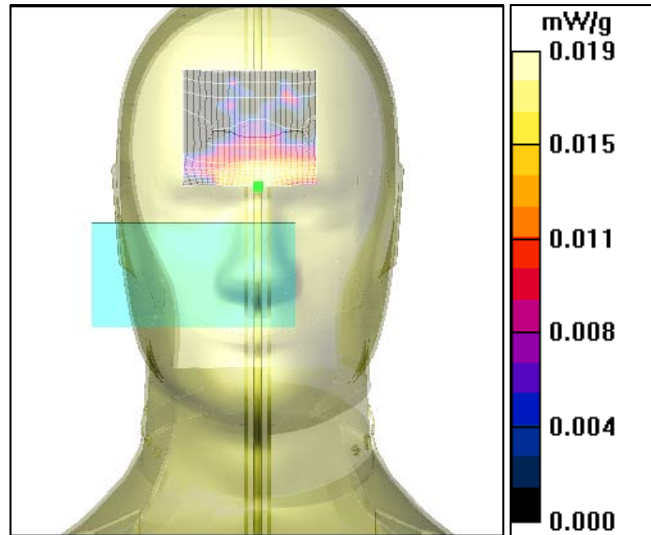
Figure 3-7: Image of the area scan for SAR detection from the DASY software.

3.7 SAR in the head when using Smart phone in the talk position and in the body when placed on the flat section of the twin SAM phantom

In this experiment, the left side head and flat section of the DASY4 twin phantom are used. The Smart phone is positioned in the talk position on the left ear and SAR is measured in the ear region. These results will help give a comparison with other measurements to be taken with the HFK in the ear region. Figure 3-8 shows the Smart phone in the talk position on the left side of the twin phantom. Also the Smart phone was positioned on the flat section of the twin phantom in contact with the bottom surface. This is shown in Figure 3-9. The maximum SAR in this region was also measured. The SAR measurement in the head region and on the flat section was carried out to show the effect of the phantom shape on the outcome of a measurement.
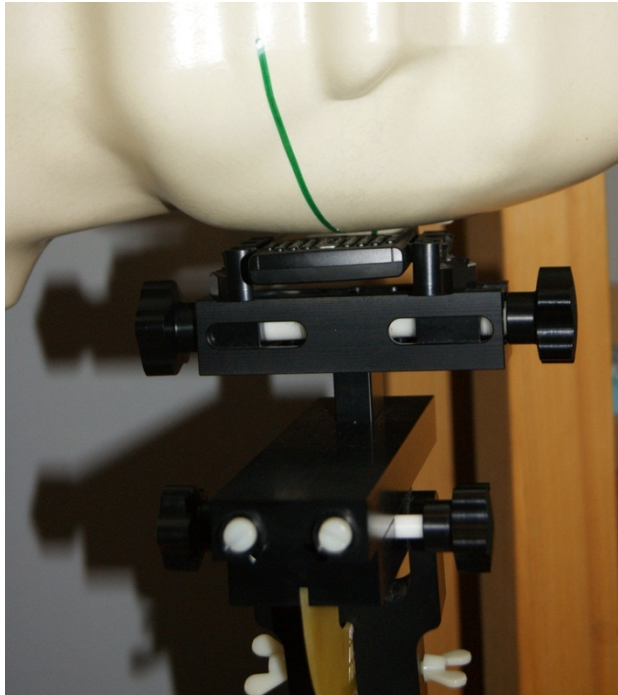
Figure 3-8: Smart phone positioned in the talk position on the left head of the twin phantom

Figure 3-9: Smart phone positioned on the flat section of the twin phantom

3.8 SAR in the head when Smart phone is in front of the face and connected to HFK when using the LouSAM head phantom

The SAR is measured in the face of the LouSAM with the phone positioned in front of it and the HFK connected to its left and right ear region in turn. The HFK is connected to the ears using sticky tape. The Smart phone is kept very close to the face with the

phone touching the nose. A full facial area scan was carried out to locate the maximum SAR region, followed by the volume scan to calculate the 1g and 10g SAR. This set up is shown in Figure 3-6. The HFK cable from the set up in Figure 3-6 is left to dangle freely. The microphone of the HFK is close to the mouth region of the LouSAM head phantom. The LouSAM is a full representative of the face with measurements limited to the frontal region of the head. With the left side of the twin phantom, measurements can only be taken at the side of the head.

3.9   SAR in the ear when HFK is connected to the Smart Phone and placed in front of the face of the twin phantom

This experiment is done with the Smart phone in front of the face with the Smart phone keypad touching the nose of the twin phantom left head and the HFK connected to its left ear. The HFK speaker is connected to the ears and the microphone to the mouth with sticky tape for all measurement scenarios considered. On the HFK wire, the microphone is located 12 cm from the ear piece. The area around the ear is scanned for the maximum 1g and 10g SAR. Figure 3-10 and 3-11 shows the Smart phone and HFK positioning on the left head of the twin phantom. In this experiment, 10 random cable positions are investigated. The ten positions are listed below:

1. HFK wire left hanging down freely: In this case, the HFK wire was allowed to drop down freely in a random manner.

2. HFK wire folded together: Natural bending points on the HFK cable are created when the cable is folded and the tie is attached to it by the manufacturer ready for packaging. Once the cable tie is removed, the cable maintains this bent shape in this scenario; the cable was bunched up along its natural bend points and then allowed to hang randomly from the phone.

3. HFK wire folded to the side of the HFK microphone: The microphone of the HFK is taped to the mouth. In this scenario, the cable was bunched up along its natural bend points and then positioned next to the microphone.

4. HFK wire held by the side of the Smart phone: The cable was bunched up along its natural bend points and then positioned along the left edge of the Smart phone.

5. HFK wire held under the Smart phone: The bunched up wire is positioned along the bottom edge of the Smart phone.

6. HFK stretched wire left to dangle: The natural bending points of the cable were stretched out and the wire was allowed to loop down from the phone to the earpiece.

7. HFK wire pulled horizontally towards the flat section: The straightened wire was pulled horizontally towards the flat section and held there using some cotton thread. This created the scenario where the cable would drop naturally down to the waist when held in front of the face by the user.

8. HFK wire dangling far from the chest: To eliminate the loading effect of the body while maintaining a horizontal cable configuration, the cable was stretched horizontally away from the chest and held in place using some cotton thread.

9. HFK wire dangling to the back of the ear: The HFK wire was clumped together in a random fashion and positioned near the back of the left ear. It was held in place using cotton thread.

10. HFK wire folded to the bottom back region of the Smart phone: The cable was bunched up along its natural bend points and then positioned on the back of the Smart phone towards the bottom edge.
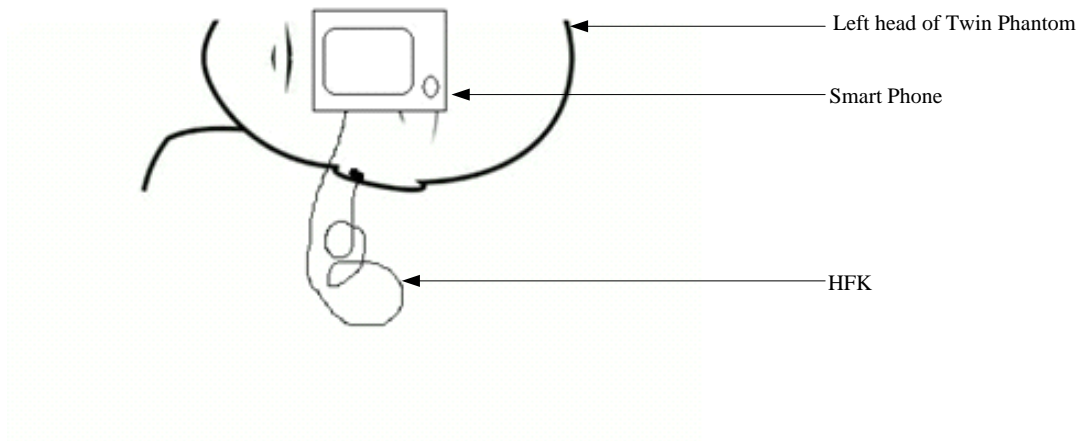
Figure 3-10: Sketch of the Smart phone in front of the face with the HFK connected to the ear**.**
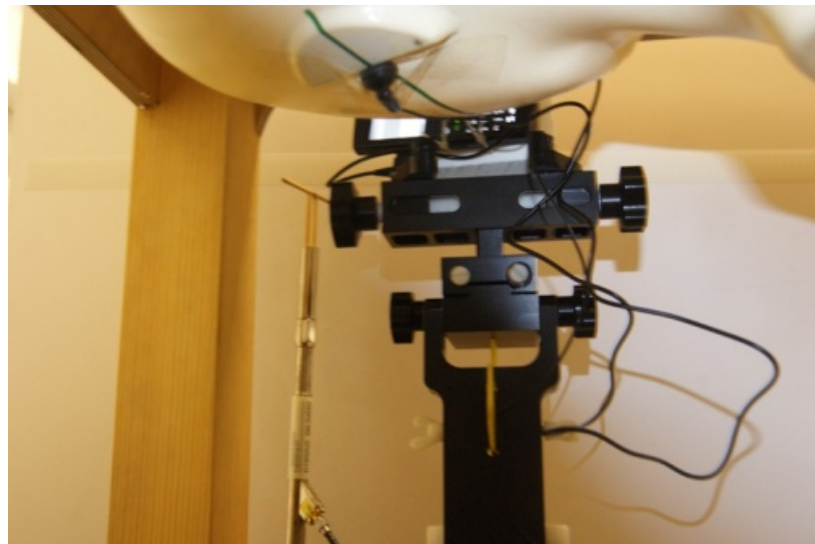
Figure 3-11: Smart phone connected to HFK positioned in front of the left head of the twin phantom

The second part of the experiment had the Smart phone placed on the flat section of the twin phantom with the HFK extending to the left ear. An area scan was completed in the ear region to obtain the maximum SAR. A picture of the setup is shown in figure 3-12. This was to check for change in SAR value when the Smartphone is not in front of the face.

Figure 3-12: Smart phone positioned in the flat section of the twin phantom with HFK connected to the ear of the left head of the phantom

3.10 Measured SAR results

In this section, the results from the experiments described above will be presented. In order to measure absolute SAR values, the electric-field probe and tissue simulating liquid must be in calibration. The equipment was out of calibration hence all the graphs are plotted by normalising the data to the maximum recorded value. This allows comparison of all the results because any errors in the system would apply to all the results equally. The maximum recorded SAR was when the Smart phone was placed on the flat section of the twin phantom, and thus all results are normalised to this value. The recorded value was 0.843mW/g.

The normalised 1g and 10g SAR results of the Smart phone (SP) in front of the face of the LouSAM head and on the left head and flat section of the twin phantom are shown in figure 3-13.
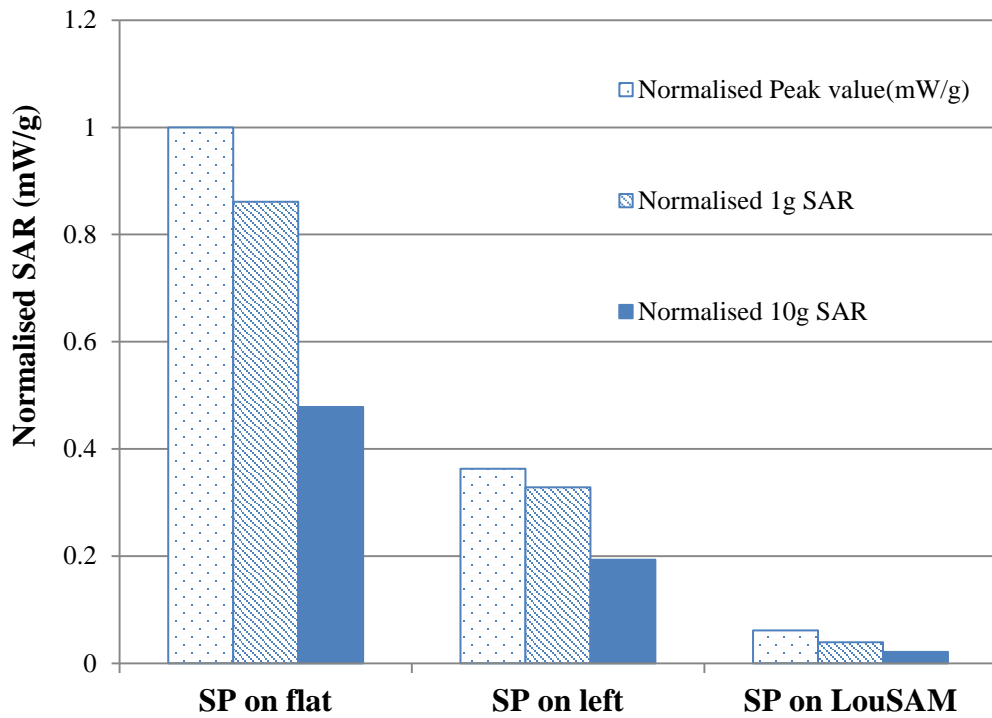
Figure 3-13: Graph of the Smart phone (SP) in different positions without the HFK

The result from the flat phantom corresponds to use of canonical phantoms for getting worst-case scenario results when representing a part of the trunk. The SAR measured in the ear region of the left head of the twin phantom is higher than that in the face region measured in the LouSAM head. This can be attributed directly to the proximity of the Smart phone to the phantom; the closer the phone is to the phantom surface, the higher the electric fields, ultimately resulting in a higher SAR. It is also important to note that the SAR in the nose of the LouSAM cannot be measured due to its shape. Since the Smart phone is touching the nose, the SAR in the phantom nose can be expected to be higher than the SAR in the rest of the face. However, in a heterogeneous head, much of the front of the nose is taken up by the air cavity of the nostrils, so even if it were possible, a 1g or 10g averaged SAR measurement in the nose may be meaningless. The Smart phone's SAR values taken in these different positions will serve as a comparison figure for measurements taken when the HFK is connected to the Smart phone.

The result of the area scans of all the HFK positions are shown in the Figure 3-14. In this case, all the scales are normalised to the maximum peak SAR observed between all 10 scenarios. This was 0.165mW/g observed in position 3.

Position 1   Position 2   Position 3

Position 4   Position 5   Position 6

Position 7   Position 8   Position 9

Position 10   No HFK
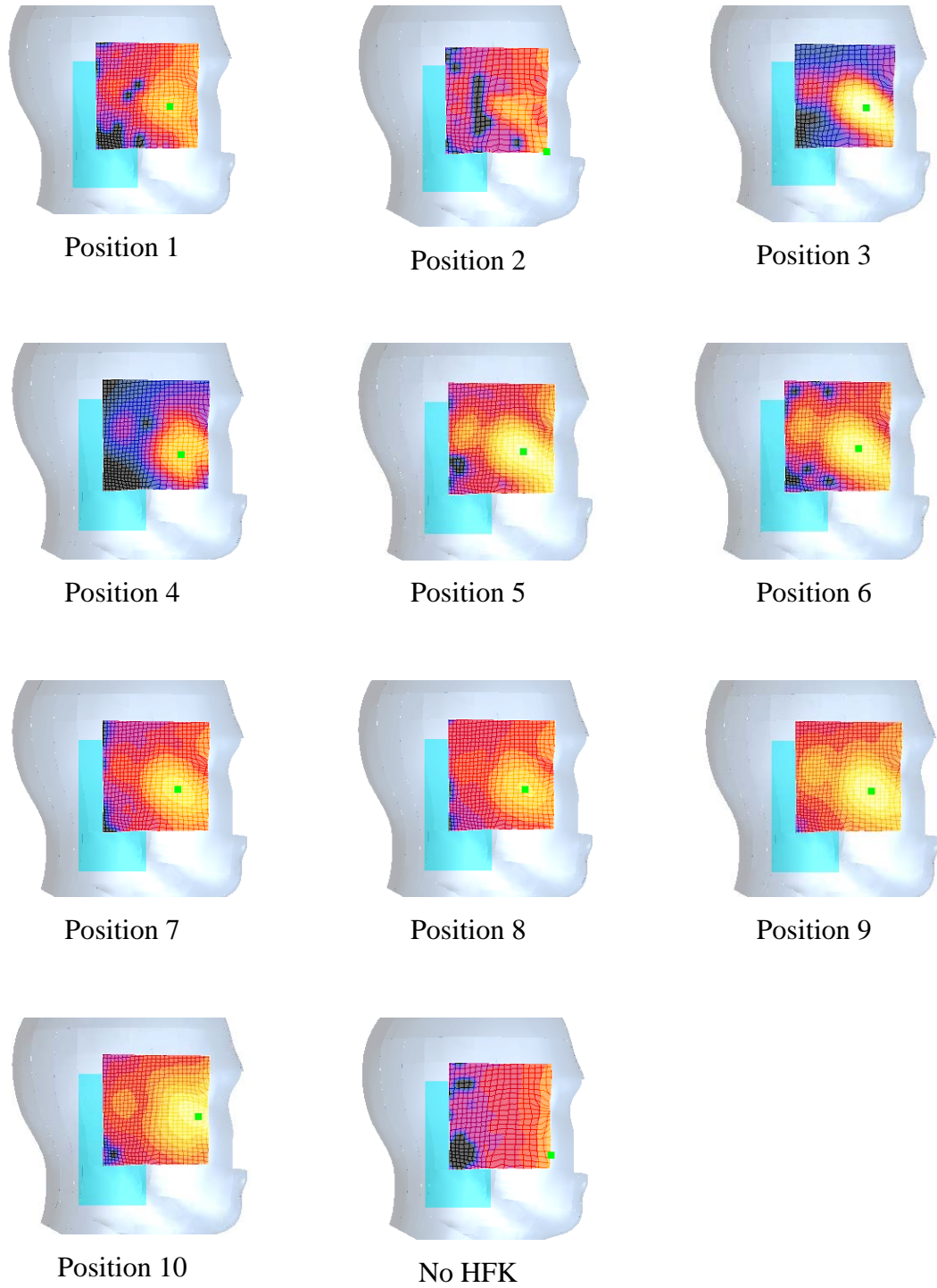
Figure 3-14: Area scan results of HFK in all 10 positions and when HFK is not connected.

Although they describe quite different scenarios, there is a noticeable similarity between the SAR scans taken in positions 5 to 9. The occurrence of a pattern in the SAR heat maps suggests there is an increased SAR effect due to the HFK, especially when compared to the *No HFK* scan result. However, it must be noted that when considering the SAR value recorded (0.306mW/g) when the phone was in the talk position (without a HFK), these 10 measurements are very low.

The result of face SAR (the SAR measured in the face using the LouSAM) with and without the HFK is compared to see the changes in the SAR value measured with the Smart phone. The graph in Figure 3-15 shows the difference in the SAR value.
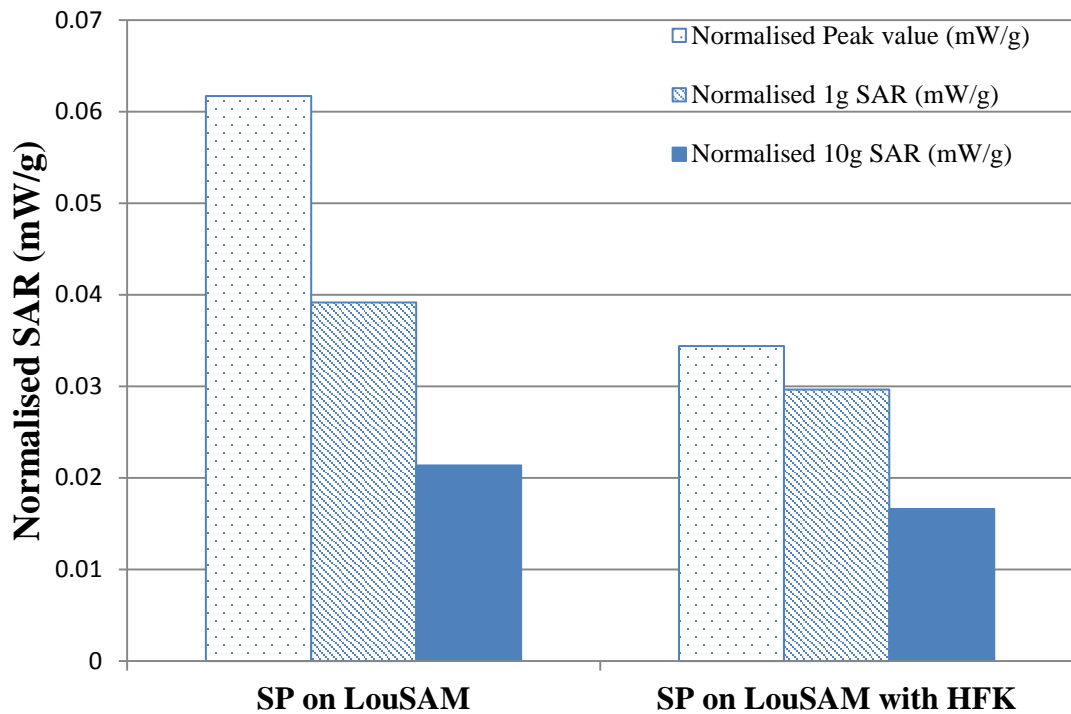
Figure 3-15: Graph of Smart phone in front of LouSAM head phantom with and without HFK.

The result shown in Figure 3-15 indicates that the peak SAR value in the face region decreases by approximately 50%. There is also a decrease in the 1g and 10g SAR values by approximately 20%. This shows that the HFK has some effect on the power absorbed in the face. This could be due to power coupling to the HFK wire or a simple case of antenna detuning. It must be noted that the measured SAR values in this scenario are very close to the noise floor of the measurement system.

The SAR value was measured in the left ear when the HFK was connected to the Smart phone while the Smart phone was in front of its face. As stated in the experimental setup section, ten random positions for the HFK wire were used. This gave options of possible wire orientation when using the HFK with the Smart phone. The graph in Figure 3-16 shows the results from the experiment for the 10 random positions.
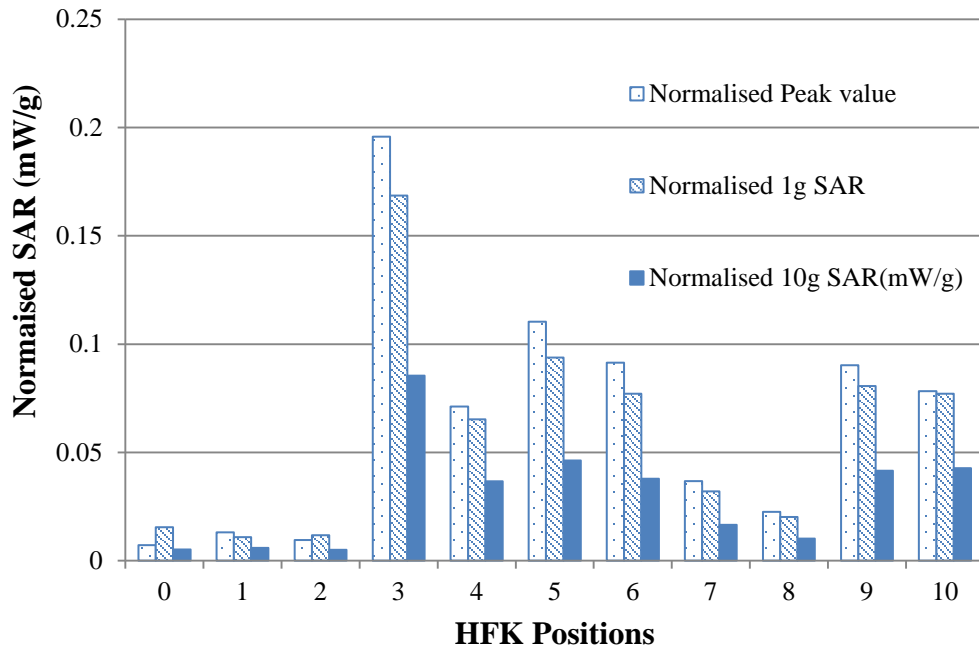
Figure 3-16: the SAR values in the ear when the HFK wire is placed in random positions (1-10) and Smart phone without HFK (0)

For reference purposes, the ear SAR without the HFK is plotted as "0" on the graph. Overall, the results indicate the SAR values in the ear region due to the HFK are very small compared to that produced by the phone placed touching the ear. In position 1 and 2, the HFK wire had no impact on the ear SAR. When compared to the reference, the HFK wire in position 3 increased the ear SAR more than 2000% giving considerable weight to the idea that there can be coupling from the handset to the HFK and subsequent radiation from the ear piece. In fact, the peak SAR recorded is almost half that recorded when the Smart phone is in the talk position.

Position 4, 5, 6, 9 and 10 also show significant increases in ear SAR compared to the reference. In position 7 and 8, there is a minimal increase in ear SAR. In terms of the measured SAR level, position 1, 2, 7 and 8 can be grouped together since their results

are in close region. Also position 4, 5, 6, 9 and 10 can be grouped together as their results are in the same region. Position 3 however was a very peculiar case. To confirm the result from position 3, the experiment was repeated at a later date. Positioning the wire in the exact position was challenging but with the aid of a picture taken, a similar wire position was achieved. The SAR results from the first and second experiments are presented in Figure 3-17. Although the results do not show an exact match, the new SAR values are significantly higher than those obtained from all the other nine wire positions. The result from the second experiment was not exactly the same as the initial one but it is still significantly higher than those results obtained from other positions. A picture of the 3rd position can be seen in Figure 3-11.
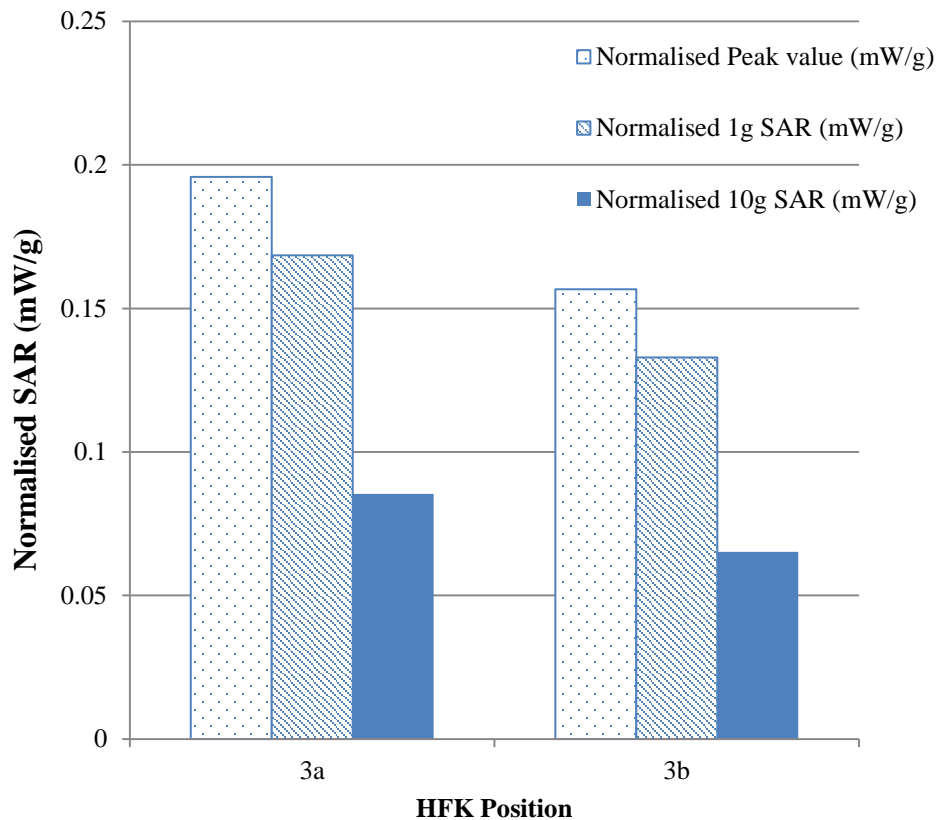
Figure 3-17: 3rd position of HFK wire carried out twice to confirm result

This result shows there is a high level of coupling between the Smart phone and the cable of the HFK. A table showing the change in 1g and 10g SAR value when the HFK are in the 10 positions when compared to when no HFK is shown in Table 3-1.

Position	Change in 1g SAR (dB)	Change in 10g SAR (dB)
1	-1.5	0.5
2	-1.2	-0.1
3	10.4	12.1
4	6.3	8.49
5	7.8	9.4
6	7.0	8.6
7	3.2	5.0
8	1.2	2.9
9	7.2	9.0
10	7.0	9.1

Table 3-1: Changes in 1g and 10g SAR value

In positions 4, 5, 9 and 10, the HFK cable length to the ear is short. The HFK cable is bunched up and the effective length from the SP to the ear is short. The bunched part of the cable can be likened to a coil. The average increase in the 1g SAR is 7.1dB with a maximum of 7.8dB and a minimum of 6.3dB.

In position 5, the HFK cable is in a parallel position to the antenna. This leads to coupling of the cable with the antenna and an increase in current flow on the HFK cable. Position 5 is described in the Figure 3-18.
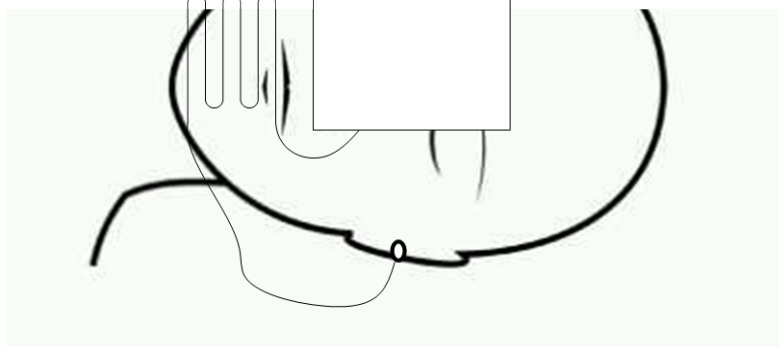
Figure 3-18: Smart phone with HFK wire bunched by the side of the antenna

In position 4, the folded HFK cable is perpendicular to the antenna. In this position, the coupling of the cable with the antenna is reduced thus leading to slightly lower current and lower SAR value. Position 4 is explained with the Figure 3-19.
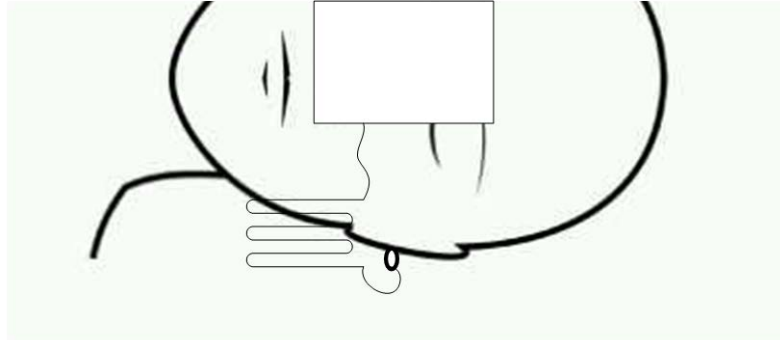
Figure 3-19: Smart phone with HFK wire bunched perpendicular to the antenna region

In position 10, the same coupling effect of the scrunched HFK cable can be seen like it is in position 5. This led to an increase in the SAR value similar to those seen in positions 4 and 5. Position 10 can be described with the Figure 3-20.
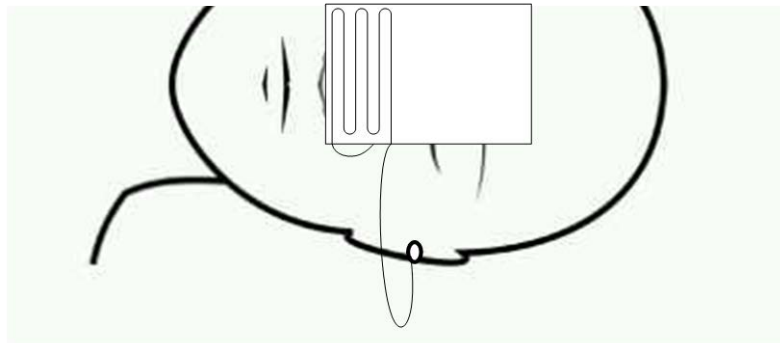
Figure 3-20: Smart phone with the HFK wire bunched at the back on the antenna region

In positions 7 and 8, the HFK cable is stretched out. The proximity of the cable to the antenna is minimal and most of the cable is not in the near-field region of the antenna. In this case, reduced coupling and current effect is felt hence the minor change in the SAR value.

In position 1 and 2, there is an interesting reduction in the SAR value. The 1g SAR and 10g SAR is reduced beyond the case where there was no HFK connected to the SP. This can be said to be measurements in the noise floor. With measurements in the noise floor region, there is a possibility of error in the measurement. The connection point of the cable is not close to the antenna in position 1 and 2. Also since the HFK cable is not drawn across the antenna region, there is no coupling effect and increase in current flow in the cable to affect the SAR value. It can be concluded that the HFK cable has little or no effect on the SAR value in these two positions.

3.11 SAR measurement using the iSAR Kit

The experiments done with the DASY kit gave some results prompting further investigation. Positions 4, 5, and 10 were re-analysed with another SAR measuring device. The iSAR machine was used for this measurement. The iSAR is produced by SPEAG. The iSAR head is an immediate SAR measurement system. The iSAR head has a shape that follows the ear to mouth line of the SAM head phantom. It is capable of analysing RF performance of a wireless device in less than 1 second. It simulates the area scan of the ear as required by IEC 62209-1, IEEE 1528 and FCC OET65. The measurement of the wireless device is done using the 256 sensors on the top surface simultaneously. These sensors are embedded in an absorbing material simulating head tissue. The iSAR can operate between 0.5 – 3GHz [21].

The measurement from this machine was done to verify how the HFK position influenced the current flow in the SP hence affecting the SAR distribution. The results from the iSAR are presented below. The results presented here are normalised to the maximum SAR value obtained while taking measurements. The SAR values here are not a direct comparison to the results from the DASY4. These results are to show the trend of the results expected when the HFK are in certain positions.

For the experiment with the iSAR, six scenarios were considered.

- ***a.*** Smart phone with no HFK connected
- ***b.*** Smart phone with HFK folded by the side
- ***c.*** Smart phone with HFK folded and placed on the back of the phone
- ***d.*** Smart phone with HFK folded to the bottom
- ***e.*** HFK on sensors while connected to Smart phone
- ***f.*** Smart phone with HFK isolated from sensors

Images showing the locations of the HFKs in each of the above scenarios, along with their SAR heat maps are shown in the Table 3-2.
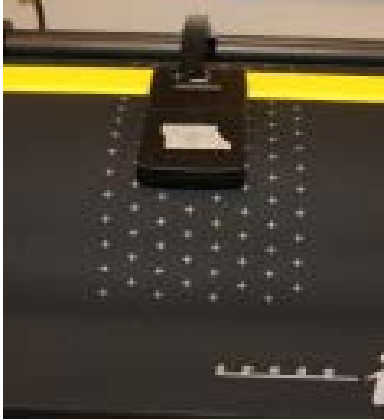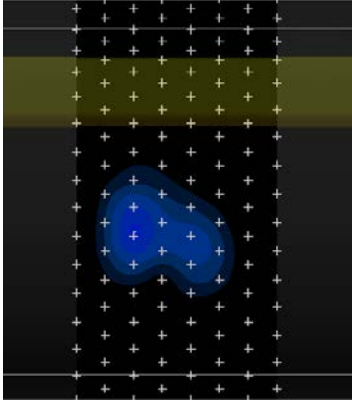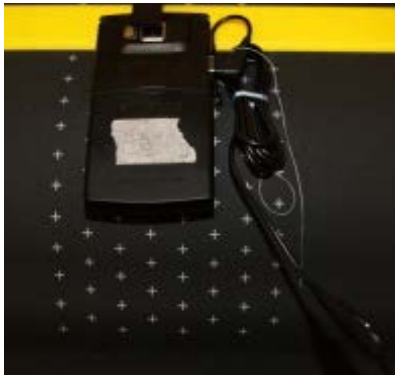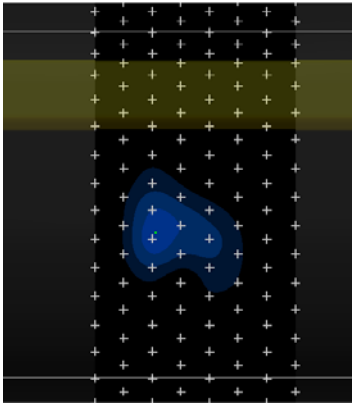
	iSAR picture	SAR heat map
a.		
b.		

Table 3-2: Smart pone in position *a-b* and SAR distribution imagine
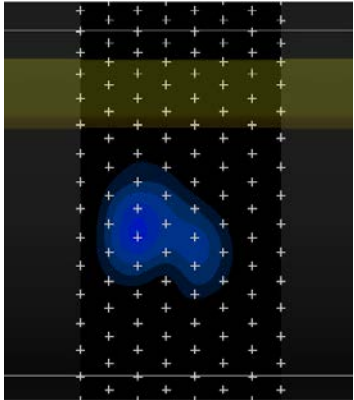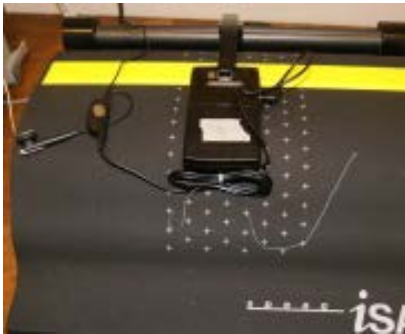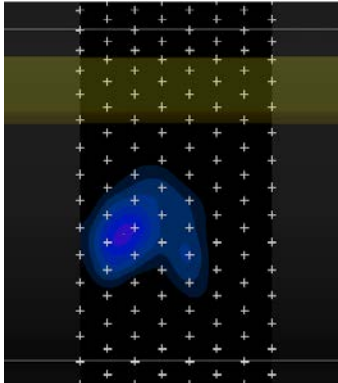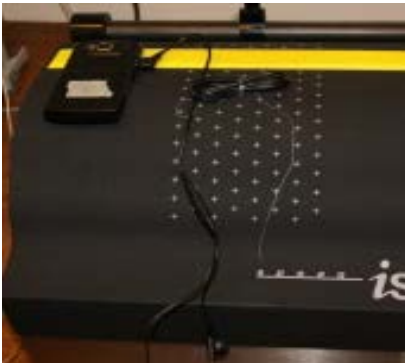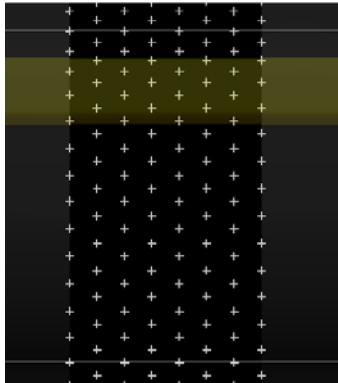
	iSAR picture	SAR heat map
c.		
d.		
e.		

Table 3-3: Smart pone in position *c-e* and SAR distribution imagine
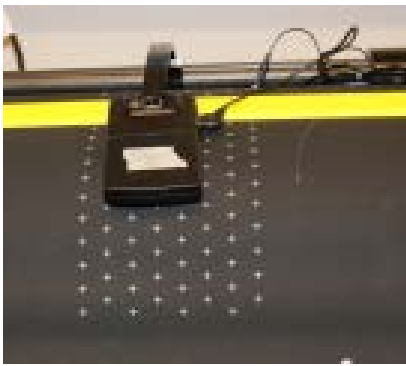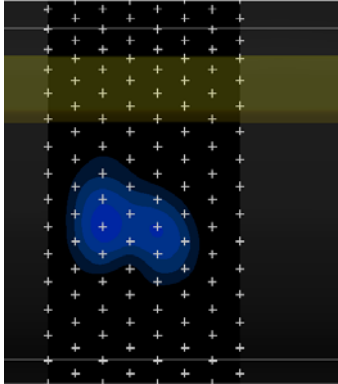
	iSAR picture	SAR heat map
f.		

Table 3-4: Smart pone in position *f* and SAR distribution imagine

The normalised result from the illustration experiments in Table 3-2 to Table 3-4 is presented in Figure 3-21.
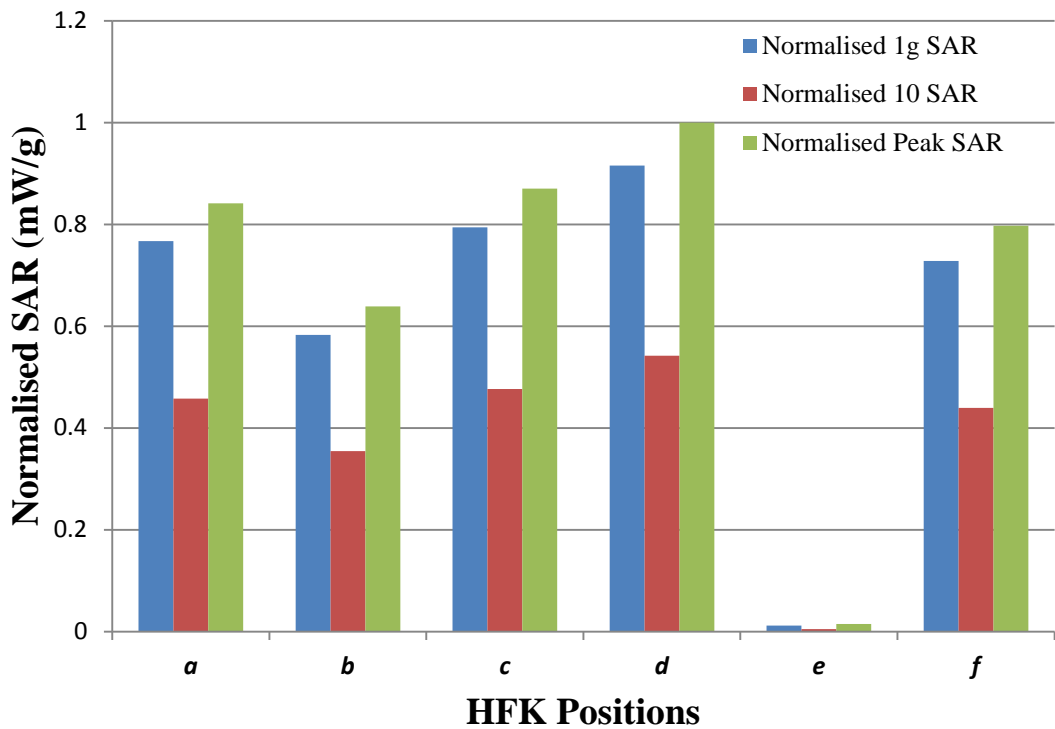
Figure 3-21: Normalised results from measurements with the iSAR kit

From the SAR distribution pattern and result presented, comparing position *c* with position *a* which is when the SP is not connected to HFK, there is no detuning of the system. The SAR heat map also remains the same. Comparing position *a* and *b*, there is

a 25% drop in the 1g SAR value but there is no change in the SAR distribution. This could mean the antenna is being detuned by the HFK when in that position. For position *d*, there was a 19% increase in the 1g SAR value when compared to position *a*. The SAR distribution pattern shifted down compared to that of position *a*. Also the maximum SAR position shifted down. All these pattern changes occurred closer to the HFK position at the bottom of the Smart phone.

3.12 Conclusions

This chapter has investigated through a comprehensive set of measurements, the effects of using a hands free kit with a mobile phone on the power absorbed inside the users head. The novelty of the work arises from the use of a Smart phone, which is more likely to be used in conjunction with a HFK in front of the face rather than attached to the waist. The *in front of face* phantom, known as the LouSAM, was also used to investigate the effects of the HFK on the power absorbed in the face region. Industry standard equipment has been used for measuring the specific absorption rate (SAR).

The detailed analysis of the results showed that none of the measurements exceeded the SAR recorded with the Smart phone located in the talk position. These results are therefore in agreement with those presented in a majority of other studies.

However, it was found that the HFK did not completely eliminate radiation into the head. In all measurements where the HFK wire was bunched up (making its apparent length shorter), the SAR in the ear region increased. In particular, the SAR recorded when the HFK was in position 3 (The HFK cable was bunched up along its natural bend points and then positioned next to the microphone) was approximately half that observed in the normal talk position. This demonstrates a significant amount of energy coupling to the wire resulting in re-radiation into the head. Although this did not exceed the SAR safety standard limits, it leaves open the possibility that certain locations of the HFK relative to the phone may produce a SAR value that goes beyond the talk position SAR. A very important consideration is that the earpiece bypasses the skull and positions itself much closer to the brain when inserted into the ear. Therefore, even if the SAR values measured with the earpiece placed on the surface of the twin phantom meet safety standards, once inserted into the ear, they may not. This certainly

warrants further investigation. Whenever the HFK cable was fully extended and located away from the Smart phone, there was no significant change in the ear region SAR.

The chapter also presented SAR measurements taken with the LouSAM, which previously had not been used in the literature for this kind of experiment. The results from the experiment with the phone in front of face with and without the HFK using the LouSAM head phantom showed that the SAR measured in the face reduced when the HFK was connected to the Smart phone. Since the SAR in the face is very small to start with, minor changes when including the HFK may just be due to background noise.

References

[1]   International Telecommunications Division, "The world in 2010: ICT facts and figures," in *ITU Telecom World*, 2010.

[2]   C. Chou and A. Guy, "Effects of electromagnetic fields on isolated nerve and muscle preparations," *Microwave Theory and Techniques, IEEE*, 1978.

[3]   E. Ofli, C. Li, N. Chavannes, and N. Kuster, "Analysis and optimization of mobile phone antenna radiation performance in the presence of head and hand phantoms," *Turk. J. Elec. Engin*, vol. 16, no. 1, pp. 67–77, 2008.

[4]   G. Bit-Babik, C. Chou, A. Faraone, A. Gessner, M. Kanda, and Q. Balzano, "Estimation of the SAR in the human head and body due to radiofrequency radiation exposure from handheld mobile phones with hands-free accessories," *Radiation Research*, 2003.

[5]   ICNIRP, "Guidelines for limiting exposure to time-varying electric, magnetic, and electromagnetic fields (up to 300 GHz)," *Health physics*, vol. 4, no. 74, pp. 494–522, 1998.

[6]   IEEE Standards Co-ordinatingCommitee, "IEEE C95. 1-1992: IEEE Standard for Safety Levels with Respect to Human Exposure to Radio Frequency Electromagnetic Fields, 3 kHz to 300 GHz, The," *Inc., New York, NY*, vol. 1991, 1992.

[7]   IEC62209-2, "Human exposure to radio frequency fields from hand-held and body-mounted wireless communication devices- Human models, instrumentation, and procedures," *International Electrotechnical Commission*, 2010.

[8]   M. T. Camp, "Development of the Bluetooth version 1.0 specification," *2000 IEEE Emerging Technologies Symposium on Broadband, Wireless Internet Access. Digest of Papers (Cat. No.00EX414)*, p. 7.

[9] "Which?," *Special Report: Mobile Phone Risks*, pp. 11–17, Apr-2000.

[10] M. I. Manning and C. H. B. Gabriel, "SAR Tests on Mobile Phones used with and without Hands-Free Kits," no. July, 2000.

[11] S. E. Troulis, W. G. Scanlon, and N. E. Evans, "Effect of a hands-free wire on specific absorption rate for a waist-mounted 1.8 GHz cellular telephone handset.," *Physics in medicine and biology*, vol. 48, no. 12, pp. 1675–84, Jun. 2003.

[12] S. Porter and M. Capstick, "SAR associated with the use of hands-free mobile telephones," *EMC Europe*, 2004.

[13] S. J. Porter, M. H. Capstick, F. Faraci, and I. D. Flintoft, "SAR testing of Hands-free Mobile Telephones," *MTHR*, 2005.

[14] S. J. Porter, M. H. Capstick, F. Faraci, I. D. Flintoft, and A. C. Marvin, "SAR and induced current measurements on wired hands-free mobile telephones," *IEE*, pp. 9–13, 2004.

[15] IndexSAR, "https://http://www.indexsar.com/." .

[16] S. Kühn, E. Cabot, A. Christ, M. Capstick, and N. Kuster, "Assessment of the radio-frequency electromagnetic fields induced in the human body from mobile phones used with hands-free kits.," *Physics in medicine and biology*, vol. 54, no. 18, pp. 5493–508, Sep. 2009.

[17] Schmid and Partner Engineering AG, "DASY4 Manual."

[18] C. J. Panagamuwa, W. Whittow, J. C. Vardaxoglou, and P. McEvoy, "A study of the validation of RF energy Specific Absorption Rates for simulations of anatomically correct head FDTD simulations and truncated DASY4 standard equipment measurements," in *Proceedings of the EuCAP 2006.*, 2006, vol. 2006, no. October, pp. 2–6.

[19] C. J. Panagamuwa, W. G. Whittow, R. M. Edwards, and J. . Vardaxoglou, "Experimental Verification of a Modified Specific Anthropomorphic Mannequin (SAM) head used for SAR measurement," in *Loughborough Antenna & Propagation Conference*, 2007, vol. 00, no. April, pp. 261–264.

[20] Samsung, "Smartphone SGH-i600 User's Guide," 2006.

[21] SPEAG, *iSAR System Handbook*. 2011.

4 Comparison between CTIA Hand Phantom and Different Human Hands for Over the Air (OTA) Power Measurements

4.1 Introduction

The performance of an antenna can be negatively impacted by the presence of objects in its near-field. This can take the form of antenna detuning (increased mismatch loss), decrease in antenna efficiency and changing of the far-field radiation pattern. Alleviating these issues in a modern mobile phone is particularly challenging because the user's hand and head are generally in the antenna near-field. In certain circumstances, users may see significant drops in the received and transmitted signal strengths and when added to the energy lost as dielectric heating in the head and hand, may result in a dropped call. The more likely outcome however is for the phone to compensate by boosting its transmit power, which results in a higher SAR in the user and a faster battery drainage.

The mobile phone antenna position plays a crucial part in signal strength. In early designs, mainly due to the technology available at the time, mobile phone manufacturers placed the antennas protruding out from the top of their phones. This had the benefit of reducing the effect of the hand on the antenna. Mobile phone evolution saw antennas change from being long protruding elements outside the phone body to very small parts inside the phone body. With the general reduction in phone size, the challenge of the antenna design and position inside the phone casing increased.

The handling of mobile phone varies from one individual to another. This is also dependent on the mobile phone size and shape. Mobile phones manufactured in the beginning of the third millennium came with instructions on how to handle the phone in order to reduce interference with phone signal. In 2010, Apple launched the iPhone 4

[1]. The iPhone 4 has its antennas as the steel band around the phone edge. It was observed after release that the phone signal dropped when the phone was gripped in a particular way in the hand. The hand would short circuit one antenna to another causing massive detuning. To reduce this effect, Apple suggested a protective case to eliminate antenna contact with the human hand. This example illustrates the challenges faced by the antenna engineer when considering the unavoidable human interaction.

In order to include the hand effect on the mobile phone during over the air (OTA) testing, the Cellular Telecommunications Industry Association (CTIA) produced a series of artificial hand phantoms [2]. This allows mobile phone manufacturers to budget for the decrease in antenna sensitivity and the effective radiated power. In the work presented in this chapter, OTA measurements are taken from an internal antenna mobile phone held by one of these CTIA hand phantoms and then compared to those taken with real hands. The chapter presents results and analysis of measured data collected from 33 volunteers.

4.2 Background study on Human proximity effect to Mobile Phone performance

Understanding the interaction of mobile phones and human beings has been a crucial part in the advancement of mobile telecommunications technology. The proximity of the human body to a mobile phone affects the input impedance, far-field radiation pattern, radiation efficiency and the magnitude of the near-field of the antenna. In [3], this was investigated with a finite difference time domain (FDTD) technique using a phone with a quarter wavelength monopole antenna and a block to represent the hand and a sphere representing the head. The investigation was carried out at 900MHz and 1900MHz. Measurements were taken with and without the head and hand model. It was concluded that the presence of the human body detuned the quarter wavelength monopole antenna and the radiation pattern changed significantly. Also, about 45% of the power was lost in the phantoms for both frequencies tested.

In [4], the interaction of human body was further investigated using more antennas. The antennas for this experiment included a monopole, side-mounted planar inverted F, top-

mounted bent inverted F and back-mounted planar inverted F, all on a block shaped mobile phone. This was to model internal and external antenna positions in the mobile phone. The investigation was carried out using FDTD simulation and more detailed information was used in modelling the head and hand. The investigation was done at 915MHz. It was concluded that the presence of the head and hand had an effect on the input impedance, radiation and gain for all the antennas used in the investigation. The SAR in the head was also analysed mathematically and it was concluded that the head absorbs an average of 50% of the power delivered to the antenna when there is a separation of 2cm between the head and the handset. It also showed that using a back-mounted planar inverted F reduced the SAR in the head. In [5], the effect of the hand on internal and external antenna of mobile phone was also investigated. It was concluded that in the design of antennas for mobile phones, the whole antenna platform which comprises of the ground plane, battery, camera and other components in the antenna region should be taken into consideration. It also concluded the hand degrades the antenna performance reducing its efficiency by about 50%.

The effect of the hand was investigated in [6] using a homogeneous and inhomogeneous hand phantom with 4 mobiles phones. The phones used were a candy bar phone with a helix antenna, a flip phone with a helix antenna and a candy bar phone with PIFA antenna at the bottom and another with the antenna at the top. The investigation was carried out using the SEMCAD X simulation tool from SPEAG. The results in [6] showed that the homogeneous hand phantom and inhomogeneous hand phantom had negligible effect on the OTA results. Hence the use of a homogenous phantom to represent the hand when testing hand effects on the phone was approved. It also concluded that the hand size and palm–phone distance had an effect on the antenna performance especially in the phone with the antenna at the bottom. Also a sensitivity test was carried out to check the impact of the index finger on the antenna. The antenna response changed according to the sensitivity of the touch. There was up to a 6.5dB difference in the total radiated power depending on the positioning of the hand. With this, a further conclusion was drawn that the grip of the hand phantom on the phone had an impact on the antenna performance. In [7], a homogeneous and inhomogeneous block hand model was designed in accordance to the CTIA hand properties. The fingers were modelled as cylinders and the palm and thumb as bricks. The skin and bones also

took the same shape for the inhomogeneous hand. The hands were used to check the effect of the hand on SAR in the head at 900MHz and 1800MHz. The result showed that the SAR in the head reduced when the hands were present.

In [8], the effect of the hand on the mobile phone was also investigated but this was from a SAR point of view. A flip phone with helix antenna and a candy bar phone with PIFA antenna similar to the one used in [6] were used in this investigation. It was concluded that the SAR value increased in the head depending on the hand grip on the phone. The conclusion in [8] confirms as stated in [6] that the grip of the mobile phone affects its performance. In [9], the same set up as [6] was used to check the effect of the hand phantom on the mobile phone performance. But in [9], the impact of the position of the index finger was also investigated. The investigation was carried out using the SEMCAD X simulation tool at 900MHz and 1800MHz. It was concluded that the hand grip had a significant effect on the performance of the mobile phone. This is affected by the hand size, distance between the palm and the phone and the position of the phone in the hand phantom. The investigation showed that the index finger position has a strong impact on the OTA performance. In [10], an experimental approach was used to study the effect of the hand and head on the mobile phone. A PIFA antenna designed to resonate at 900MHz, 1800MHz and 2000MHz was used for the experiment. An IXB-90R hand phantom and a head phantom from IndexSar [11] were used for the experiment. Total efficiency and impedance matching was measured for when the antenna was in free space, in the hand and in the hand beside the head. For the talk position, six hand grip positions were used in this experiment. It was concluded that the antenna performance depends on how the mobile phone is held in the hand. Papers [6], [8], [9] observed that the index finger affected the antenna performance and impact of SAR in the head. Further investigation was conducted in [12] using the SEMCAD X to check the SAR and efficiency performance of the phone antenna as the index finger is moved away from the antenna. A candy bar phone with internal PIFA antenna at the top back region was used. It was concluded that the index finger position affects the SAR and OTA parameters of the phone. In [13], a study on how the phone is held in different positions was performed. It was also concluded that the index finger is a major factor affecting the phone's performance. It was recommended that the hand needs to be considered in OTA performance testing of mobile phones. In [14], [15], a study on how

the mobile phone is gripped when in the talk position was conducted. From numerous videos taken, screenshots to extract different grips were taken. Data obtained was converted to CAD format and all investigations were carried out with a FDTD simulation tool. From the video recording of 100 participants, the study showed that the index finger was mostly placed in the back region of the mobile phone [14]. Also in [14], it was concluded that the hand had more detrimental effects on the communication system compared to when the phone is placed on the torso of the SAM phantom. The authors in [15] investigated the effects of the phone user's hand on PIFA antennas in mobile phones using data acquired from [14]. A CAD model of the human hand was used for the simulation from data acquired from [14]. The effect of the hand was compared with that of the upper torso. It was concluded that the hand, especially the index finger has an impact on the antenna performance and SAR in the head. Further studies were carried out in [16] to compare the effect of the hand when the phone is in data mode and talk mode. Two data mode grip positions were considered along with two talk mode grip positions. In the talk mode, the investigation concluded that the index finger contributed to over 70% of the power absorbed by the hand and reduced communication performance. The data mode investigation showed that the fingers and its surrounding tissues are the only factors that affect the antenna performance. The radiation efficiency of a handheld mobile phone was tested in [17]. The experiment was carried out in an anechoic chamber with a phone with a helix antenna and another with an integrated patch antenna. It was concluded that the hand position had a large impact on the radiation efficiency while the tilt angle of the phone and the separation distance between the phone and the head had little impact on the radiation efficiency in both phones. The dimension and location of the antenna is taking into consideration in [18]. In the work, the guidelines to design and location of antenna is given to reduce the effect of the hand on the antenna. The work was done using FDTD based simulation. It was concluded the hand and hand grip should be considered when designing antennas for mobile terminals.

Numerical analysis of antenna performance around the human body was carried out in [19]. For this analysis, three different handsets with a monopole antenna, side mounted dual PIFA and a back mounted PIFA were used. This study showed a body affected the antenna's input impedance, radiation pattern and received power. It was suggested that

this interaction should be considered when developing antennas used in proximity to the body. To reduce the hand effect on the mobile phone antenna, [20] implemented an adaptive matching circuitry alongside the antenna. The matching circuit was called a Dynamic Antenna Matching (DAM) circuit. The main component of the DAM circuit is a GaAs technology based semiconductor switch (SP4T). The adaptive circuit compensated for losses caused by mismatch when the hand is placed in the antenna region. The results showed an improvement of 2-4dB when operating from 815–900MHz and 2dB when operating from 1710-1910MHz in the total efficiency of the antenna. The circuitry also helps reduce power consumption which occurs when the mobile phone is trying to boost signal power when signal strength is dropping. The DAM circuit does not affect the radiation efficiency of the antenna in a mobile phone. To reduce the hand effect on a mobile phone, [21] designed a coupled radiator antenna to replace the PIFA antennas in a mobile phone. This was carried out at GSM900. It was concluded that the antenna had sufficient bandwidth and efficiency when in free space and human hand.

In [22], an antenna selection system to compensate for the finger effect was proposed. In this system, two antenna elements were used. The antenna element which was least affected by the index finger was selected. The selection process involved the use of capacitance sensor located close to the antenna element and an RF switch performing the antenna selection based on information given by the sensors [22]. The experiment was carried out at 1800MHz comparing the finger effect on a single element and a two element antenna. The hand was modelled using a vinyl glove filled with tissue simulating liquid. The result showed a minimum of 2dB improvement in total efficiency when using the two element antenna in comparison to the single element antenna. In [23] the radiation performance of the mobile phone antenna in the presence of the head and hand was improved by optimizing the antenna. This was carried out in SEMCAD X using a genetic algorithm based optimization technique. The antenna CAD file was converted to parameters and optimization was performed in two steps. First the antenna was designed to work in free space and secondly the head and hand phantom was introduced to the system. The antenna was then optimized to work at required frequency with the presence of the head and hand. A comprehensive review on antennas in mobile phones for the past 15 years was carried out and a plan for the antenna system for the

new generation phone is proposed in [24]. The effect of the body on the antenna system in a phone was examined. It concluded the body had a detrimental impact on the antenna system. The work proposed the use of MIMO antenna system in the mobile phone to improve the system.

The studies highlighted so far have shown a negative impact of the hand on the antenna in a mobile phone. In [25], a hand phantom was used to investigate efficiency, antenna match and total radiated power (TRP) of a mobile phone, which showed the opposite. The investigation showed that the hand phantom increased the TRP at lower band and reduced TRP at higher band. It was concluded that this was due to the ability of the hand phantom to extend the ground plane.

For OTA power measurements for mobile phones, the CTIA recommends the inclusion of the hand phantom in the test procedure [2]. Some homogeneous hand phantoms showing different phone grips were developed to be used in the OTA power measurements. This was done to help standardize all measurements including the hand phantom and phone grip. The CTIA hand phantom is gaining increased prominence in today's mobile communication field. The ICES TC34 SC2 working group is also working on assessing the feasibility of including the hand phantom in the Specific Absorption Rate (SAR) measurement standard [26].

In the work presented in this chapter, the CTIA hand is tested and compared to the human hand. In all the literature reviewed the CTIA hand has not been tested to verify how best it represents the human hand. In this work, the impact of the index finger proximity to the antenna region of a phone with its antenna in the top back region was tested. This work also investigates the effects a metallic ring worn on the index finger has on the received power by the antenna compared to when the ring is not worn. The work presented here is all experiment-based with participants with different hand sizes. Both left and right hands were used in this experiment.

4.3 Experimental setup for comparison of CTIA Hand Phantom and Different Human Hands

The purpose of this study was to answer the following questions

1. How well does the CTIA phantom hand compare to real human hands when conducting OTA power measurements?

2. What effect does the hand size and index finger location have on OTA power measurements?

3. Does a metallic ring on the index finger have an effect on OTA power measurements?

4. Is there a difference between the left and right hand grips when conducting OTA power measurements?

In the experiment carried out, personal information of the participants' were neither taken nor published in any part of this work. There is no image of the any participant involved in this work. In the process of data storage, the participants were labelled with numbers to keep their identity anonymous. The participants were well informed of the experimental procedure. The experiment was carried out with the guideline of the ICNIRP for radiation exposure.

The power level transmitted from the mobile phone was set at maximum level. The maximum level is set according to the ICNIRP standard. This power level is within guideline and it's a power level a mobile phone user can be exposed to under normal working condition. Although the mobile phone is transmitting at maximum power, the distance between the head and the mobile phone is about 60 cm. This drastically reduces the SAR in the head.

The experiment was conducted in a semi-anechoic chamber at Loughborough University. For the experiment, a Nokia 6220c mobile phone was used. The Nokia

6220c was selected for this experiment because of the position of its antenna which is located at the top back region of the phone. This is shown in the figure 4-1.
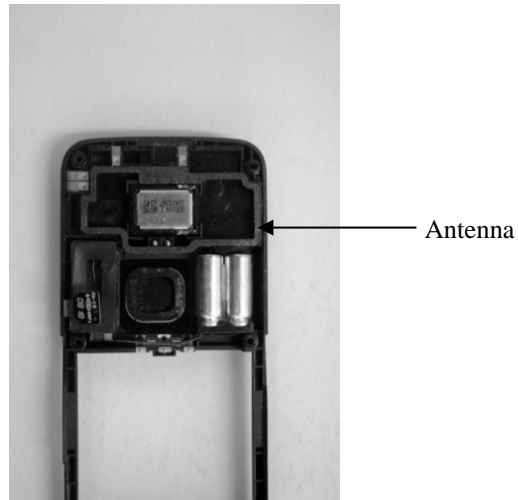
Figure 4-1: Antenna location of the Nokia 6220c

The mobile phone was mounted on a rig using two thin cables and supported with a block of ROHACELL® 31 HF[27]. The rig was kept in a fixed position in order to reduce changing variables in the experiment. With the phone in a fixed position, the participant's hand position was the only changing factor. For communication with the phone, a dipole antenna connected to an Agilent 8922A was used to simulate the base station operating at GSM 1800, Chanel 512 (1710MHz). The phone was instructed to transmit at maximum power. Figure 4-2 shows the setup of the base station and mobile phone position.
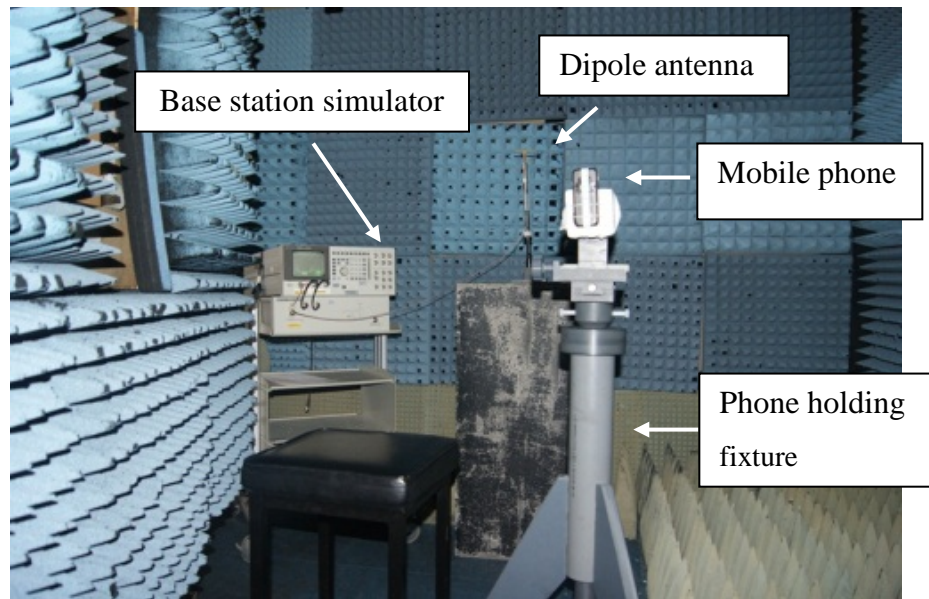
Figure 4-2: Measurement setup in the anechoic chamber

A broadband horn antenna connected to an Advantest R3182 spectrum analyzer was positioned approximately 2m from the back of the phone. The photograph in Figure 4-2 was taken from the location of the horn antenna. The phone was set to transmission level 1. At level 1, it communicates with the base station at maximum power. This power from the phone was measured using the spectrum analyzer. The screenshot of the spectrum analyzer measurement is shown in figure 4-3. The red dot is a marker for the point where the power is measured at 1800MHz. The envelope around the point of power resonance is the area over which measured power is averaged.
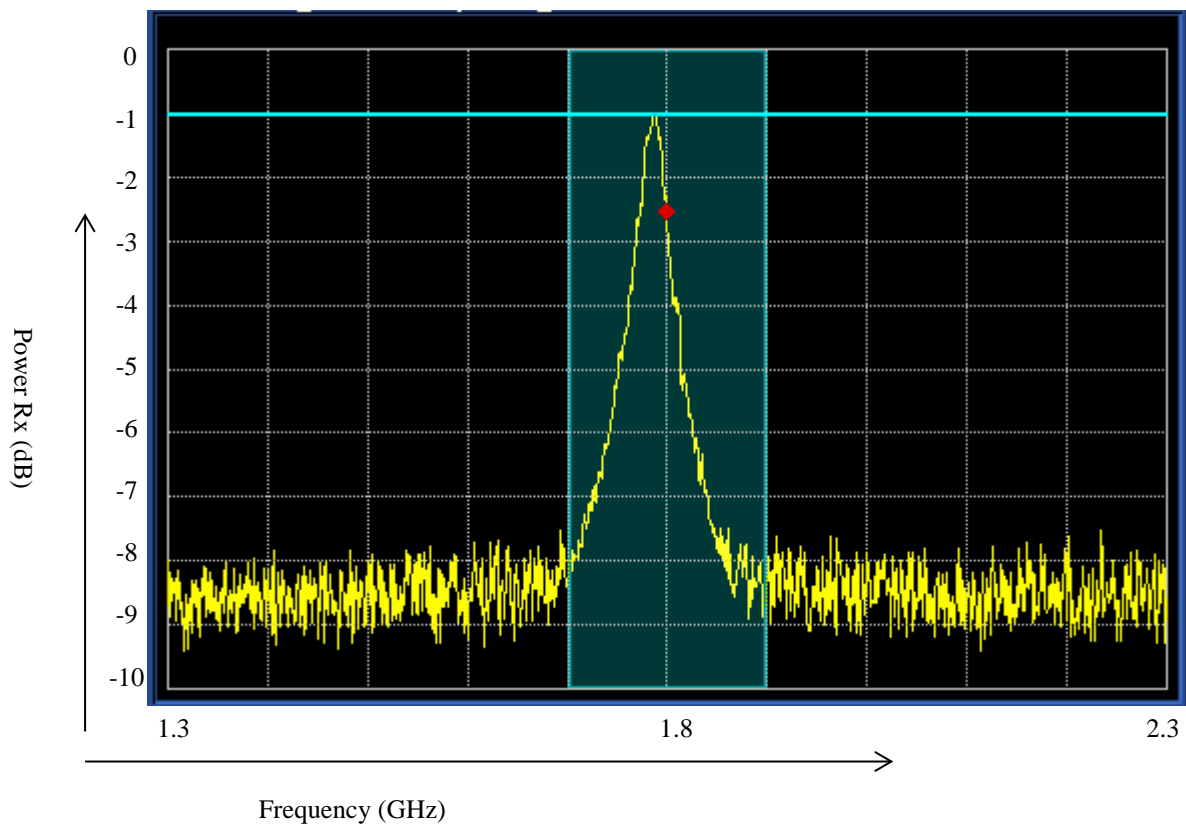
Figure 4-3: Screenshot of the trace from the spectrum analyzer

Participants were asked to sit to the left of the mobile phone and to grip the phone with their right hand. The same procedure was repeated with the left hand with the participants sat to the right of the mobile phone. The stool on which the participants sat was kept in the same location to ensure the participant's bodies were approximately in the same position with respect to the phone. The separation distance between the phone and horn antenna was kept constant for the duration of the experiment. A schematic of the setup for the experiment is shown in the figure 4-4.
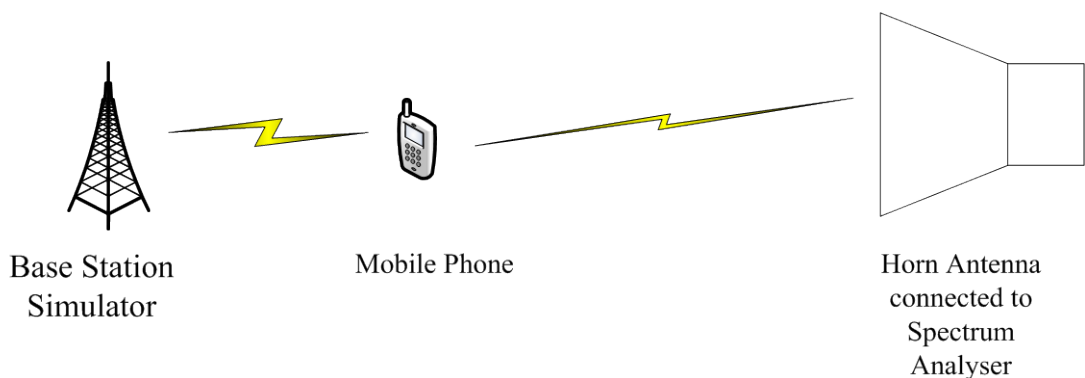
Figure 4-4: Base station – Mobile Phone – Spectrum analyser interaction

Thirty three participants took part in the experimental study. Measurements were taken with and without a ring worn on the index finger. This ring used was metallic. The idea of using a ring on the finger was to check how fashion accessories affect the phone antenna. The index finger positions were carefully controlled using markers on the back of the phone. Paper tape was fixed vertically along the centre of the back and marked with three 10mm spacing. The top most position (Position 1) was directly over the phone antenna and Position 4 was 30mm vertically down from the top region of the antenna position. Figure 4-5 shows the mobile phone with the marking of each position of the finger. Position 2 and Position 3 are between when the antenna is fully covered and when the antenna is not covered (i.e. between Position 1 and Position 4 respectively).

Figure 4-5: Mobile phone with markings of finger positions

The participants were asked to hold the phone in a similar fashion to the CTIA hand phantom SHO V2RB shown in figure 4-6 acquired from SPEAG. The hand phantom is made from a silicon and carbon mixture with $\varepsilon_r = 27$ and $\sigma = 0.99$ S/m ($\pm 20\%$) at 1800MHz [2]. The key dimensions of the hand phantom in the grip position are given in table 4-1 and a figure of the hand phantom from different views is shown in figure 4-6. The height is the length of the hand and the width is the breadth of the hand.

Hand dimension	Measured value (mm)
Height	205
Wrist width	61
Hand width	97

Table 4-1: Dimension of the CTIA hand phantom [28]
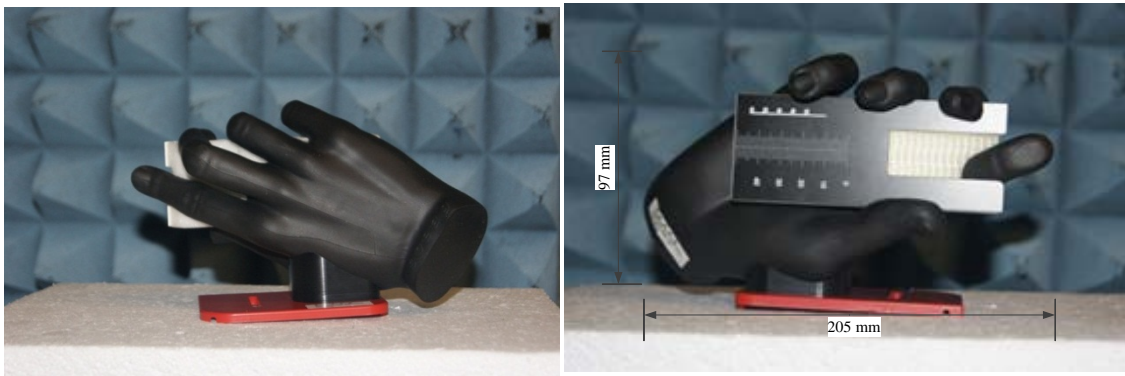
Figure 4-6: Back view and Front view of the CTIA hand phantom

To ensure the accuracy and repeatability of measurements taken under the same condition, the point where the participants put their finger is marked. The setup is such that the only moving part is the participant's finger and body when they take a seat on the stool provided. The result from the experiment varied due to different hand sizes involved in the experiment. The index finger length involved in this experiment varied from 7cm to 11.5cm.

Each of the thirty three participants had their index finger with and without a ring placed on the 4 positions marked on the mobile phone and the received powers were measured. This procedure was also carried out without the ring on the CTIA hand phantom in the 4 positions. For the purpose of quantifying repeatability, the CTIA hand phantom was measured twice. The maximum error between the two measurements with the hand phantom was 1dB. In Section 4.4, the results from the experiment will be presented and compared with that of the CTIA hand phantom.

4.4 Analysis of Results

For the purpose of analysis, a measurement was taken with the mobile phone on the rig setup and in communication with the base station simulator. This was done without a participant in the setup and all subsequent measurements were normalised to this measurement. The maximum power received at the horn antenna at the transmit frequency was -4.37dBm.

The variation of the measured power from the mean is expressed as standard deviation. The lower the standard deviation the closer the measured data to the mean of the data and otherwise if the standard deviation is higher. The table below shows the standard deviation of the measured power for all finger positions with and without a ring worn on the index finger.

	Left hand	Left hand - Ring	Right hand	Right hand - Ring
Position 1	2.29	2.37	1.88	1.99
Position 2	1.49	1.22	1.26	1.51
Position 3	1.20	1.14	1.12	1.03
Position 4	1.34	1.04	1.01	1.03

Table 4-2: Standard deviation of the measured power

Prior to the experiment, the measurement was repeated 4 times to check for repeatability. The results showed the measurement was within 1dB of each other. The margin of error for the measurements taken is shown in the table below.

	Left hand	Left hand - Ring	Right hand	Right hand - Ring
Position 1	±0.78	±0.81	±0.64	±0.68
Position 2	±0.51	±0.42	±0.43	±0.51
Position 3	±0.41	±0.39	±0.38	±0.35
Position 4	±0.46	±0.36	±0.34	±0.35

Table 4-3: Margin error of the measured power

The analysis of results will be broken down according to finger position (Position 1-4) with and without ring. Also hand dimensions will be considered in understanding the results.

To reduce the margin of error and changing variables in the experiment, the following steps were taken:

> ➢ The positions of the equipment were marked in case it moved in order to maintain same position in the experiment.

> ➢ The finger position was marked on the mobile phone to guide the participants during experiments.

> ➢ The stool position was marked to maintain the same position during the experiment.

In position 1, the index finger made contact with the region of the casing directly above the antenna. Maximum received power measurements were taken with the left and right index finger in position 1, in both cases with and without the ring on the index finger. As far as possible, the participant was asked to replicate the CTIA hand grip. The set of four results for each of the participants is plotted in Graph 4-1 along with the result for the hand phantom. The received power is very low at position 1. This is due to the finger being placed on top of the antenna region. Normalised to the maximum received power without the participant, the hand phantom reading is -9.2dB and the average of all measurements taken at position 1 is -9.0dB. The horizontal orange line shows the hand phantom result to aid the visualization.
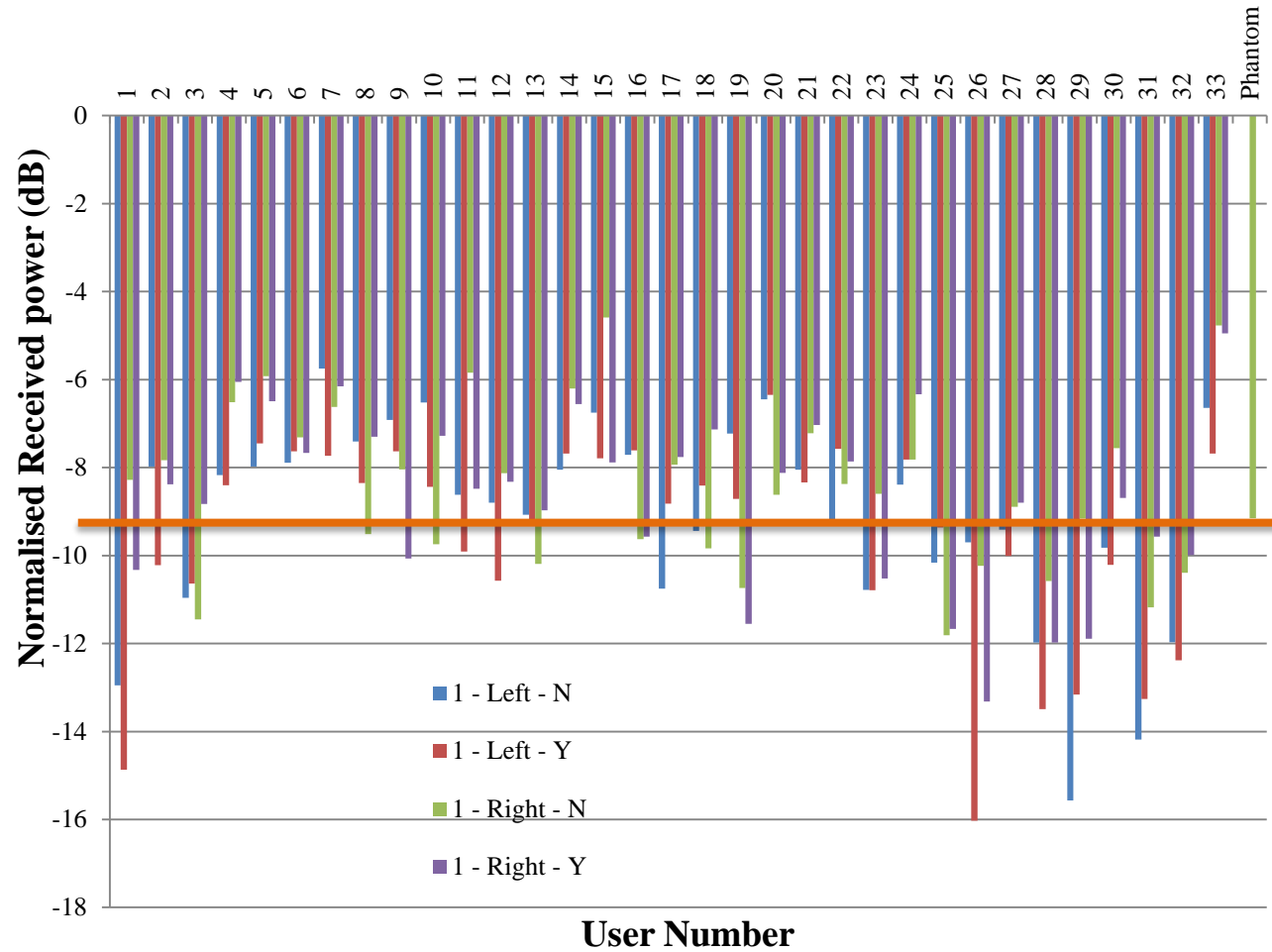
Graph 4-1: All measured results compared to phantom hand at Position 1

In position 2, the index finger is at the 10mm mark on the mobile phone. More of the antenna is now exposed. The result for the measurements taken is shown in the graph 4-2. At this point, it can be observed that the measured received power is generally higher compared to measurements taken from position 1. The normalised received power when the hand phantom is in position 2 is -5.5dB and the average for all participants is -5.8dB.
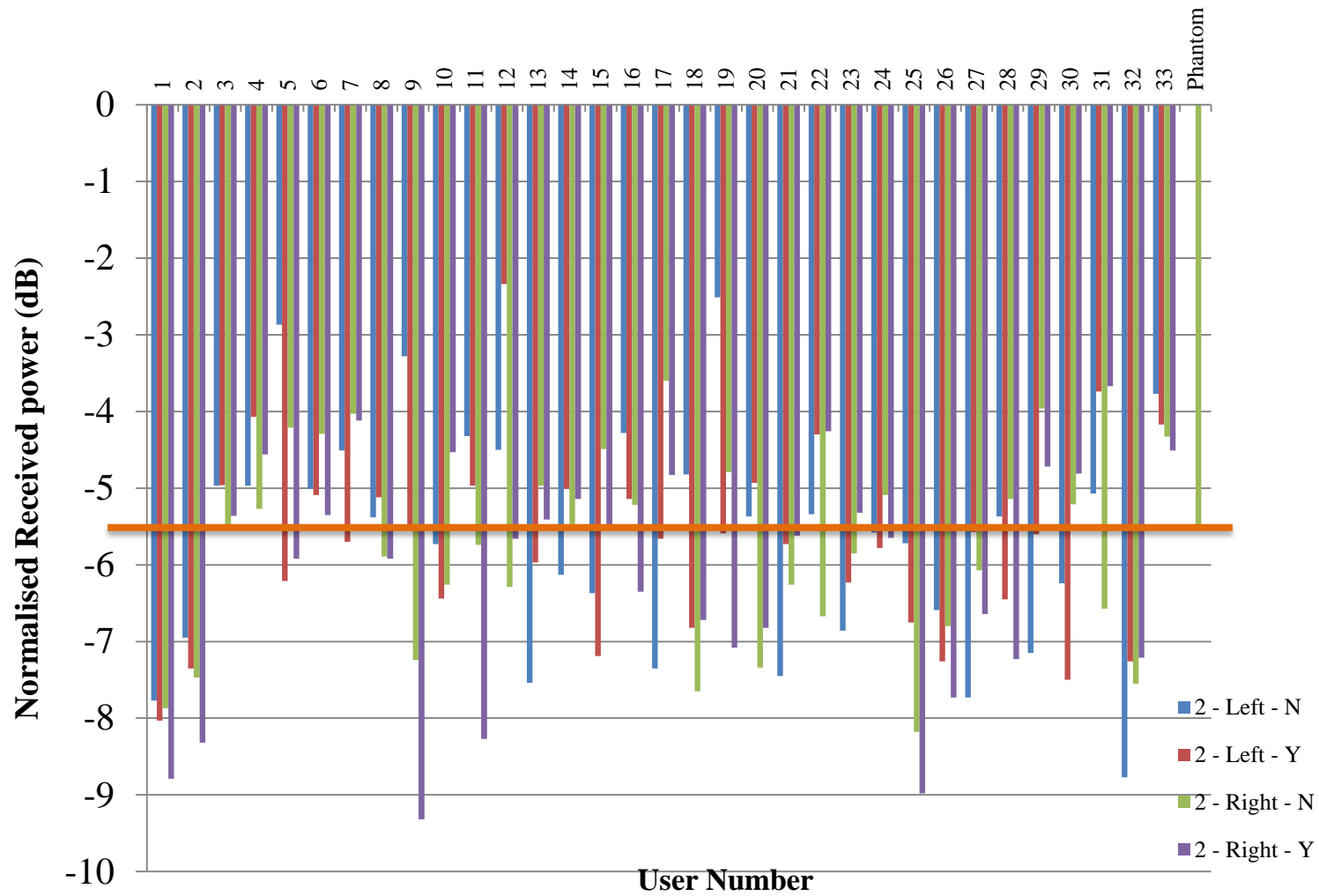
Graph 4-2 : All measured results compared to phantom hand at Position 2

The graph 4-3 below shows received power when the finger is at position 3. At position 3, the index finger is 20mm from the top of the antenna region. At this point, a large region of the antenna is exposed and there is less disruption. The normalised received power at this position with the phantom hand is -2.9dB and the average for the human hands is -2.6dB.
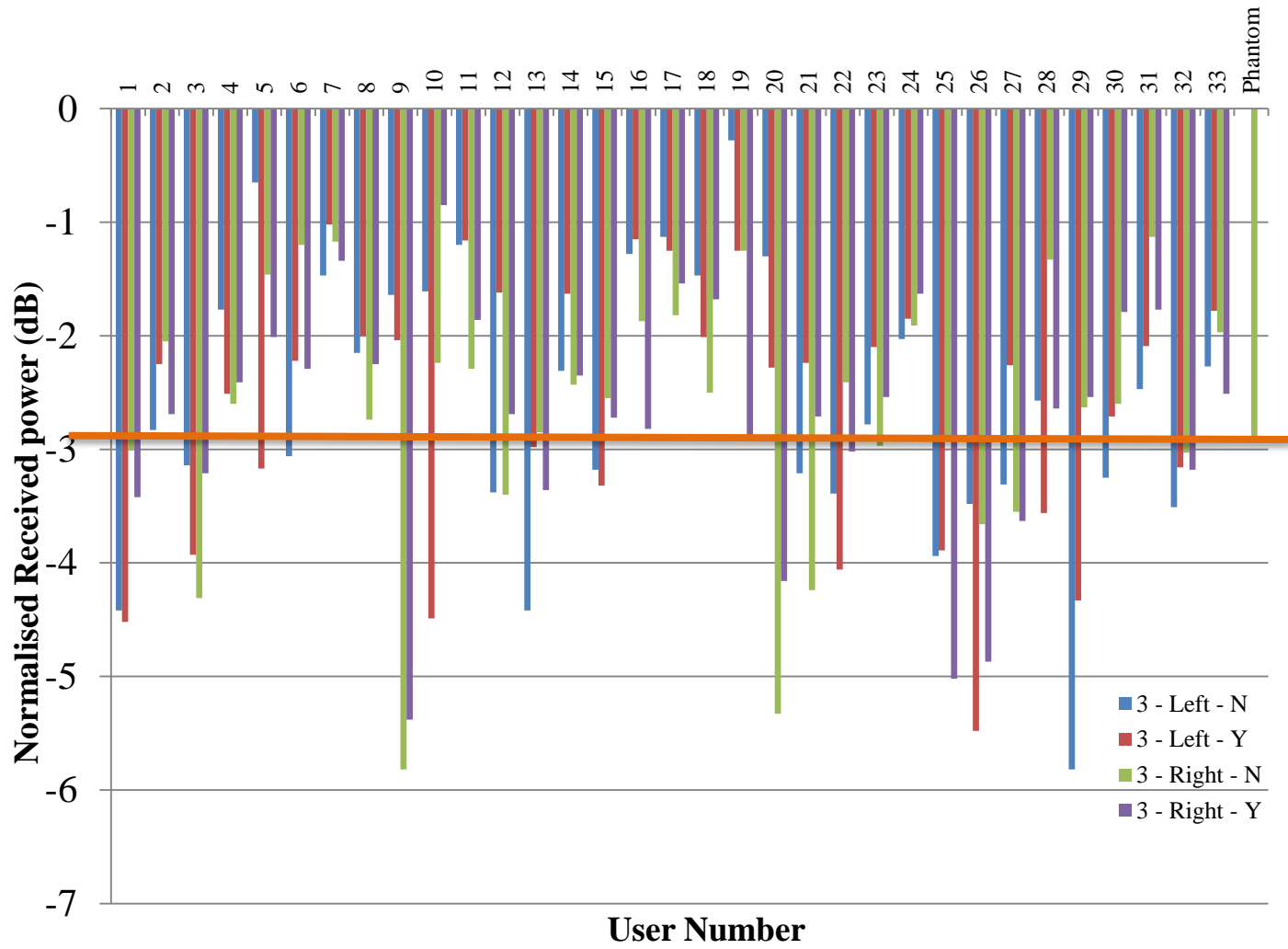
Graph 4-3: All measured results compared to phantom hand at Position 3

At position 4, the finger is hardly covering the antenna region of the phone. But the hand still has an impact on the received power. At this point, the hand is 30mm away from the top region of the antenna area. Graph 4-4 shows the normalised received power when the human hand and phantom hand are at position 4. The received power when the hand phantom is used is -2.1dB and the average for the human hands is -1.5dB.
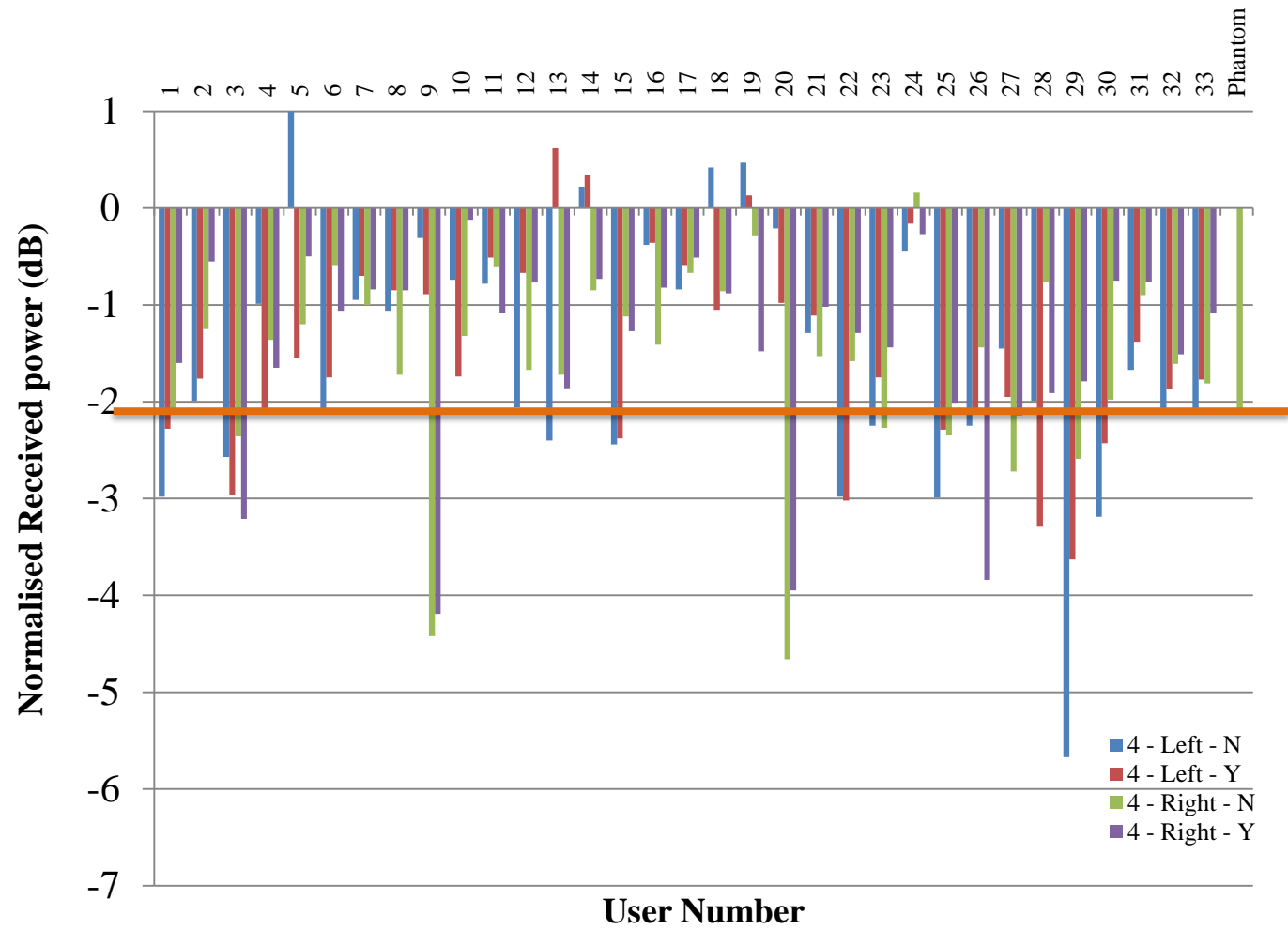
Graph 4-4: All measured results compared to phantom hand at Position 4

The average of power received for each position averaged over all participants is compared to that of the phantom. Graph 4-5 shows a common trend in the increase of power received as the hand moves away from the antenna region. There is good agreement between the Participant average and the CTIA phantom hand.
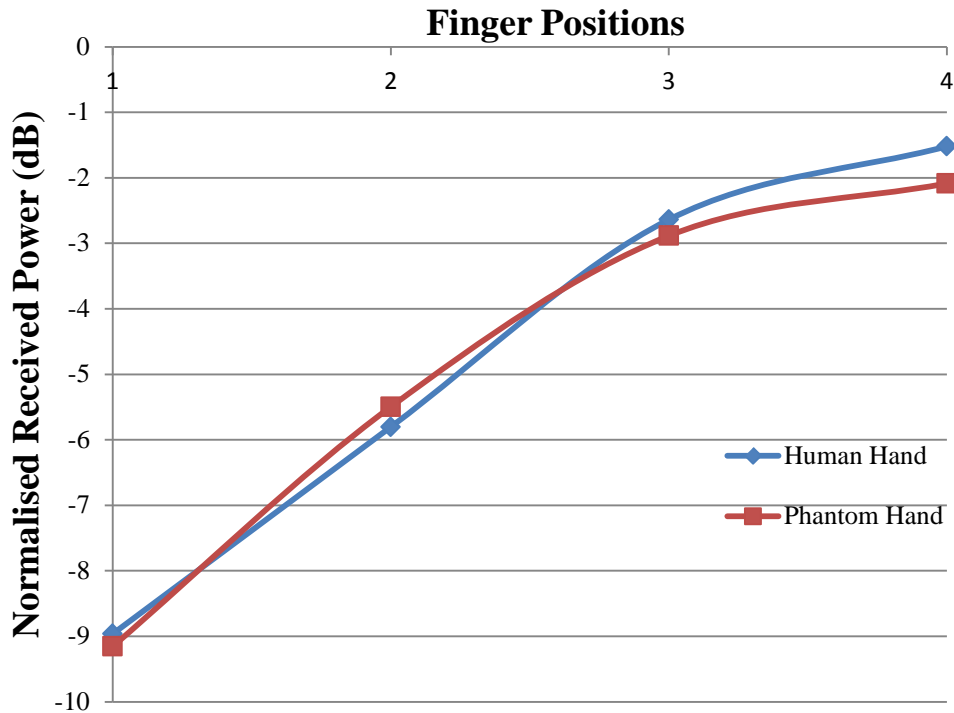
Graph 4-5: Change in received power from different finger position

The results of the measurements taken with the participant's hands included left and right hand with and without ring. The comparison of the average received power from both hands under the two conditions is shown in the graph 4-6. The two hands showed negligible difference on received power with and without the ring. When the ring was placed on the ring finger, and the hand was gripping the phone, the proximity of the ring to the antenna was greater than approximately 6cm. With this separation distance, the ring does not seem to have any noticeable effect on the radiation characteristics of the antenna. The proximity of the index finger has a much greater influence.

Since the mobile phone antenna is not symmetrical, one can expect it to behave differently depending on whether it is held in the left or right hand. In this experiment,

for both left and right hand, the index finger always touched the back of the phone in the same four locations (positions 1 to 4). Even though the other fingers and palm were in mirrored locations (for the left and right hands), their impact on the received power was negligible compared to the location of the index finger tip. One could expect a different result if the index finger position was offset to one side of the phone.
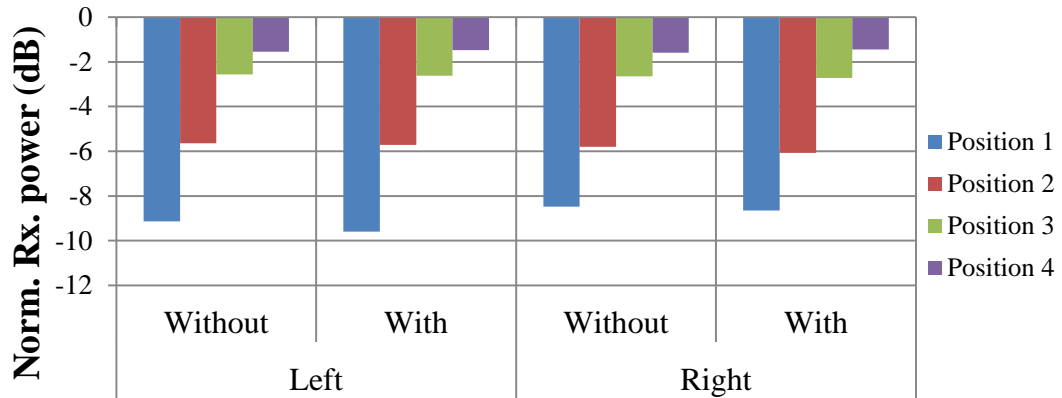
Graph 4-6: Average received power for 4 finger positions

The normalised received power for each participant is plotted against that participant's index finger length. This is done for both left and right hands, and the four index finger positions (1 to 4). Graph 4-7 shows the lines of best fit for each of the four index finger positions. In finger positions 1, 2 and 3, there is a marked decrease in the received power as the finger length increases. In general, longer finger lengths are associated with bigger hands. As a result, one can expect the footprint of the index finger on the back of the phone to be larger for longer fingers. This would cause a larger disturbance in the antenna's near-field, thus leading to a reduction in the received power. At position 4, the index finger is clear of the antenna and so has less of an effect on its radiation characteristics. Furthermore, for a larger hand, when the index finger is in position 4, the palm is completely off the phone so the size of it becomes inconsequential.
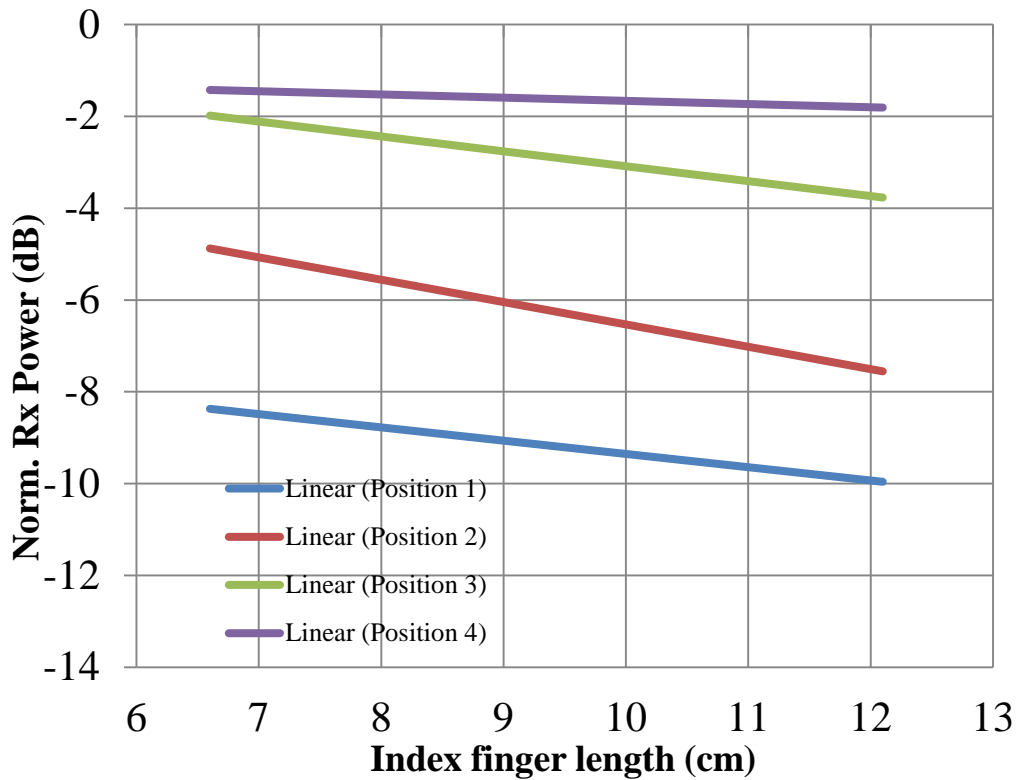
Graph 4-7: Trend of received power for different index finger lengths

4.5   Conclusion

This study has looked at how the user's hand holding a mobile phone affects the power transmitted from it. There is a significant reduction in the power received at the spectrum analyser when the user's finger is placed directly over the phone antenna. This is to be expected and is consistent with the findings of the reviewed papers. It should be kept in mind that a drop in the received power at the spectrum analyser does not necessarily mean a reduction in the transmitted power. This can only be established by monitoring the power fed to the antenna or by measuring the full 3D far-field radiation pattern. The latter was not possible on health and safety grounds as well as the time constraints of the participants. Nevertheless, following other simulation based studies elsewhere, it can be assumed that there will be significant drop in radiated power due to antenna mismatch and efficiency degradation. The normalised average received power was -9dB, which is a significant reduction; in some cases, the received power dropped by approximately 15dB.

The study also looked at whether the choice of left or right hand gripping the mobile phone has any effect on the received power at the spectrum analyser. In this instant, there was negligible difference. For antennas and index finger locations that are significantly non-symmetric about the centre of the phone, one can expect the antenna behaviour to vary. This is based on the observation of what happens when the index finger covers, or even partly covers the antenna element.

Another aspect investigated was the effect a ring worn on the index finger has on the received power at the spectrum analyser. No noticeable effect was observed. It can be surmised that metallic finger rings, when located away from the radiating element, has very little impact on the antenna performance. If the antenna is positioned at the bottom of the phone, a ring on the wedding ring finger would be very close to the radiating element and may have an influence on the antenna performance. With the increasing number of antennas required by modern phones, antenna placement at the bottom of the handset has become common place. This could be an avenue for investigation in the future.

Finally, this study also tried to verify the suitability of the CTIA hand phantom to represent human hands in OTA mobile phone measurements. Averaging results over 33 participants, the CTIA hand phantom provided a very close match. As highlighted by the significant deviations from the average value (as much as 15dB reductions in received power), the mobile phone antenna is very sensitive to the location of the index finger. For a majority of people who use the *index finger at the back of the phone* style grip, the index finger is most likely to be placed in broadly defined region at the top of the phone. This region extends from the middle to the edge of the phone where the bottom three fingers are located. This comes from the tendency of the user to press the speaker, which is located centrally on the reverse side of the phone into the ear using the index finger. However, for this particular CTIA hand model, the index finger will always be located in a central line of any small to medium width phone placed in it. Therefore, it is possible that for antenna designs that are heavily biased to one side of the mobile phone body, the CTIA hand phantom may significantly underestimate the level of detuning. This must be considered when carrying out OTA measurements.

Reference

[1]   Apple,   "http://www.apple.com/pr/library/2010/06/07Apple-Presents-iPhone-4.html,"   2010.   [Online].   Available: http://www.apple.com/pr/library/2010/06/07Apple-Presents-iPhone-4.html.

[2]   P. Makikyro, M. Nurkalla, H. Shapter, J. Torres, P. Wireless, B. Chan, and L. Magana, "Test Plan for Mobile Station Over the Air Performance," *CTIA Certification*, 2011.

[3]   J. Toftgard, S. N. Hornsleth, and J. B. Andersen, "Effects on portable antennas of the presence of a person," *IEEE Transactions on Antennas and Propagation*, vol. 41, no. 6, 1993.

[4]   M. Jensen and Y. Rahmat-Samii, "EM interaction of handset antennas and a human in personal communications," *Proceedings of the IEEE*, vol. 83, no. 9406485, 1995.

[5]   Q. Guo, R. Mittra, F. Lei, and Z. Li, "Interaction between internal antenna and external antenna of mobile phone and hand effect," *IEEE Transactions on Antennas and Propagation*, vol. 61, no. 2, pp. 862–870, 2013.

[6]   C. Li, E. Ofli, N. Chavannes, and N. Kuster, "The effects of hand phantom on mobile phone antenna OTA performance," in *European Conference on Antennas and Propagation*, 2007, no. c, pp. 1–5.

[7]   H. Suzanna and S. Hassan, "A comparative study on the effect of quasi-block hand model specific absorption rate measurement," *Loughborough Antenna & Propagation Conference*, no. November, pp. 1–4, 2011.

[8]   C. Li, M. Douglas, E. Ofli, B. Derat, and N. Kuster, "User's hand effect on the Specific Absorption Rate in the head," *2011 IEEE International Symposium on Antennas and Propagation (APSURSI)*, pp. 141–144, Jul. 2011.

[9]   E. Ofli, N. Chavannes, and N. Kuster, "Effects of Hand Phantom on Mobile Phone Antenna Performance," *IEEE Transactions on Antennas and Propagation*, vol. 57, no. 9, pp. 2763–2770, Sep. 2009.

[10]   M. Berg, M. Sonkki, and E. Salonen, "Experimental study of hand and head effects to mobile phone antenna radiation properties," *Antennas and Propagation, …*, vol. 1, pp. 437–440, 2009.

[11]   IndexSAR, "https://http://www.indexsar.com/." .

[12]   C. Li, E. Ofli, N. Chavannes, and N. Kuster, "SAR and efficiency performance of mobile phone antenna with different user hand positions," *IEEE Antennas and Propagation Society International Symposium*, pp. 412–415, 2009.

[13] C. Li, E. Ofli, N. Chavannes, E. Cherubini, H. U. Gerber, and N. Kuster, "Effects of hand phantom and different use patterns on mobile phone antenna radiation performance," *2008 IEEE Antennas and Propagation Society International Symposium*, pp. 3659–3662, 2008.

[14] M. Pelosi, O. Franek, M. B. Knudsen, and G. F. Pedersen, "User's Proximity Effects in Mobile Phones," in *European Conference on Antennas and Propagation*, 2009, pp. 1022–1024.

[15] M. Pelosi, O. Franek, G. F. Pedersen, and M. Knudsen, "User's Impact on PIFA Antennas in Mobile Phones," *VTC Spring 2009 - IEEE 69th Vehicular Technology Conference*, pp. 1–5, Apr. 2009.

[16] M. Pelosi, O. Franek, M. B. Knudsen, G. F. Pedersen, and J. B. Andersen, "Antenna Proximity Effects for Talk and Data Modes in Mobile Phones," *IEEE Antennas and Propagation Magazine*, vol. 52, no. 3, pp. 15–27, Jun. 2010.

[17] G. F. Pedersen, M. Tartiere, and M. B. Knudsen, "Radiation efficiency of handheld phones," *Vehicular Technology Conference Proceedings IEEE*, vol. 2, pp. 1381–1385, 2000.

[18] J. Ilvonen and O. Kivekas, "Mobile terminal antenna performance with the user's hand: Effect of antenna dimensioning and location," *IEEE Antennas and Wireless Propagation Letters*, vol. 10, pp. 772–775, 2011.

[19] Y. Rahmat-samii and K. W. Kim, "Antennas and Human in Personal Communications: Application of Modern EM Computational Techniques," *12th International Conference on Microwaves and Radar. MIKON '98*, vol. 4, pp. 36–55, 1998.

[20] P. Ramachandran, Z. D. Milosavljevic, and C. Beckman, "Adaptive matching circuitry for compensation of finger effect on handset antennas," *European Conference on Antennas and Propagation*, pp. 801– 804, 2009.

[21] A. S. Omar, L. Young, M. Engineering, P. Bhartia, I. Bahl, A. House, P. Bharita, K. Jung, C. W. Jung, M. Park, Y. Chung, D. Kim, B. Kim, H. Wi, T. Kim, B. Lee, and S. National, "A COMPACT COUPLED RADIATOR ANTENNA WITH REDUCED HAND EFFECT FOR MOBILE HANDSET," *Microwave and Optical Technology Letters*, vol. 53, no. 9, pp. 1964–1967, 2011.

[22] R. Valkonen, S. Myllymaki, A. Huttunen, J. Holopainen, J. Ilvonen, P. Vainikainen, and H. Jantunen, "Compensation of finger effect on a mobile terminal antenna by antenna selection," *International Conference on Electromagnetics in Advanced Applications (ICEAA)*, pp. 364–367, 2010.

[23] E. Ofli, C. Li, N. Chavannes, and N. Kuster, "Analysis and optimization of mobile phone antenna radiation performance in the presence of head and hand phantoms," *Turk. J. Elec. Engin*, vol. 16, no. 1, pp. 67–77, 2008.

[24]   B. Z. Ying, "Antennas in Cellular Phones for Mobile Communications," *Proceedings of the IEEE*, vol. 100, no. 7, pp. 2286–2296, Jul. 2012.

[25]   P. Hui, "Positive hand effects on mobile handset antennas," *2008 Asia-Pacific Microwave Conference*, pp. 1–4, Dec. 2008.

[26]   R. Petersen, "ICES (SCC-39) Annual Report," *IEEE*, vol. 34, no. November, pp. 2011–2012, 2012.

[27]   Evonik, "Dielectric Properties ROHACELL ®," 2011.

[28]   SPEAG, *OTA Phantoms User Manual*. 2011.

5   Isolation of the On-body channel using Selection Combining at 2.4 GHz

5.1   Introduction

This chapter examines a method for determining the importance of the on-body channel [1] in short range wireless communications at 2.4GHz. The method examines selection combining [2] for experiments with and without a human but using duplicated geometries.

2.4GHz is an ISM band [3] that is used by many different types of services, for example Wi-Fi [4] and Bluetooth [5]. Both 802.11 and Bluetooth have been discussed extensively as candidates for body area networks (BANs) and it is therefore a reasonable choice of frequency.

In these experiments a human was used rather than the phantoms discussed in chapter 3, Section 3.6 in relation to the hands free kit. Phantoms have a drawback in that they do not have a fat-layer and a skin-layer [6]. On-body antennas need to be stable regardless of the thickness of the fat/skin layer and therefore a human volunteer was advantageous.

A particular goal of on-body antennas is that they should be omnidirectional [7]. However, because the body absorbs a great deal of the energy radiated by any antenna close to it, in essence blocking part of the far-field pattern omnidirectionality is generally impossible. A possible solution therefore is to have more than one antenna located on different spots on the body and achieve a better antenna by superposition. This has the advantage of allowing some form of space diversity [8]. Two or more antennas can then be combined to improve the characteristics of the channel.

5.2 Body centric measurement

Advances in technology have made it possible to have wearable hardware for communication and sensing incorporated in the personal area network (PAN) and body area network (BAN). Body centric communication systems play a very important role in the fourth generation communication system (4G) [7] . To support antenna and propagation research on wireless personal area networks, the IEEE 802.15 standardization group was established [9]. Applications have been applied to athletes, paramedics, fire-fighters and military personnel. This can be seen as a trend triggered by innovation in mobile phones [7].

Extensive research has been done in body centric communications [7], [9–15]. It was concluded in [7] that the monopole is the best for on-body propagation in comparison to top loaded monopole and PIFA antenna. Also in [7] , it was suggested that antennas that direct their radiation along the body surface with appropriate polarisation are needed for on-body links. It was further explained that this is a generalized view. Specifying the radiation pattern requirement for a system is difficult. For maximum path gain, links between antennas on-body should have monopolar like pattern with polarisation oriented normal to the body surface.

In carrying out on-body measurements, various approaches have been followed. Some researchers opt for simulation packages combined with mathematically modelled phantoms [16–18] while some have used real phantoms filled with tissue simulating liquid to represent various parts of the body [19–22]. Several experiments have also been seen using volunteers for the on-body measurement [11], [23], [24]. All these methods have helped understand and improve technology development for body area network. In [25–27], antennas were worn on volunteers for experiments on fading interactions with various environments. In [28], a simulator was used for the on-body measurement with various movements. This gives the opportunity to perform the experiment while changing different variables to suit the environment expected for the experiment. In [29], a phantom was used to check the performance of antennas in a multipath environment. The experiment was done in a reverberation chamber for repeatability. The employment of a phantom reduces variation in results attributed to movement of the body. In [21], a study was done to determine the effects of antenna

proximity to the body. This was done using rectangular and cylindrical phantoms to represent the human torso and compared with results obtained using volunteers. The experiment showed that a cylindrical phantom can be used to represent the human torso in a situation where repeatability in experiment is important.

Embedding of technology on and in the body is a growing trend in the field of mobile communications [30]. The human body introduces undesirable effect to the antenna in the near field. This is important in terms of safety and electronic performance.

On body radio propagation has helped improve telemedicine. Patients can be monitored without coming in contact with a doctor. Telemedicine system can be categorised in two systems, the system on the body surface and the one internal with implants in the body [12]. In [31], work was done on an infant telemeter. It was concluded a loop antenna in best for communication in an on-body system. The different body centric applications combined with global positioning system (GPS), navigation system, cellular, Bluetooth and UWB has made it possible to achieve the low power signal budget using body centric antennas [32].

5.3   Multiple Input Multiple Output (MIMO)

Buildings and trees affect the line of sight of communication thereby causing path loss, reflection, scattering and fading. The signals tend to be scattered by the environment so that when they reach the receiver there are multiple versions of the same signal each with slightly different phase and amplitude. Phase differences cause smearing of the signal. MIMO antenna systems provide a partial solution to this problem.

MIMO is a radio system where there may be multiple antennas at both the transmitting and receiving sides. The signals can be combined to form a stronger signal or compared with a sample of the original signal sent. In the case where the signal is compared, the signal with the highest correlation with the sample of the original signal is selected to be received. These sent signals are orthogonal to each other to avoid interference.

MIMO systems can be seen as an expansion to smart antennas [33]. Smart antennas are antennas that use antenna arrays and programming technology to improve antenna

capability. MIMO systems which are sometimes referred to as *volume to volume systems* [33] and have emerged as one of the most important technological advances in wireless communication. It has given opportunity for increasing data rate and reducing bit error rate (BER) and inter-symbol interference (ISI) in communication. MIMO technology has been used in commercial wireless and network products such as broadband wireless systems, wireless local area network and beyond.

There are three popular forms of Multiple Antenna systems. They are as follows:

5.3.1   Multiple Input Single Output (MISO)

A MISO system is made up of multiple antennas on the transmitter and an antenna on the receiver.
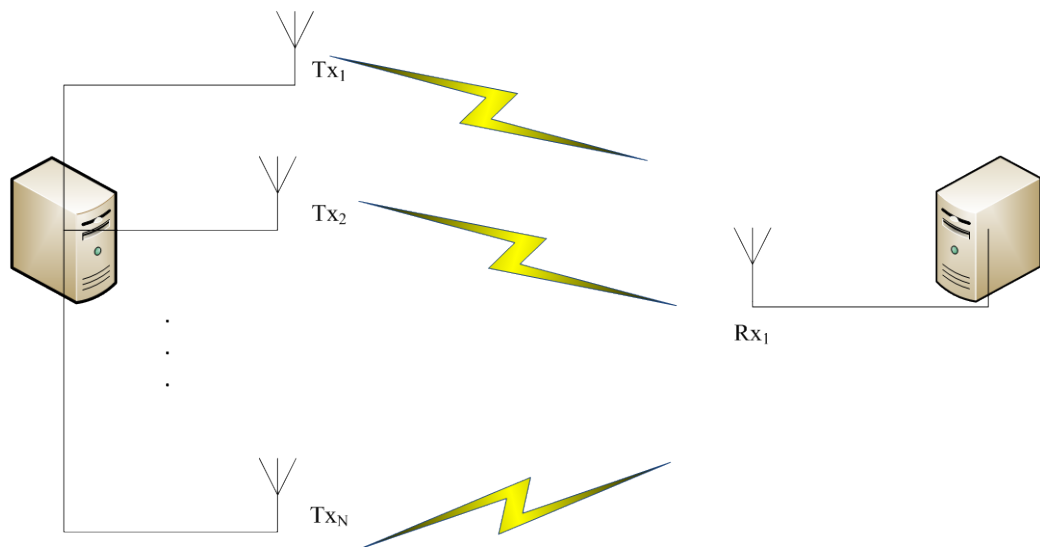
Figure 5-1: A Multiple Input Single Output (MISO) system.

5.3.2   Single Input Multiple Output (SIMO)

A SIMO system is made up of a single antenna on the transmitter and multiple antennas on the receiver.
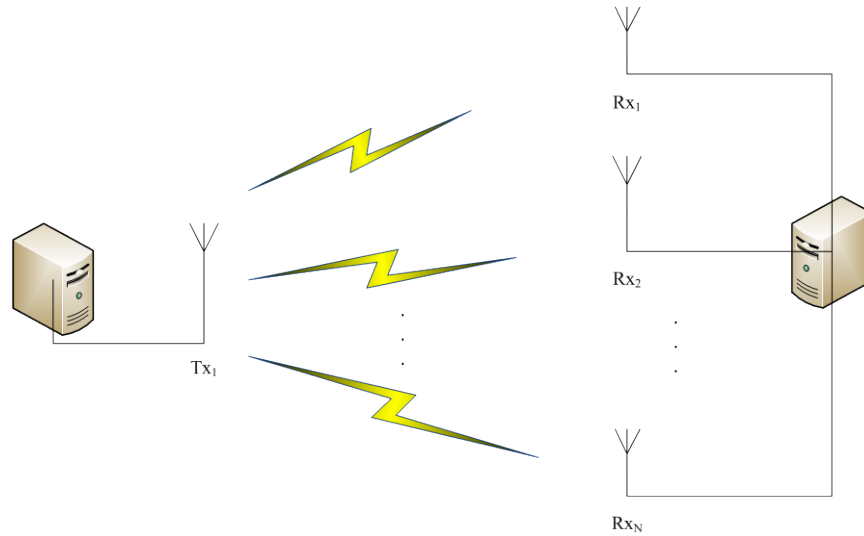
Figure 5-2: A Single Output Multiple Input (SIMO) system.

5.3.3   Multiple Input Multiple Output (MIMO)

A MIMO system is made up of multiple antennas on both the receiver and transmitter.
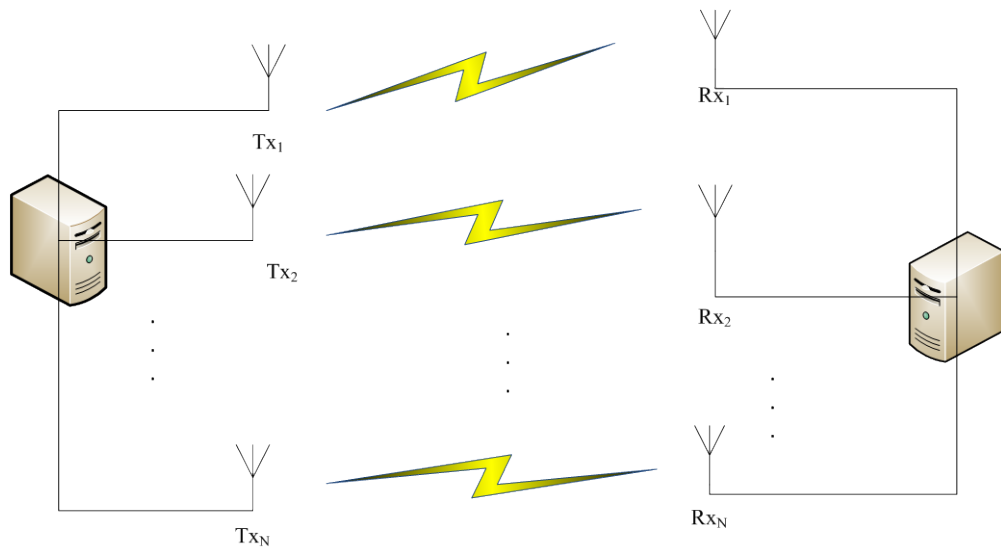
Figure 5-3: A Multiple Input Multiple Output System (MIMO) system.

MIMO systems exploit the channel in two ways, using diversity and transmission of several parallel channels [34].

5.4   Multipath and On-body antennas

The wavefront from an omnidirectional antenna expands as the surface of a sphere with radius *r* where *r* is the distance between the antenna and the point at which the wavefront is measured. Although omnidirectional antennas are difficult to realise the general behaviour of an RF signal is that it expands (grows wider) as the range increases. In the channel, each part of the wavefront will encounter objects that reflect, refract, diffract and interact with the signal. The single wavefront from a transmitting antenna therefore becomes many duplicated wavefronts each having the same content but each with its own attenuation and phase characteristics. At the receiver these separate wavefronts combine and interfere both constructively and deconstructively. The phenomena is called multipath and the result at the receiver is called multipath interference [35] or multipath fading.

Typically delay spread is a characteristic used to determine the amount of multipath present. Delay spread can be described as the time between the arrival of the strongest signal and the last reflected signal. Typical values for delay spread are < 50ns for homes, ~100ns in offices, ~200 – 300ns for manufacturing floors [36]. In multipath we sometimes see signal nulling. This occurs when the reflected waves occur exactly out of phase with the main signal and thus null it out completely [36]. The problem can be partially overcome using more than one antenna with some form of diversity.

5.5   Overview of Diversity schemes

Diversity gain can be defined as the improvement in average signal-to-noise ratio (SNR) from a combination of signals from a diversity antenna system compared to the SNR from one antenna is the same system [37]. When signals are received, they experience a fluctuation in signal level. This variation experienced in signal level is called fading. Diversity is a way of combatting fading when sending and receiving signal in a wireless environment. Diversity schemes provide multiple inputs and aim for uncorrelated fading

at the receiving antennas. The degree of non-correlation of the signal is important to combatting fading in the end result of the receiver. There are two types of fading: long-term and short-term fading. Long term fading is caused by obstruction from building and natural features [35]. It represents long term variation in received power level. It is determined by the local mean of a fast fading signal. Short term fading is as a result of constructive and destructive combination of multipath. It is referred to as a rapid change in the received signal in space, time and frequency.

To reduce long-term fading, macroscopic diversity is used and to reduce short-term fading, microscopic diversity is used [38]. For the purpose of this work, short-term fading is of interest and microscopic diversity was used to combat the effect of multipath at the receiver. In microscopic diversity, two or more antennas or multiple frequencies on the same antennas are required. There are six diversity schemes applicable with the multiple antenna or frequencies. These are space, frequency, polarisation, field component, angle and time [39]. All of these six seek to separate the antennas so that they each interact with a different part of the wavefront.

Space diversity then allows us to sample the wavefront at different points using separated antennas at differing positions on the body. In the experiments described later two receiving antennas were used. The next stage involved selecting one of two channels. The process of selection is called combining. Later experiments were carried out to gauge the effect of the on-body channel on combining.

For the purpose of this research space diversity is considered. Space diversity is the physical separation of the antennas by a distance to provide signals with low correlation in their fading and avoid coupling in the antennas. It is easy to implement and requires no frequency spectrum resources. This space diversity will be used along with the combining technique called selective combining.

There are four combining schemes that can be used with the listed diversity schemes. These are selective combining, switched combining, maximal ratio combining and equal gain combining [39].

In [7], [40] and [41], diversity was investigated. The transmitter was connected to the belt and the receiver to the chest, back, wrist, head and ankle position. In [7], selection combining (SC), equal gain combining (EGC) and maximal ratio combining (MRC)

were tested with the transmitter on the belt and the receiver on the head and ankle. It was discovered that the best diversity technique was when the transmitter was on the belt and the receiver was on the head using the MRC. This was achieved using a monopole antenna. In [40], diversity gain was measured using monopoles, printed inverted F antenna and planar inverted F antenna. The MRC proved to be the best combining technique. The printed-IFA gave better results hence concluding that the orientation of the antenna is important in diversity gain. In [41], diversity measurement was carried out on body. Space diversity and pattern diversity was investigated on the body. With the space diversity, SC, EGC and MRC were applied. The result concluded as given in [7] that the MRC is a better diversity combining scheme with on-body propagation. In the pattern diversity in [41], an annular slot monopole antenna was used. The radiation pattern pointed away from the body surface. The MRC gave the better diversity combining technique. However, the diversity gain was lower compared with the space diversity technique. Again from [7], [40] and [41], it can be concluded that diversity reduces fading and useful gain can be achieved by using small antenna pairs with small spacing.

In [40] and [41], multipath was taken into consideration. In [40], the diversity measurement was done in the chamber, lab and office. The office gave the best diversity gain result. This is due to the rich multipath presence. In [41], the diversity gain was higher in the laboratory than the anechoic chamber and office. [41] used printed IFA with pattern diversity while [40] used monopole with spatial diversity. In [29], the performance of on-body antenna was tested in a repeatable multipath environment. The path gain was measured using the $|S_{21}|$ data between the two antennas connected to a phantom. This was done using two sets of five different antennas. It was concluded that efficient communication over the body surface is possible if the antenna radiates tangential to the tissue surface regardless of the environment.

5.6   Selection combining (SC)

SC is a simple diversity technique. In this technique, the strongest signal from the diversity branch is selected at the receiver. The more branches the higher the probability

of a better signal at the receiver. In this work, a two-branch diversity system will be considered. The selection combining for a two-branch system can be described mathematically by:

$$s_k = \begin{cases} s_{1k}, & if \ |s_{1k}| > |s_{2k}| \\ s_{2k,} & if \ |s_{2k}| > |s_{1k}| \end{cases}$$

5.1

Where, s_{1k} and s_{2k} are decision variables at the first and second diversity path and s_k is the decision variable at the output of the receiver.

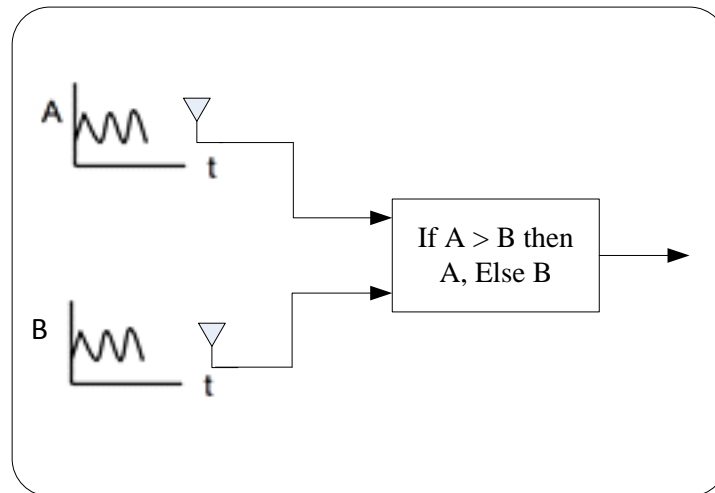SC is shown in the figure 5-4 for a two-branch diversity receiver.

Figure 5-4: Selection Combining for a 2-branch diversity system

5.6.1 Background work on selection combining

Selection combining is commonly used in receivers because it is economical to implement [42], [43]. The effect of noise on the switching rate between two branches was considered in [44]. This was studied in a noisy environment using Rayleigh and Rician fading. The switching rate between a noisy and noise free environment was compared. It was concluded that the switching rate is greater in a noisy environment than a noise-free environment. SC effect was compared in different modulation schemes in [45]. In [45], selection combining is chosen over other diversity techniques because of its simplicity, easy implementation and reduced power consumption in the receiver. A performance analysis of SC in an indoor mobile communication environment was

performed in [46]. The SNR and system reliability were considered. It was concluded the SNR improved as the number of diversity branch is increased. SNR was also improved with only one extra path. This also applies to the reliability of the system in an indoor environment. In [47], the theoretical and measured SC for four dipole antenna with 2λ spacing between them was computed. The cumulative distribution function of the theoretical and measured SC had a 1dB difference. It showed the predictability of the SC by theory. SC in the experiment would therefore be predicted and compared with results for validation purposes.

The simplicity in SC has made it possible to combine it with other diversity techniques to achieve better signal. In [48], [49], the SC was combined with maximal ratio combining to improve received signal. This system was called a hybrid selection/maximal ratio combining system. The SC was achieved by having a multiple antennas on each branch. When the SC is carried out on each branch the next stage was to perform MRC on the result from the branches. It was concluded that the system provided improved performance without requiring additional electronics and power compared with the combination of the SC and MRC is referred to as generalized selection combining (GSC) [2], [50–54]. With GSC, the signal to noise ratio was calculated in [52] this was later modified for non-identical Rayleigh fading statistics in [53]. In [55], the SC was combined with MRC for arrays of antennas working in the millimetre wave band for an indoor wireless channel. The system takes the advantage of arranging multiple antennas on a small surface. Combination of selection combining with channel models is being investigated. In [56], SC is analysed in a Nakagami-m fading channel. It was also investigated in [57] using a Rayleigh fading channel. [58] investigated it over a Weibull fading channel.

In an on-body system, there is complexity in the antenna-body interaction [59]. These effects include near-field coupling, radiation pattern fragmentation, and a shift in antenna impedance which will overall affect the efficiency and reliability of the system [60]. In [59], communication between on-body antennas and off-body antennas was investigated using various diversity technique in an indoor environment at 868MHz while the body was in motion. The cross-correlation between signals received on different branches on the body was measurement to be less than 0.6. In [8] and [58], measurement and simulation of on-body antenna with various diversity techniques was

carried out at 868MHz. The cross-correlation between branched was less than 0.7 and the diversity gain increased as the experiment moved from the anechoic to a multipath environment.

The use of diversity schemes with wearable antenna is tested in [62] using selection combining (SC) and maximal ratio combining (MRC). Multiple wearable textile antennas are integrated on the garment of a firefighter. The antennas were positioned in front and the back of the jacket. The test was carried indoors. The firefighter walked around in a room where there was line of sight and no line of sight with the transmitter. The work showed that diversity scheme gives an advantage of improving performance of on-body antenna system.

SC is chosen for this work based on its simplicity. The results will be used to further establish coupling effects with the human body during communication.

5.7   Monopole antenna on a circular ground plane

The antenna sets constructed for the on-body measurement consisted of two identical quarter-wavelength monopole antennas on an isolated circular ground plane. The circular ground plane minimised unwanted surface corner reflections due to less than infinite ground plane size. The monopole perpendicular to the surface of the body is known to produce surface waves that interact well with human tissue [63]. Isolation using a 50mm thick polystyrene disk lifted the antenna a repeatable distance off the skin. The antenna was built to resonate at 2.4GHz. The resonant wavelength is given by

$$\lambda = \frac{c}{f}$$

5.2

Where λ (m) is the wavelength, c is the speed of light $(3 \times 10^8 m/s)$ and f (Hz) is frequency. With the equation above, the wavelength of an antenna operating at 2.4GHz is ≈ 0.125m. For a quarter wavelength monopole antenna, the antenna length is ideally 31.25mm. The ground plane of the antenna is made circular. This helps avoid corner effects introduced by more typical rectangular shaped ground planes and makes the

antenna independent in azimuthal alignment with the body part to which is will be attached. After some initial simulations the ground plane is set at 100mm diameter. This is set to meet the requirement of the ground plane being a minimum of a quarter-wavelength [64] and also for convenience when mounting it on the body. The ground plane was built from a one sided copper FR4 substrate. Figures 5-5 and 5-6 show the dimension of the antenna.
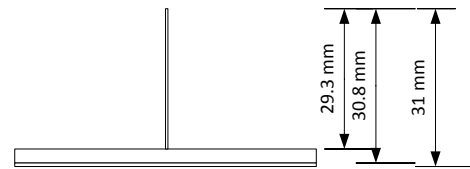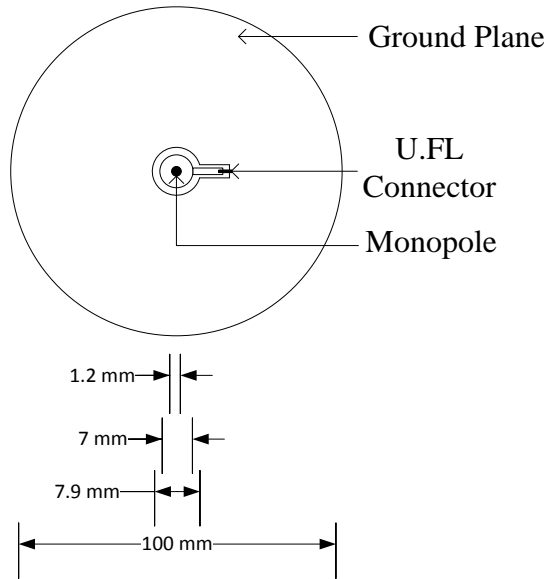

Figure 5-5: Top view of the monopole antenna   Figure 5-6: Side view of the monopole antenna

The antenna was simulated using the Empire XCcel EM simulation package [65]. In the simulation package, the antenna was initially built with the FR4 substrate and a monopole mounted in the centre with the feed from below the ground plane. The antenna was later modified with ROHACELL® 31 HF to cover the monopole and the source of the feed. This is referred to as solid air since ideally when clean it has little effect on the antenna characteristics. The property of the ROHACELL® 31 HF is given in the table 5-1.

Dielectric	Permittivity ε_r	Loss tangent δ
ROHACELL® 31 HF	1.05	< 0.0002 @ 2.5GHz

Table 5-1: Rohacell properties

This was also simulated to check for any changes in the antennas characteristics. After simulation with the ROHACELL® 31 HF, the antenna is simulated on the body. The

antenna is tuned to work at 2.4GHz when attached to the body. For the simulation on the body, the Brooks man was used to represent the human body. The Brooks man has the whole body details of a human being with all the organs well detailed for simulation purposes. Adjustments were made to the height of the monopole antenna to get the antenna resonating at 2.4GHz on the body. The ROHACELL provided protection and rigidity for the antennas which was important during measurement.

The $|S_{11}|$ of the simulated antenna with and without the ROHACELL® 31 HF is compared to check the effect of the ROHACELL® 31 HF on the antenna on and off the body. The result is presented in the graph shown in figure 5-7.
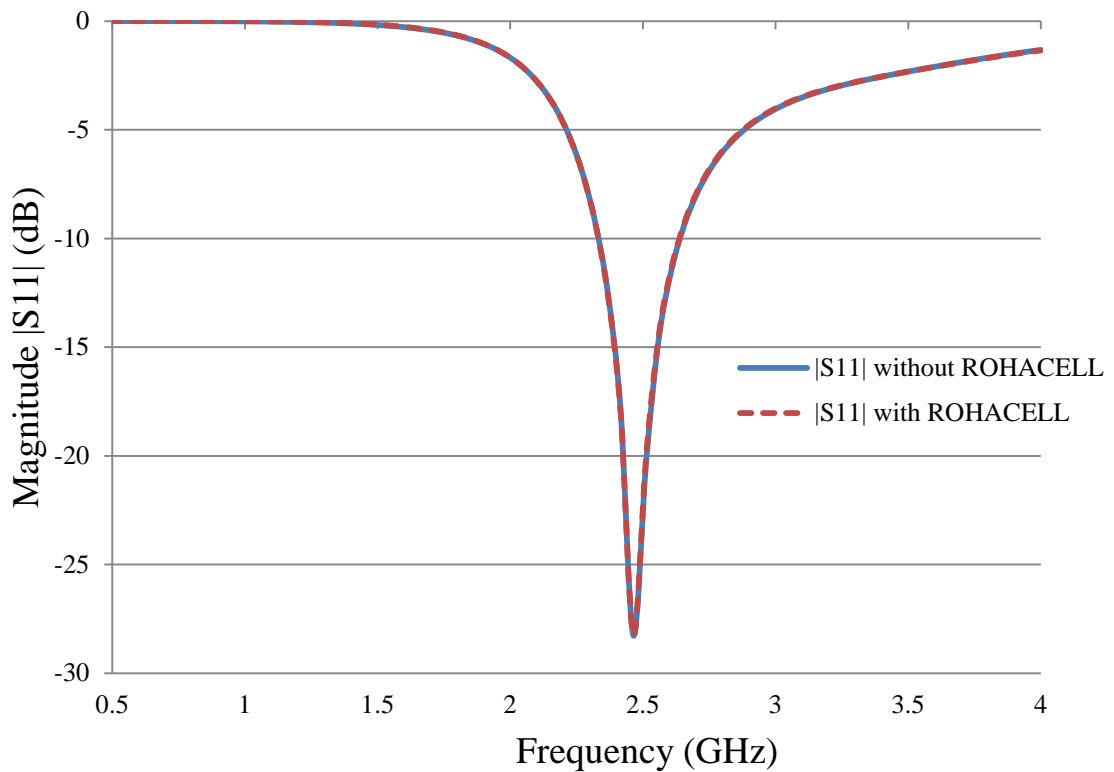

Figure 5-7: Simulated $|S_{11}|$ of a $\lambda/4$ antenna simulated with and without the rohacell radome.

The -3dB bandwidth for the antenna is 43%. The results from the result showed the antenna behaved alike with and without the rohacell. This showed the rohacell was useful to provide more rigidity for the antenna but did not change the results in any significant way.

The antenna was built in the Loughborough University Electronics workshop using the parts simulated in Empire XCcel. A U.FL-SMT PCB receptacle connector was used in

antenna. The choice of this connector was based on its size. The specifications of the connector are given in appendix I. The antenna is shown in the figure 5-8 and 5-9 without and with the rohacell respectively.

Body Side up   Body Side down

Figure 5-8: Monopole antenna without rohacell

Body Side up   Body Side down

Figure 5-9: Monopole antenna with rohacell

The built antenna was then measured in the communication division's small anechoic chamber. In the simulations carried out, it was established that the ROHACELL had insignificant effect on the antenna. For the purpose of this test in the anechoic chamber, the rohacell used to protect the connector on the ground plane was removed. The antenna efficiency and gain were checked. The $|S_{11}|$ and radiation pattern were measured in free space. The figure 5-10 and 5-11 below show the antenna mounted on

the support pole with the dimension of the support and the support pole above the positioner in the anechoic chamber.
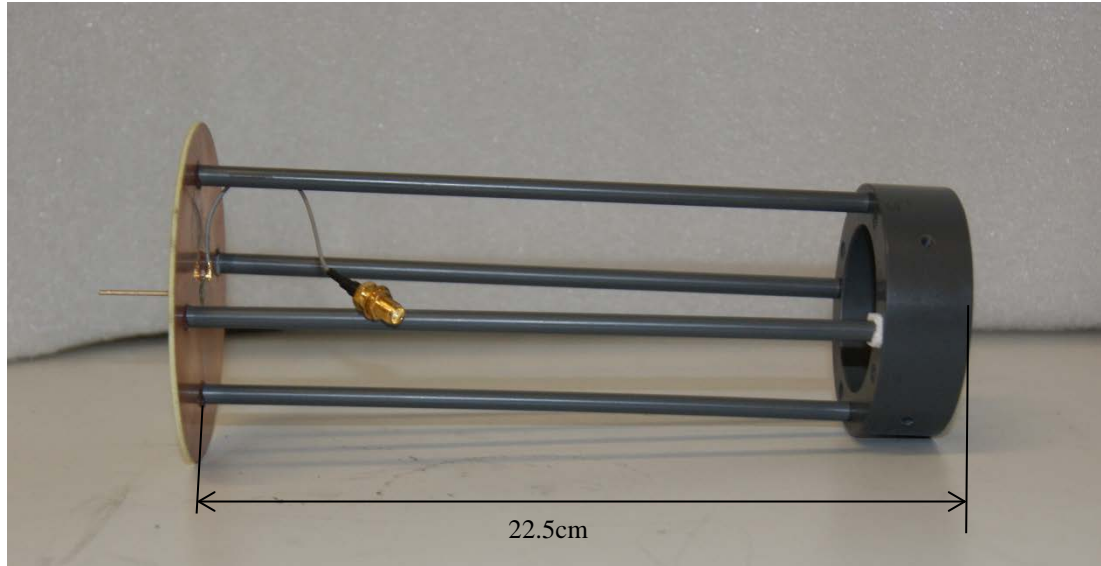

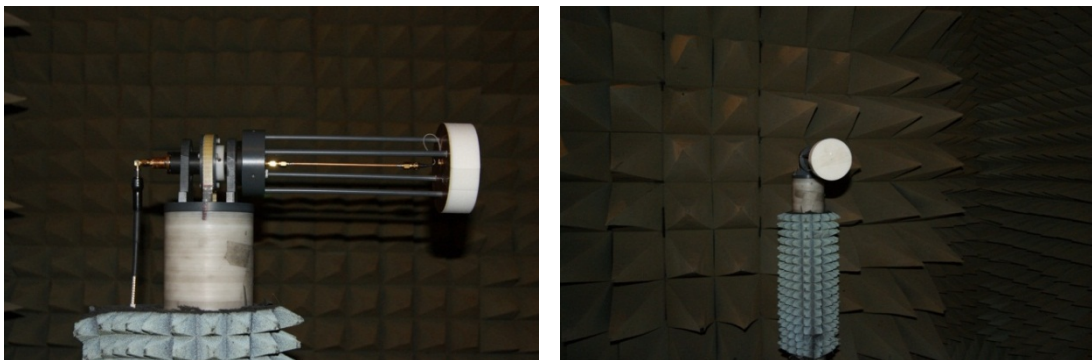Figure 5-10: Monopole antenna mounted on the support pole

Figure 5-11: Monopole antenna mounted on the support pole in the anechoic chamber

From the measurement taken in the chamber, the $|S_{11}|$ for the antenna at 2.4GHz was about -18dB. The efficiency of an antenna deals with the radiated power compared to power delivered to the antenna. In the chamber, the radiation efficiency and total efficiency of the antenna was checked. The radiation efficiency is the ratio of radiated power to the input power of the antenna while total efficiency account for the loss in the input terminal and within the antenna structure. The total efficiency of an antenna is less than the radiated efficiency of the same antenna. Efficiency is mostly expressed as a

percentage. The graph in figure 5-12 indicated the radiated and total efficiency of the monopole antenna within a frequency range.
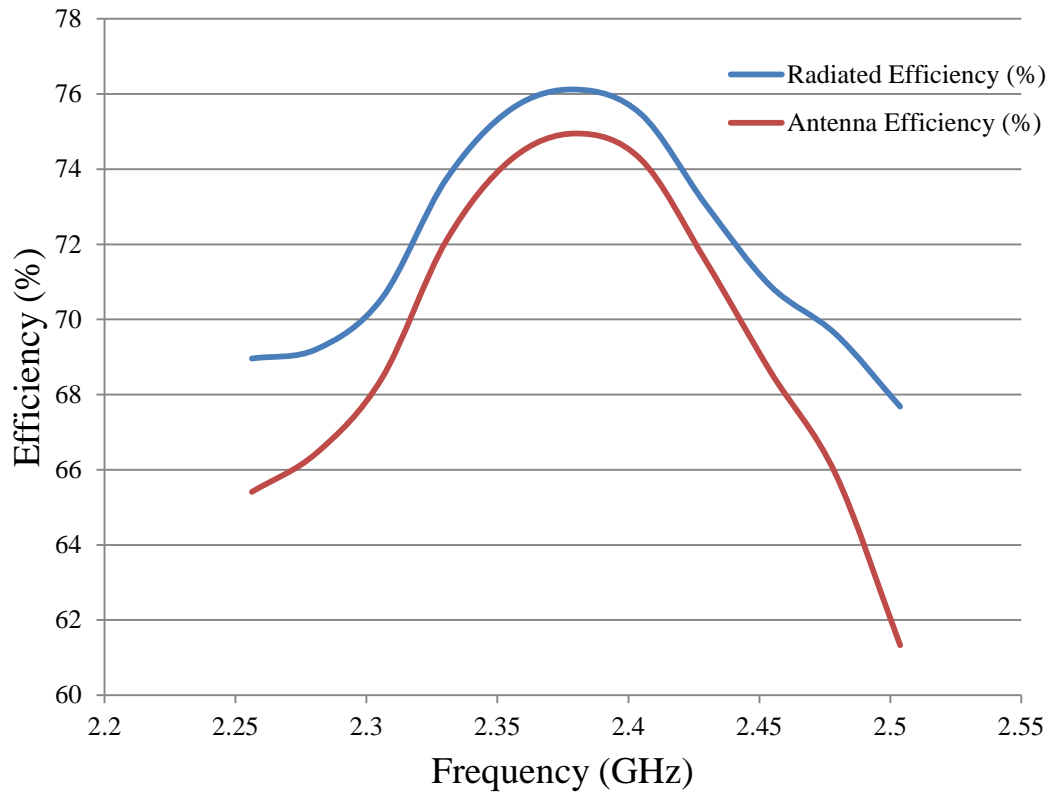

Figure 5-12: Results of the radiated and total efficiency for a $\lambda/4$ monopole without radome.

The $|S_{11}|$ of the antenna is measured with and without the rohacell (RH) protective layer. The built antenna has a higher $|S_{11}|$ than the simulated one. This can be due to material and connectors used to build the antenna. Figure 5-13 shows the $|S_{11}|$ for the simulated and built antenna with and without the RH protector.
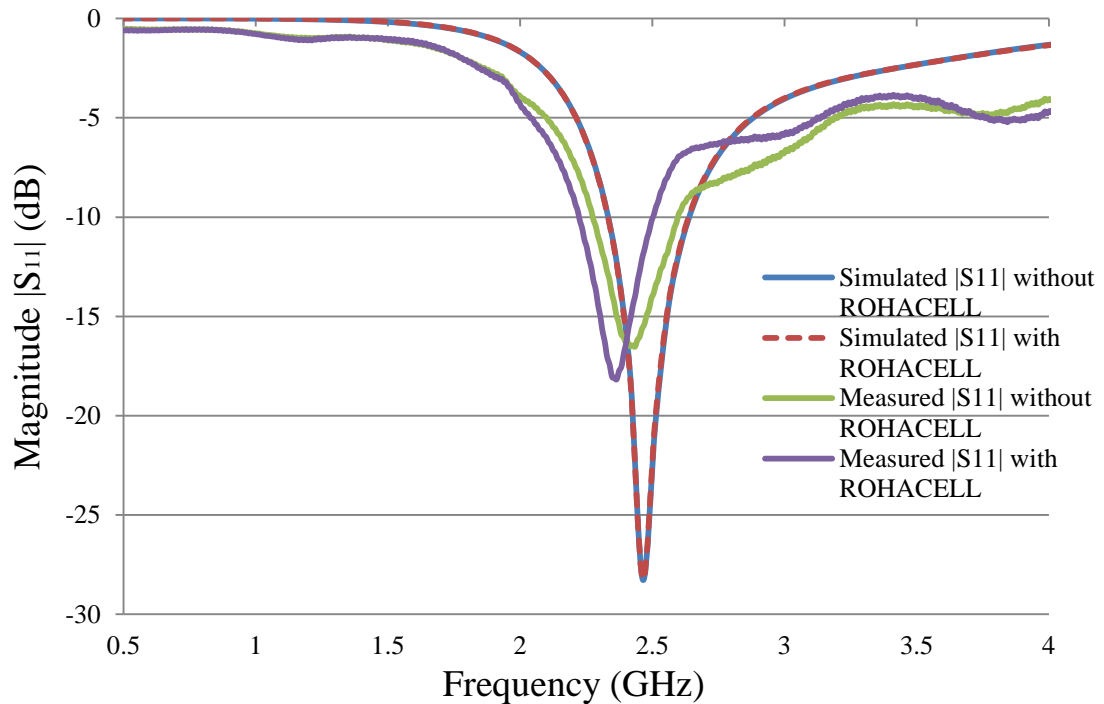
Figure 5-13: $|S_{11}|$ from simulation and built antenna with and without rohacell

The results for the measured monopole were similar but not the same as the simulations. It was seen that the antenna was more inductive than expected (longer) and therefore resonated at the lower frequency. Also it was seen that the Q of the antenna was poorer by approximately 10dB. These differences were thought to be caused mainly by cabling and soldered joints on the monopole that were not simulated. However a resonant point of -17dB and resonance close to 2.4GHz was reasonable and therefore the antenna was not tuned again. Efficiency for this experiment was not critical but measured results of 75% or more did validate that the antenna was radiating. The built antenna had a shift in frequency response to a lower frequency but with the 10dB bandwidth range, it still worked properly at 2.4GHz. An increase of around 10dB is noticed in the simulated and built antenna. The radiation pattern of the antenna with and without the rohacell protection was obtained in the anechoic chamber. This result is shown in the figure 5-14.
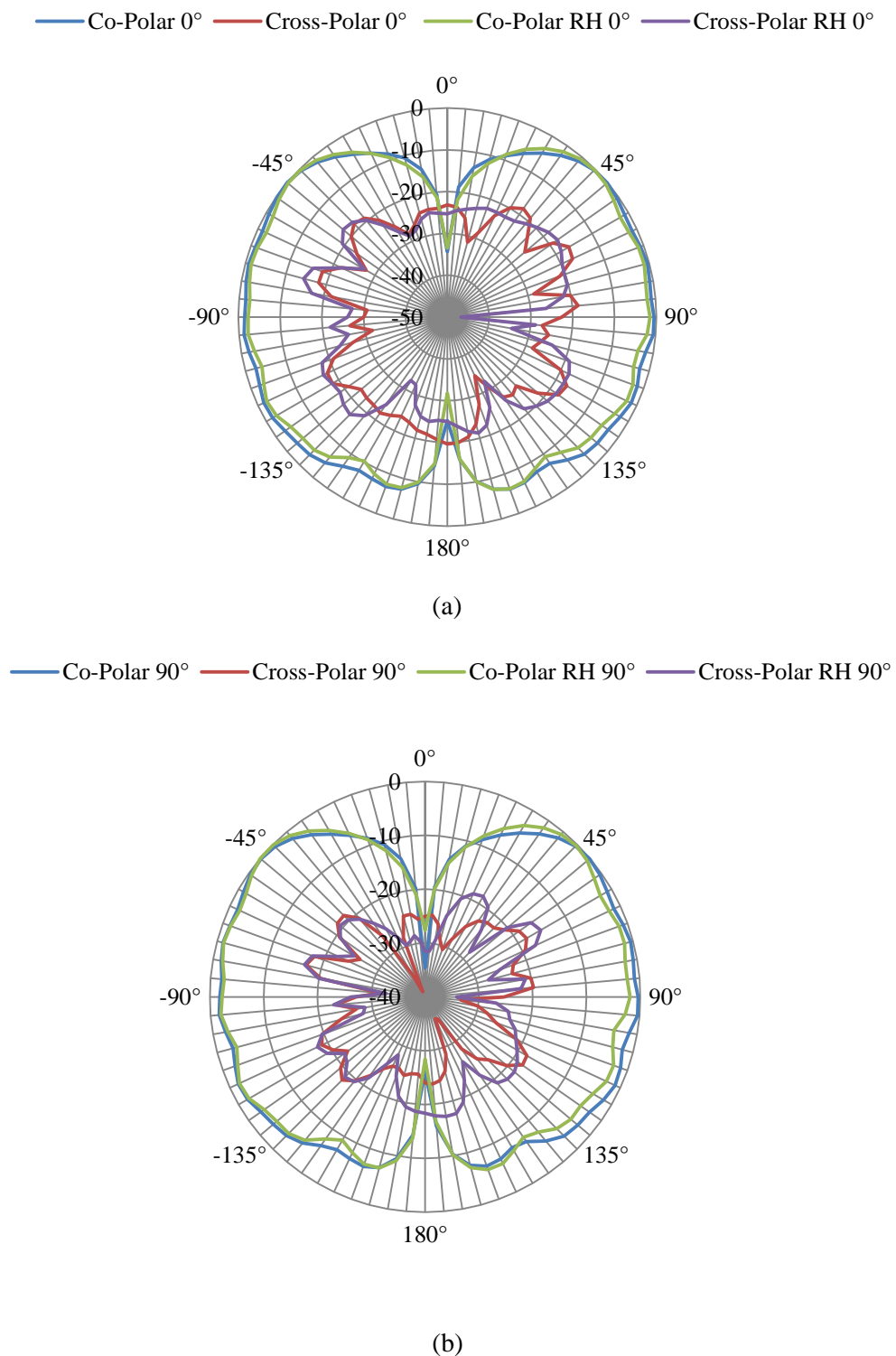
(a)

(b)

Figure 5-14: Measured radiation patterns of the monopole antenna with and without rohacell (RH)

The radiation pattern in the figure 5-14 is for the co-polar and cross-polar plane at 0° and 90° for measurement in the anechoic chamber. The results show the rohacell has minimal effect on the antenna's normal working state.

5.8 Support Rig for On-body/Off-body Combining two channel SIMO system

For the measurement to be repeatable in the same position in the on/off-body position, a non-metallic support rig was built for the antenna. The rig supports the antenna in the shoulder and waist region. The rig was constructed from wood and nylatron material. The rig is shown in the figure 5-15. In subsequent work, the rig will be seen supporting the antennas in different positions relative to the body.
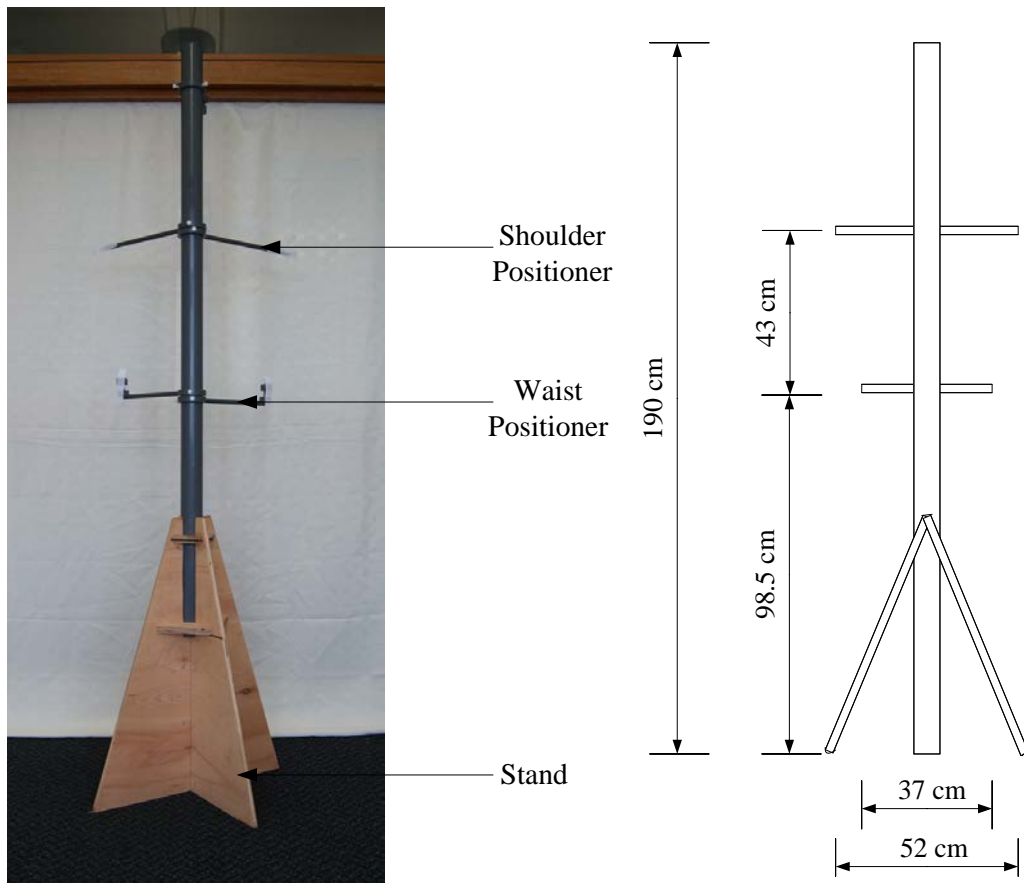
Figure 5-15: Support rig for the antennas.

5.9   Experimental setup

The communication system in this experiment is a multiple antenna system. The system is built with one transmitting antenna and two receiving antennas.

For the experiment, three different environments were used. The communications laboratory, the corridor and the centre for mobile communications research (CMCR) office. For the purpose of identification, the measurement in the communications laboratory is labelled MIL, measurement on the corridor is labelled MOC and the measurement in the CMCR office is labelled MIO. The transmitting antenna was a horn antenna. Two of the designed monopole antennas were used for the receiver. The geometry of each environment is shown in the figures 5-16, 5-17 and 5-18.
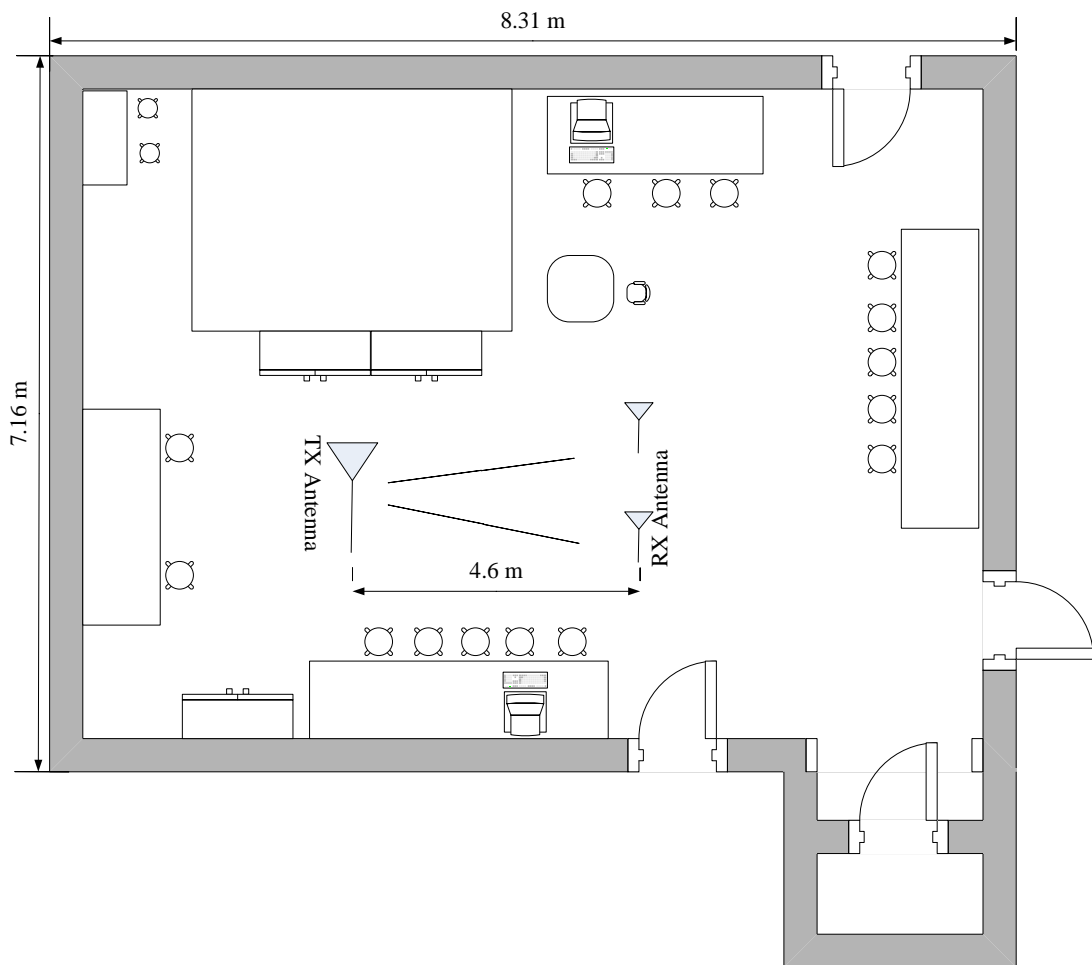

Figure 5-16: Layout of the CMCR laboratory with the antenna positioning (MIL).
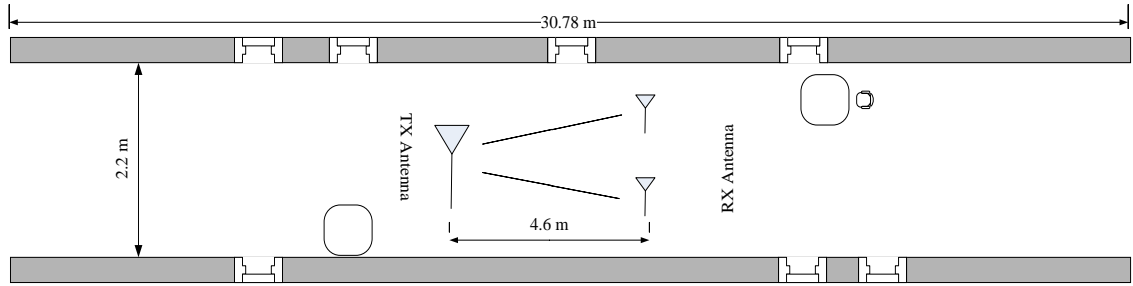
Figure 5-17: Layout of the corridor with the antenna positions for the experiment (MOC).
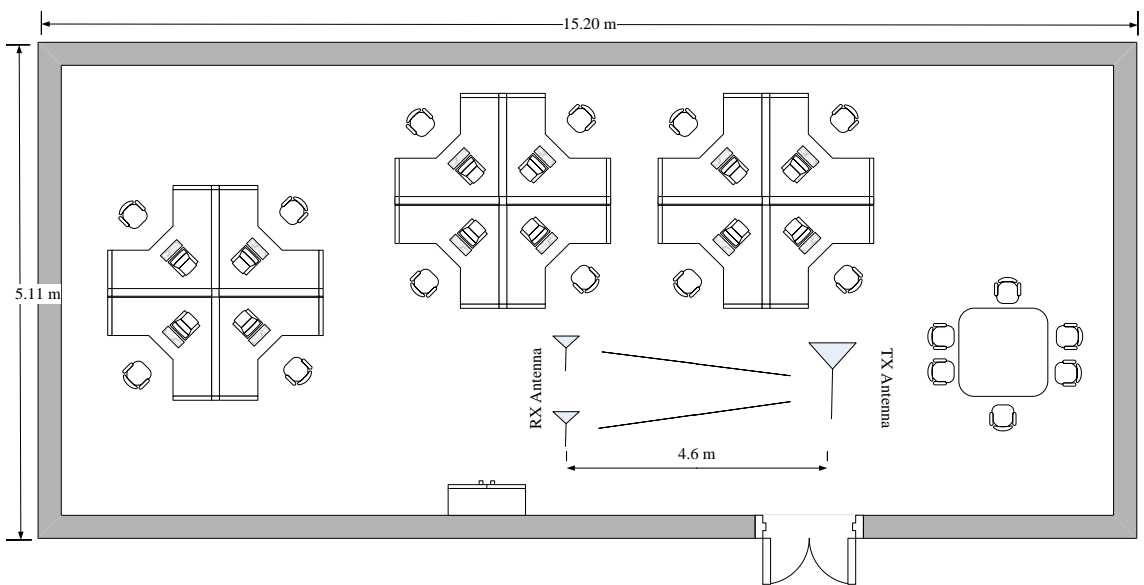

Figure 5-18: Layout of the CMCR research office and the antenna positions for the experiment (MIO).

The receiving antennas were mounted on the rig with a combination of positions between the shoulder and the waist. In total, a combination of six positions were obtained for the experiment. The six positions are left shoulder and right shoulder, left shoulder and right waist, left shoulder and left waist, right shoulder and right waist, right shoulder and left waist and left waist and right waist. The distance between each point on the body is shown in Figure 5-19 below.
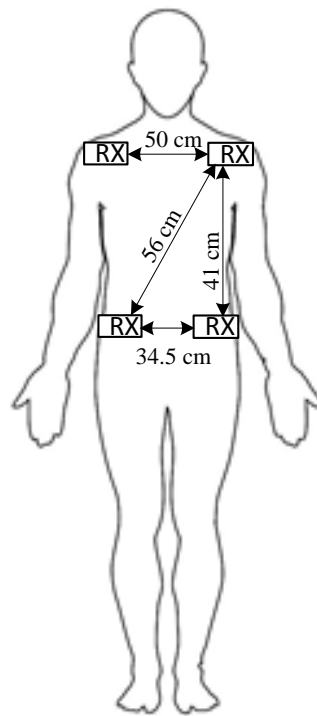
Figure 5-19: The human body with the distance between the antennas in all alignment.

Figure 5-20 and 5-21 shows the alignment listed above. The support rig was used to achieve same position when the antennas were measured in the on and off body mode.
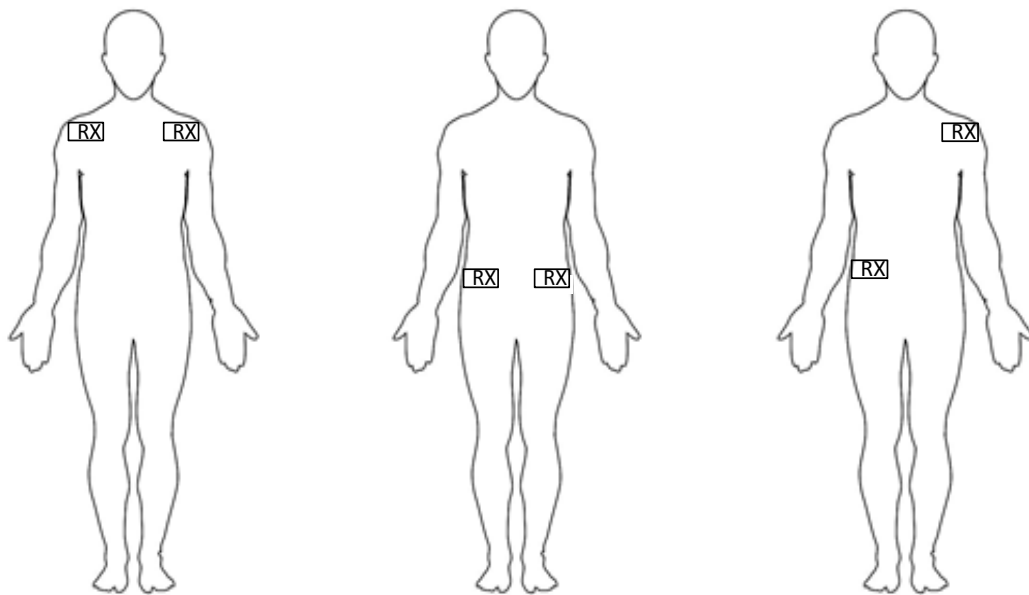

Figure 5-20: Antenna alignment for the on/off-body the experiments to be carried out in the different environments.
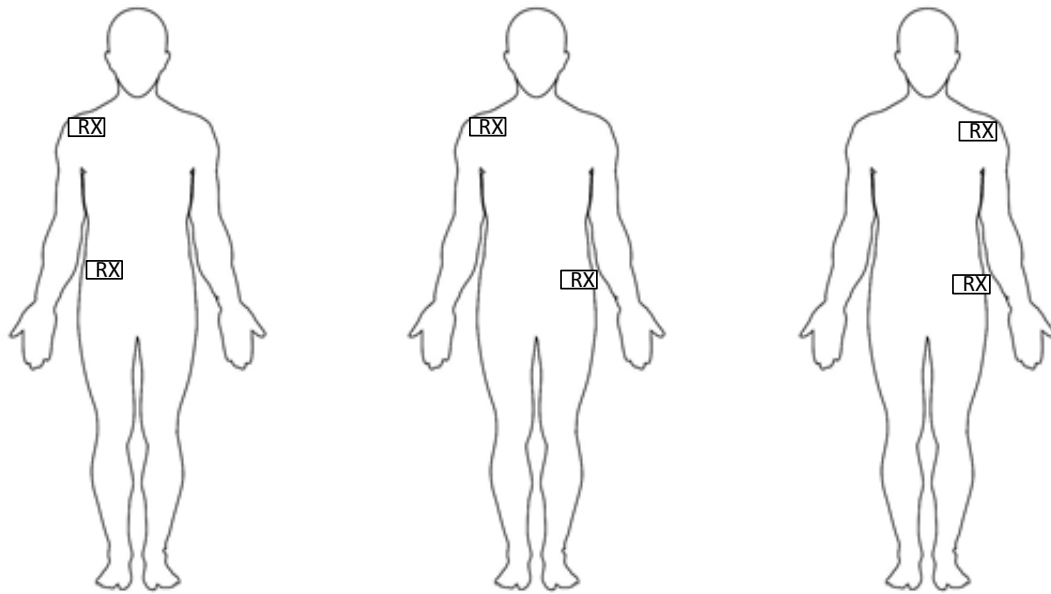
Figure 5-21: Antenna alignment for the on/off-body the experiments to be carried out in the different environments.

The experiment was carried out at 2.4GHz. An HP 8350 signal generator was used to transmit power to the antenna. Due to the power limitation of the signal generator, a power of 10.5dBm was transmitted. The received power in the antennas was measured using a LeCroy SDA 18000. The serial data analyser (SDA) is set to measure the received power in the two monopole antennas attached to its channel 1 and channel 2 simultaneously. The antennas are connected to the LeCroy SDA 18000 using 3m long RG316 cables. The cable specification can be found in the appendix. Channels 1 and 2 are set to respond to a maximum frequency of 6GHz. The sampling rate is set as 500kS/s. To select the narrowband of the signal, the transmitted power was measured with the receiving antenna attached to the Advantest R3182 spectrum analyser. The narrowband was set at 134kHz based on the signal strength**.** A picture showing the antenna connected in the left waist and right waist alignment in the on-body measurement is shown in the figure 5-22 along with an off-body alignment of the antennas on the support rig. In figure 5-22, RG316 cables can be seen connecting the antennas to the LeCroy SDA 18000.
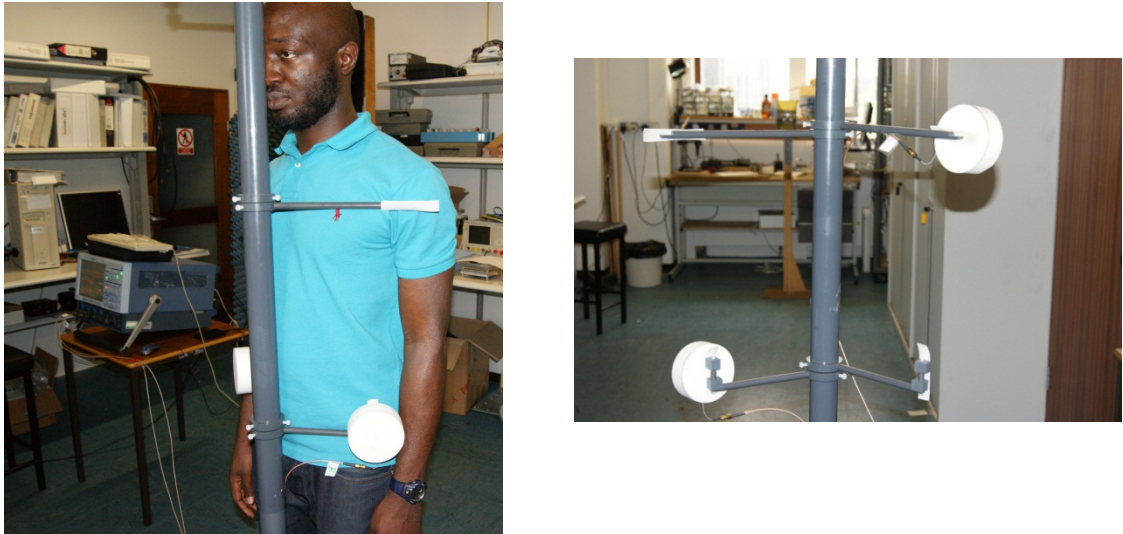
Figure 5-22: On-body alignment of the body and off-body alignment.

A schematic of the layout for the setup of the on/off-body measurement is shown in the figure 5-23.
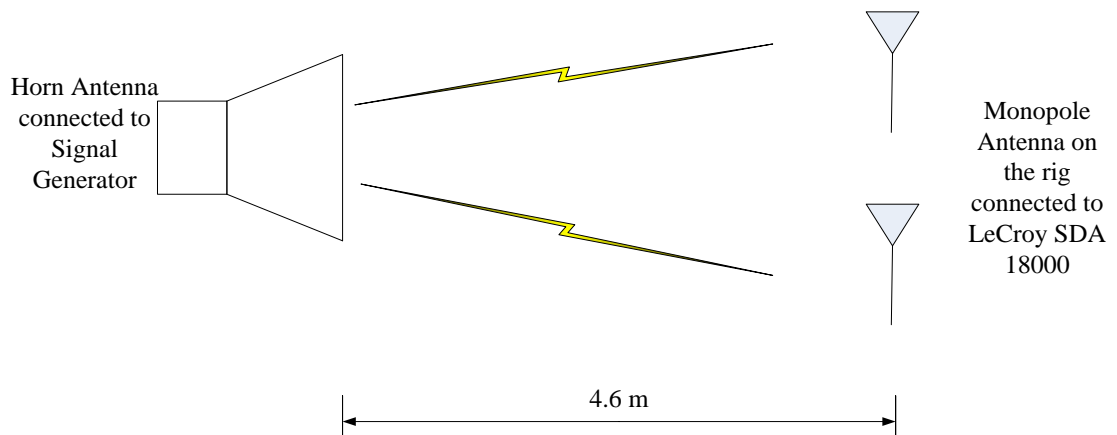
Figure 5-23: Schematic of the transmitting and receiving antennas

The distance between the transmitting horn antenna and the pole of the rig is maintained at 4.6m in all the environments. The receiving antenna was place at such distance to ensure it was in the far field region. Far field region also known as the Fraunhofer region is the region of the antenna field where the angular field distribution is independent of the distance from the antenna [66]. The Fraunhofer region is

$$R > \frac{2D^2}{\lambda} \qquad\qquad 5.3$$

R is the distance between the transmitting antenna and receiving antenna

D is the maximum dimension on the antenna

λ is the wavelength.

The maximum dimension in the monopole antenna is 10cm and for the horn antenna the maximum dimension is 24.5cm. From the result, $\frac{2D^2}{\lambda}$ is approximately 0.96m. This shows the distance between the transmitting and receiving antenna 4.6m is the far field.

Each measurement was taken for 300 seconds giving 15,000 power points in each channel. This was at a sample rate of 50 times per second (50Hz). Measurements were repeated three times for each of the six paths. In the entire test environment, during on/off-body measurement only two individuals were in the room. One individual controlled the LeCroy SDA 18000 while the other stood by the rig for the on-body measurement. Figure 5-24 below is a schematic of the experiment carried out.

Figure 5-24: Schematic for the layout of the experiment.

While the off body measurements were carried out, the two individuals stood by the LeCroy SDA 18000. Figure 5-25 is a screen shot of the measurement from the SDA attached to the receiving antennas. C1 and C2 represent the continuous waves received from the transmitter by the antennas attached to the SDA. F1 and F2 show the power level for the received signal at C1 and C2 respectively.
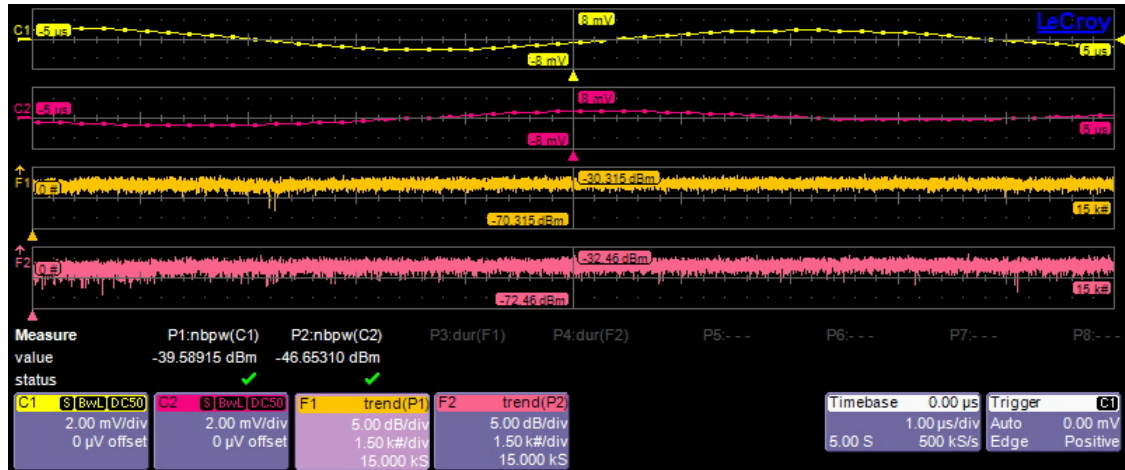
Figure 5-25: Screen shot of the LeCroy SDA 18000

In the environments the experiments were carried out, a 2-person presence was maintained. While carrying out the on-body measurements, one person stood by the rig and the other operated the LeCroy SDA 18000. During the off-body measurement, the two individuals were by the machine. This was done to reduce variables during the experiment. The results from the data collected from the measurements in different positions and locations will be presented in Section 5.10.

5.10 Results

There have been several interesting papers on the on-body channel [67], [68] and a variety of models have been put forward to describe the propagation characteristics of communication channels close to the body. For close to the body communications scenarios at 2.4GHz the on-body channel can be thought of as comprising of four parts namely, a line of sight component, a component due to scattering in the immediate environment, a creeping wave on the surface of the body and a radio wave that travels through the body. It is now generally accepted that only the first two components contribute significantly to the energy at the receiver. This is because energy absorption by the body itself is significant and the fact that propagation over the surface of the body is sharply attenuated [69].

As has been stated in Section 5.9, this experiment is concerned with SIMO [70] and seeks to determine the effectiveness of SIMO with one transmitter off the body and two receivers on the body in improving short range communications links close to humans.

The experimental setup is shown in Section 5.9. In this set of measurement approximately 540,000 power points were gathered. An average of three values was taken for all points. The results show selection combining performed on the received power in the 2 antennas. The results will be shown according to location of experiment and there will be a comparison of results taken for different alignment.

An example of the results for a selection combining performed on the received power obtained for 300 seconds is shown in the figure 5-26.
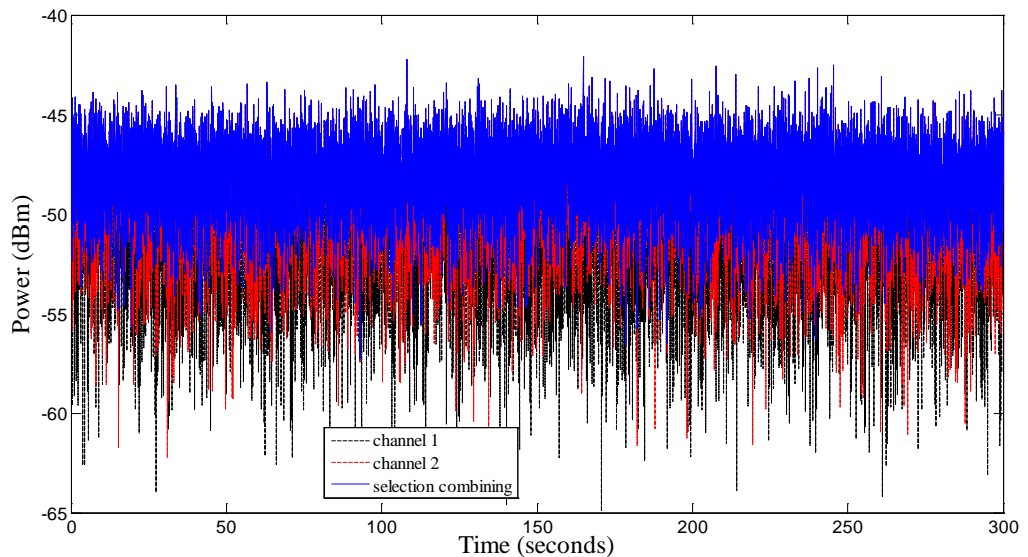

Figure 5-26: Results for 300 seconds of power measurement taken in 2 channels and selection combining carried out

For the result that will be shown, only a time sector of the data will be plotted. This will help show the variation in received power over time and the selection-combining plot. For the results shown in the following section, measured power between 160 seconds and 180 seconds was plotted. This 20 seconds of data amounted to 1000 measured power points. To show that 20 seconds of data can represent the 300 seconds record, self-similarity test were carried out. The idea of a self-similarity test was first introduced in [71]. Self-similarity occurs when a shape or object can be recreated from part of the data used to create the original shape or object. It is a reduced scale of the main object. To test for self-similarity, two parts of the data is used to test if the original object can

be recreated. If this occurs, self-similarity is possible from the data gathered. In the experiment carried out for the on/off-body selection combining, a large range of data was gathered. To make the information gathered more visible and readable, the data was cut into chunks. To confirm that a chunk of the data gather will properly represent the whole data, a self-similarity test was carried out. For the test, a range of 1000:2000 and 8000:9000 was compared to the 0:15000 points. The plot of the data is shown in the figure 5-27. This plot of the data shows that the information complies with the self-similarity test.
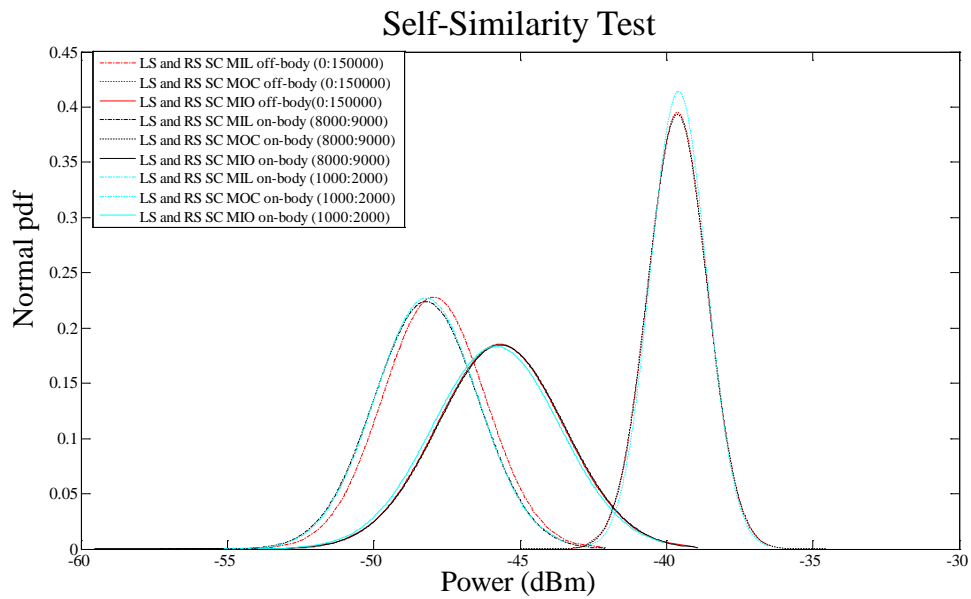

Figure 5-27: Self-similarity test using data from selection combining from the left shoulder to right shoulder

Some abbreviations will be adopted to clarify results. These abbreviations are shown in table 5-2.

Abbreviations	Meaning
RS	Right Shoulder
LS	Left Shoulder
RW	Right Waist
LW	Left Waist
SC	Selection Combining
MIL	Measurement In the Laboratory
MOC	Measurement On the Corridor
MIO	Measurement In the Office

Table 5-2: Table of Abbreviations

5.11 Results of MIL

The results from the six-antenna orientation on/off-body are presented in this section. The set up for the experiment is as described in the experimental setup. The measured power in each channel is shown along with the result after selection combining has been carried out. The graphs below show a part of the results of the selection combining carried out.
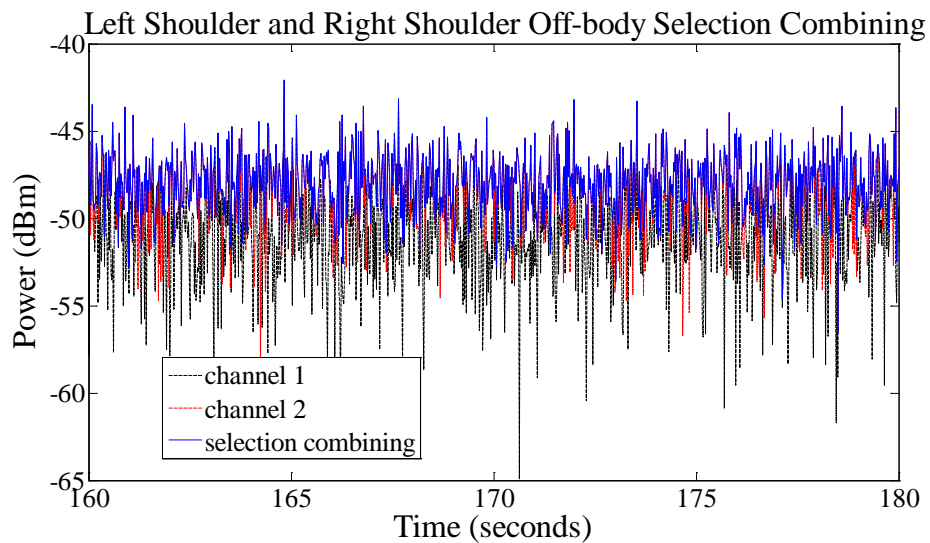

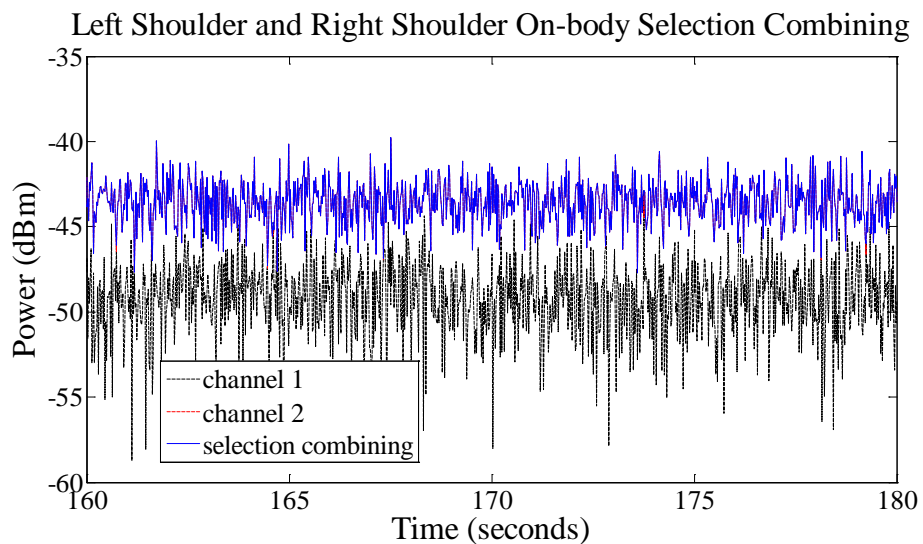Figure 5-28: LS and RS off-body selection combining

Figure 5-29: LS and RS on-body selection combining

Figure 5-30: LS and RW off-body selection combining

Figure 5-31: LS and RW on-body selection combining

For the MIL off-body measurements, the RS and RW alignment gave the maximum average received power for both channels and its selection combining. The least average power is received in the LS and RW alignment for both channels and its selection combining. For the on-body measurement in the MIL, the RS and RW also give the average maximum power for both channels and its SC. In the off-body measurement of the MIL, the maximum average received power was in channel 2 for four of the six alignments except the LS&RW and LS&LW. But in the on-body measurement for MIL, the maximum average receive power was in channel 2 for five of the six alignments except LW&RW.

5.12 Result of MOC

Parts of the results from the selection combining performed in the six-antenna position measure on the corridor are presented in the graphs below. These results are extracted from a from a 300 seconds measurement taken. 20 seconds of the measured power in channels 1 and 2 is presented along with the result when selection combining is performed.

Figure 5-32: LS and LW off-body selection combining
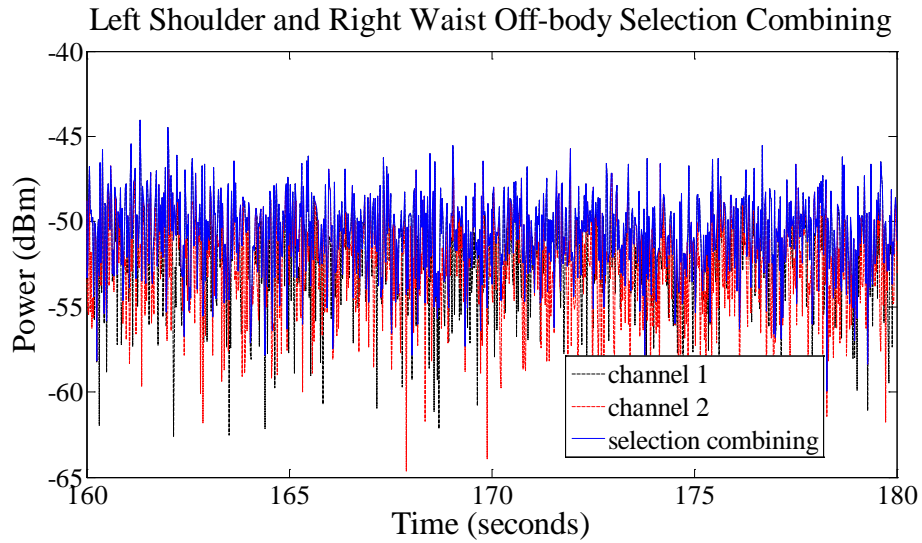
Figure 5-33: LS and LW on-body selection combining

Right Shoulder and Right Waist Off-body Selection Combining
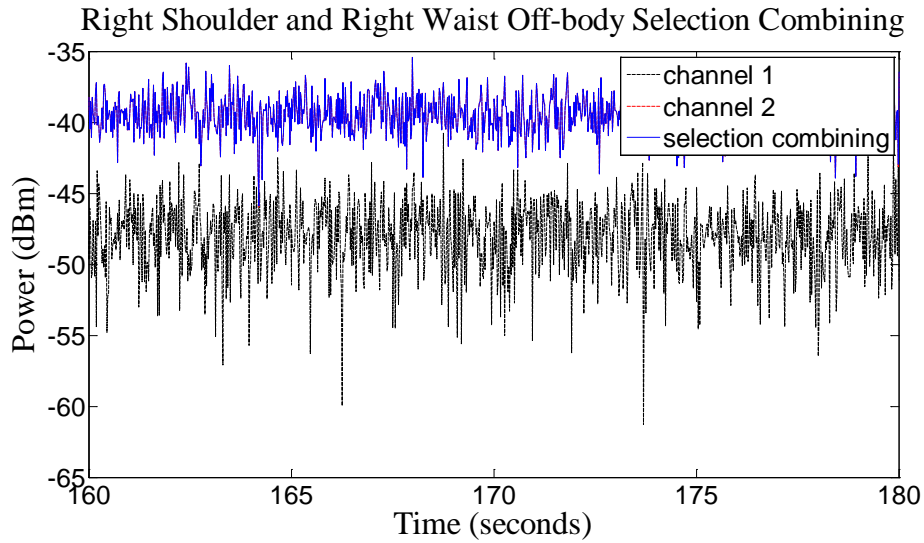
Figure 5-34: RS and RW off-body selection combining

Right Shoulder and Right Waist On-body Selection Combining
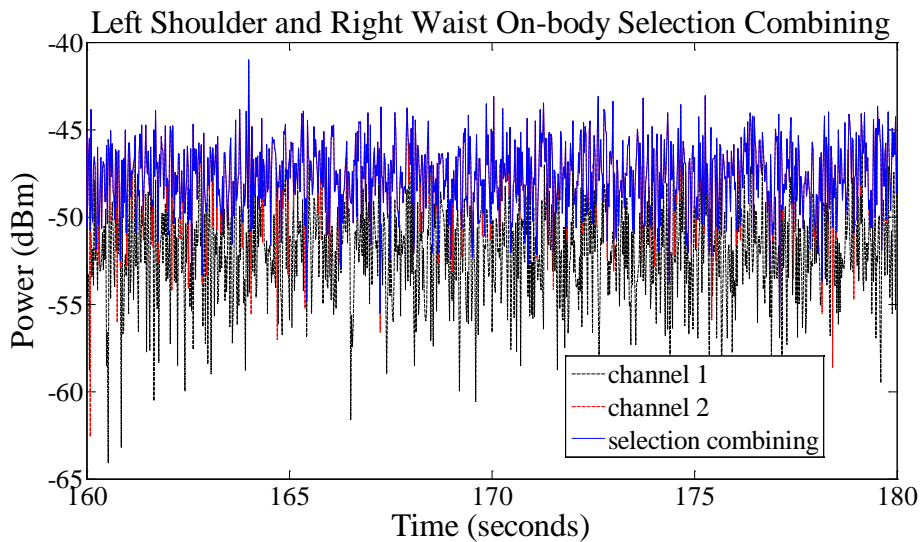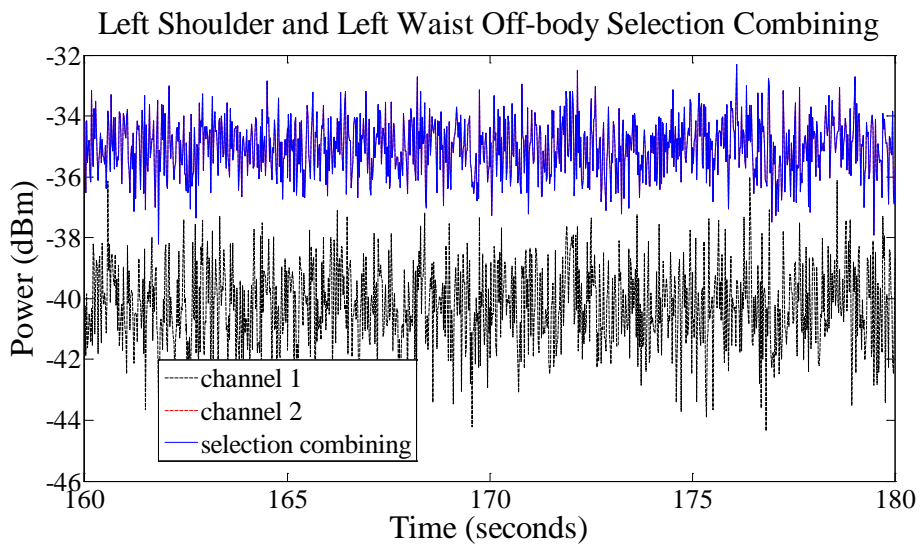
Figure 5-35: RS and RW on-body selection combining

For the MOC off-body measurements, the maximum average received power for channel 1 was from the LW&RW alignment while the maximum average received power in channel 2 was from LS&LW alignment. The LS&LW alignment had the maximum average power for the selection combining. For the on-body measurements, the maximum average received power in channel 1 was received in the LW&RW alignment while the maximum average received power in channel 2 was received in the LS&LW alignment. The maximum average power for selection combining results also came from the LS&LW alignment. The LS&LW alignment had the maximum average received power for all the channels and the selection combining. The maximum average power in the MOC off-body came from channel 1 in four of the six alignments except

for the LS&LW and RS&RW. For the on-body MOC, three of the six alignments had the maximum average in channel 1.

5.13 Results of MIO

The results presented here are measured in the CMCR office. The office has an open plan layout with 12 workstations and 2 racks for server system. The experiment was carried out when no students were present. A distance of 4.6 metres was maintained between the transmitter and receiver rig similar to the other experiment. The graphs below show a part of the on/off-body power measurement in the six different alignments.
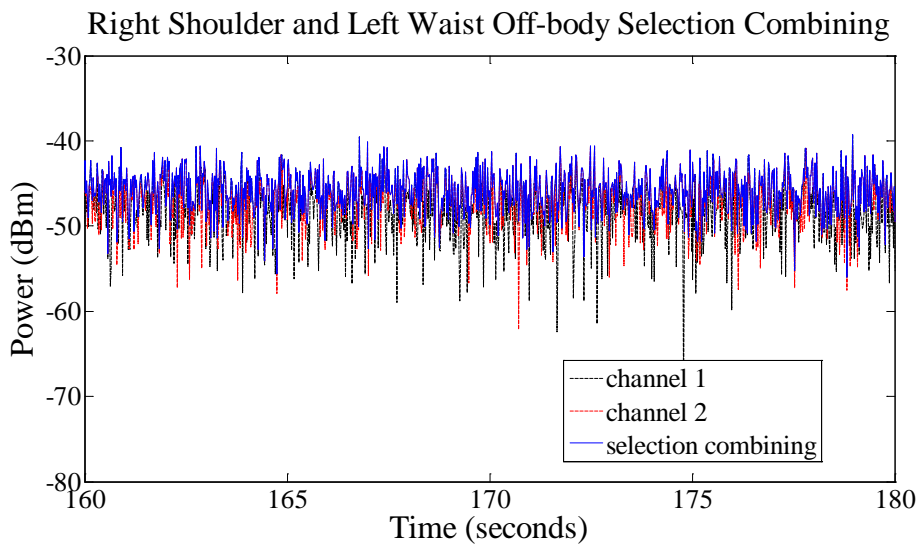
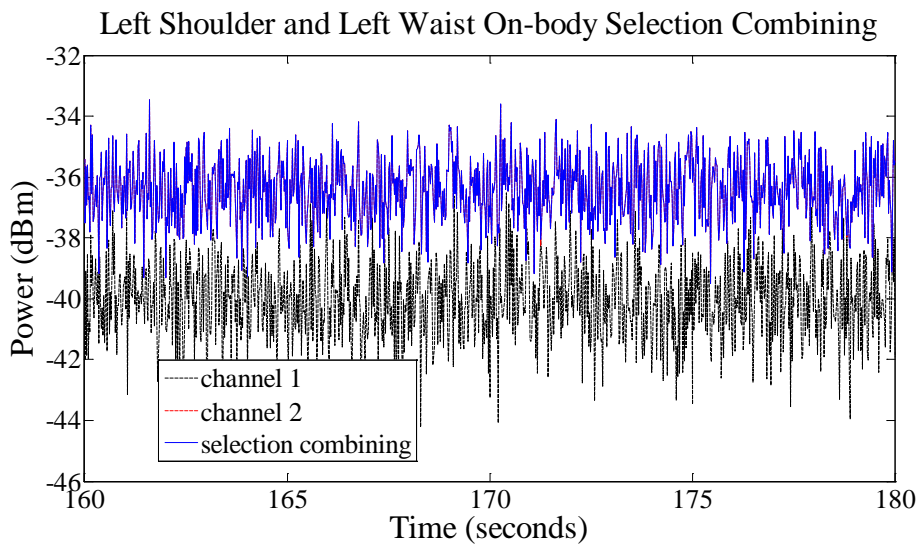
Figure 5-36: RS and LW off-body selection combining
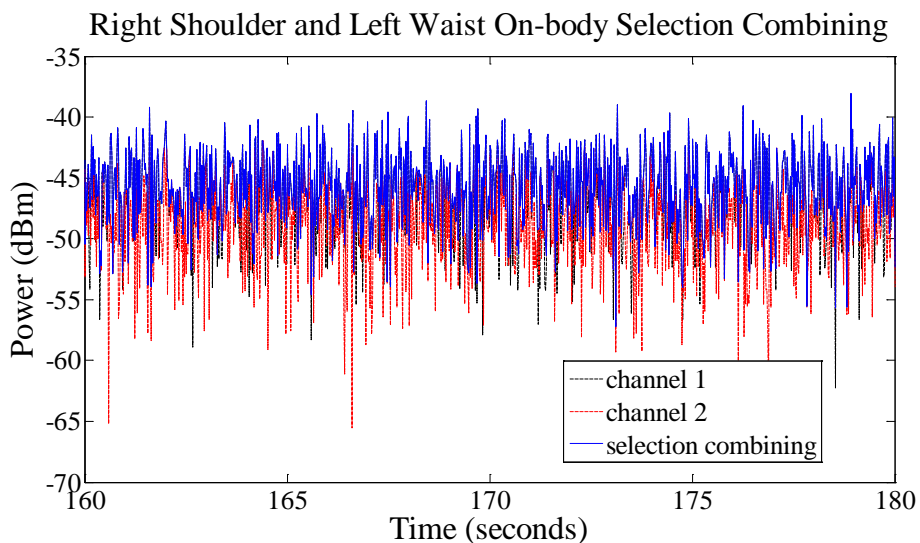
Figure 5-37: RS and LW on-body selection combining

Left Waist and Right Waist Off-body Selection Combining
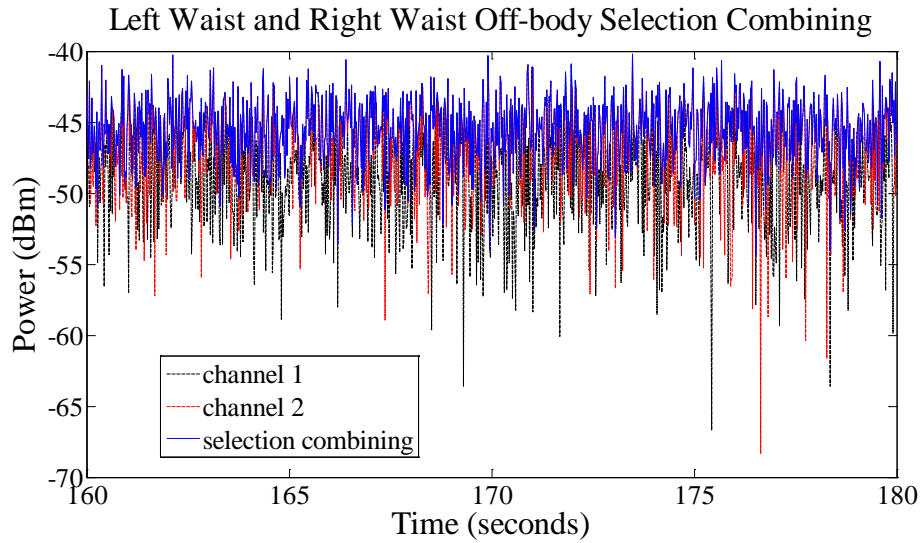
Figure 5-38: LW and RW on-body selection combining

Left Waist and Right Waist On-body Selection Combining
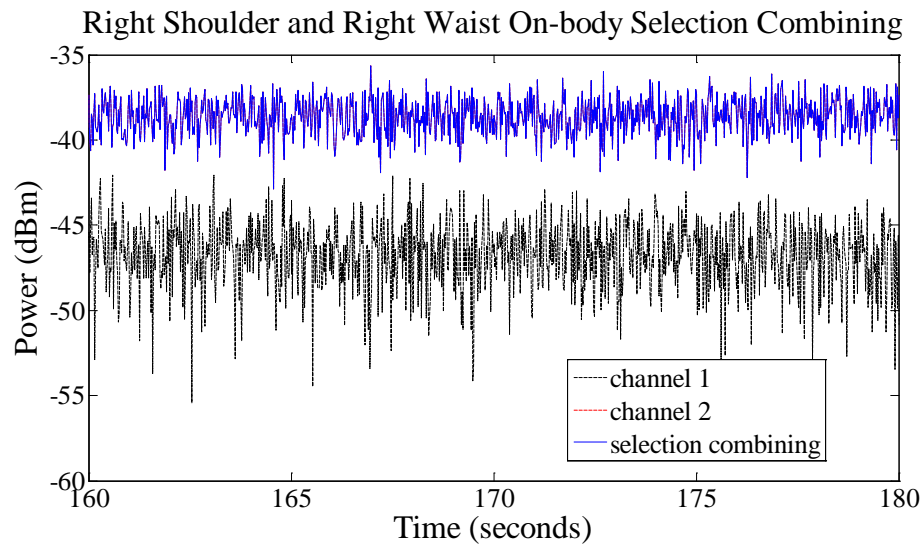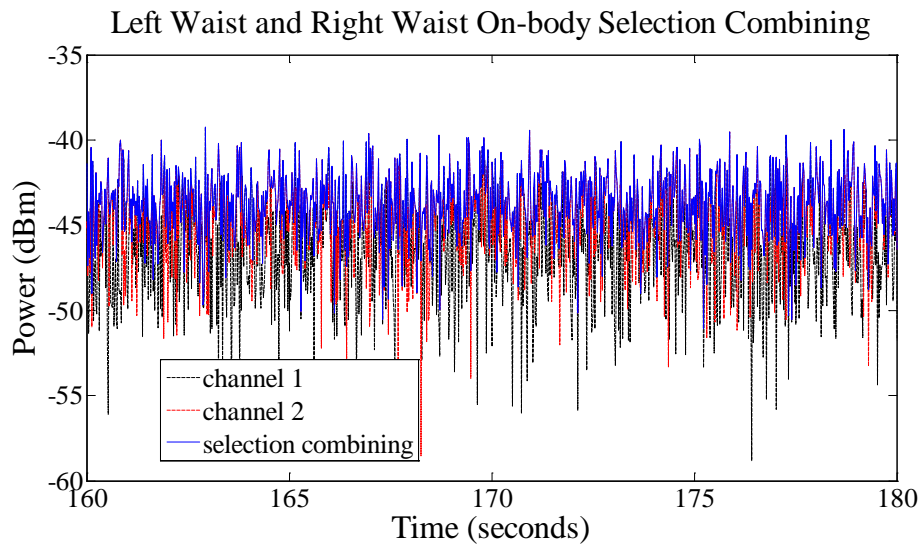
Figure 5-39: LW and RW on-body selection combining

For MIO off-body, the maximum average received power for channel 1 was from the RS&RW alignment while the maximum average received power for channel 2 came from the LS&LW alignment. The maximum average power for selection combining also came from the RS&RW alignment. For the on-body measurements, the maximum average power for channel 2 came from the LS&RW alignment. The maximum average power for the selection combining was from the RS&RW. In MIO, for the off-body measurements channel 2 had the maximum average power for five of the six alignments except RS&RW. While in the on-body measurement, channel 1 had the maximum average power in all six alignments.

5.14 Results of the Selection Combining On/Off-body for MIL

The results in this section are a comparison of the selection combined on-body and off-body measured power. The comparison of the results for the SC for MIL indicates that for all six alignments, the system performed better on the body. The on-body power measurement was on average 2.5dB better than the off-body measurement. The result presented is a 20 second section from the 300 seconds of collected data. The graphs below show a part of the selection combining for the six antenna alignments.

Figure 5-40: LS and RS selection combining
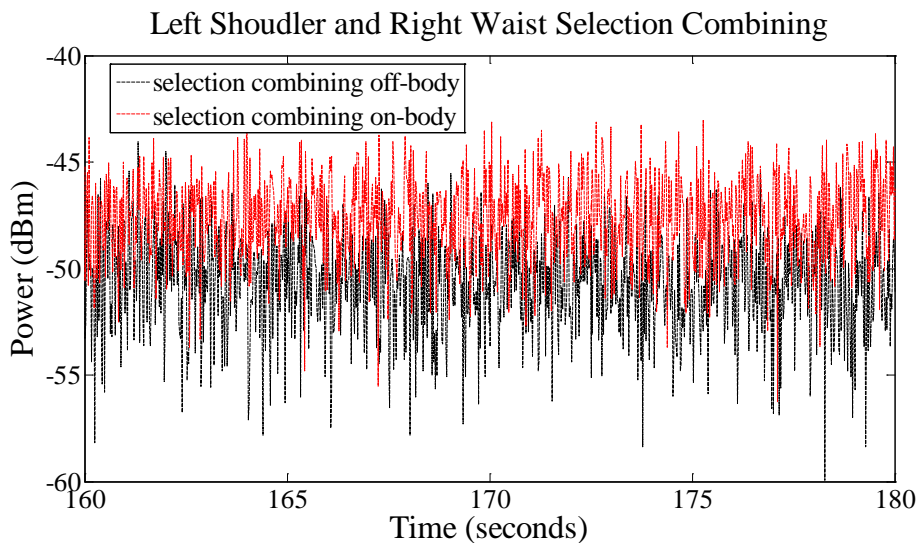
Figure 5-41: LS and RW selection combining

5.15 Results of the Selection Combining On/Off-body for MOC

The selection combined result for the on/off-body measurements taken on the corridor is presented in this section. The results for the comparison of the on/off body measurement for MOC for the six alignments indicate that the system performance fluctuated with change in antenna alignment. There is no clear indication if the system was better on-body or off-body. In this situation, the environment is assumed to have more impact on the system than the body. The graphs below show a part of the results from selection combined outcome for the six antenna alignment.

Left Shoulder and Left Waist Selection Combining

Figure 5-42: LS and LW selection combining

Right Shoulder and Right Waist Selection Combining

Figure 5-43: RS and RW selection combining
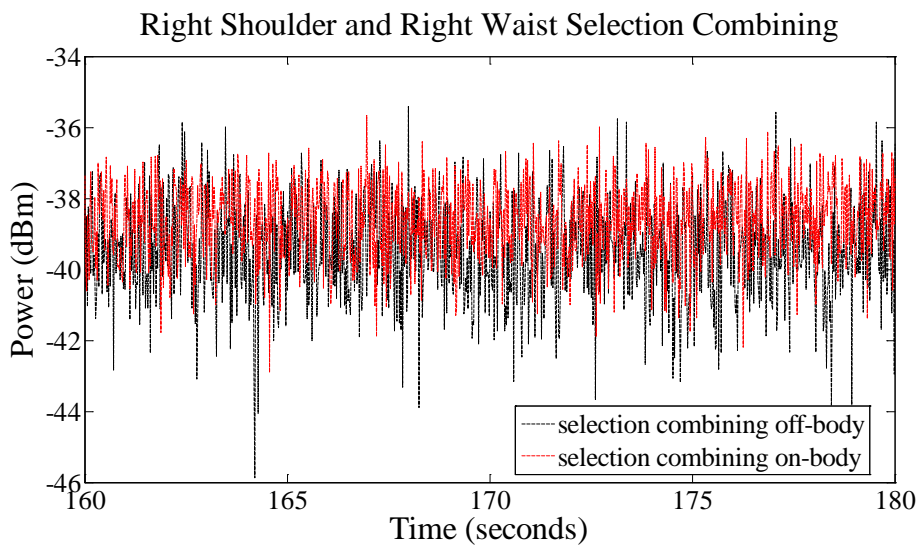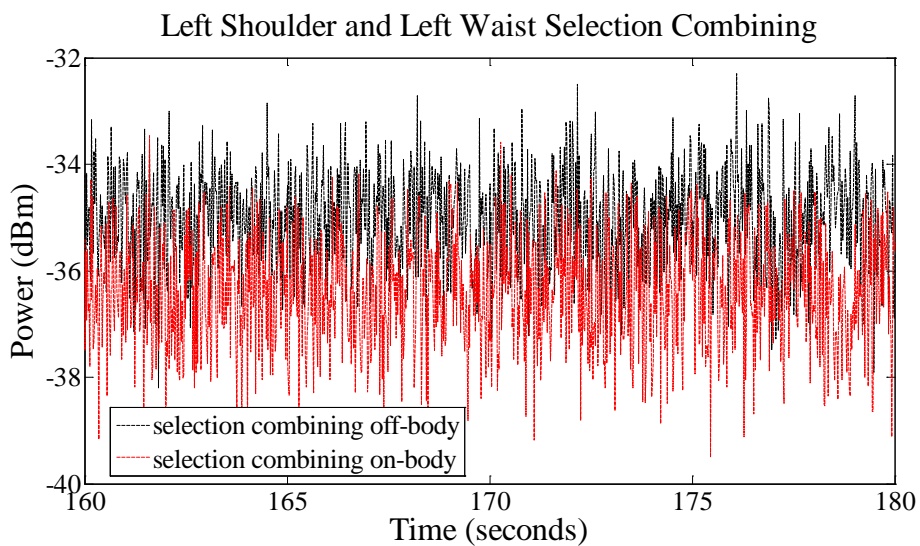
5.16 Results of the Selection Combining On/Off-body for MIO

The selection combined result for on/off-body measured power in the office is presented in this section. The results show that the performance of the system on and off body had no significant difference. It can be deduce that the environment plays a major role in the effect on the received power. The graphs below show a part of the six-antenna alignment for on/off-body.
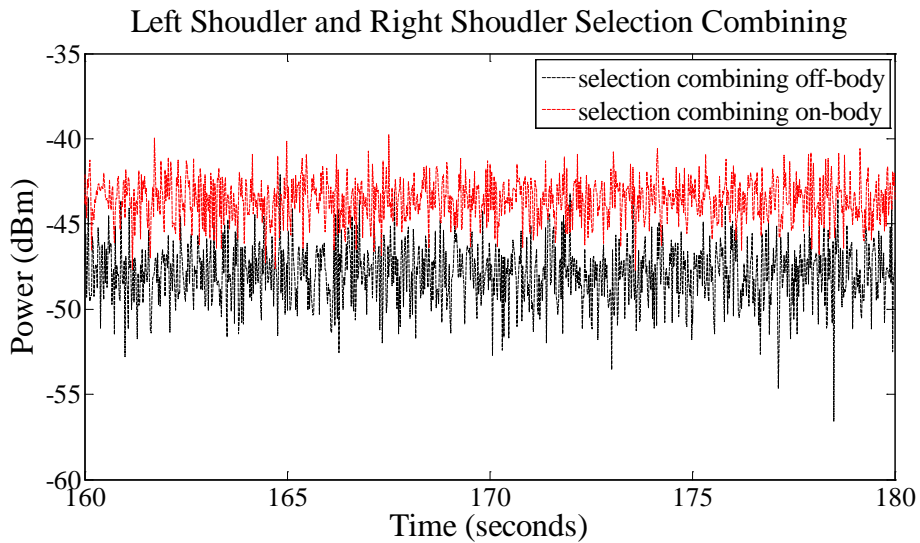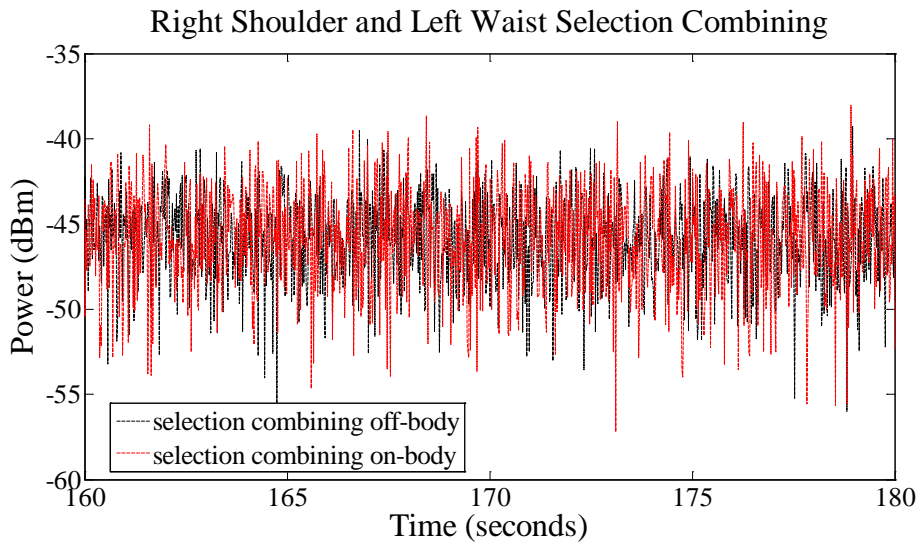

Figure 5-44: RS and LW selection combining
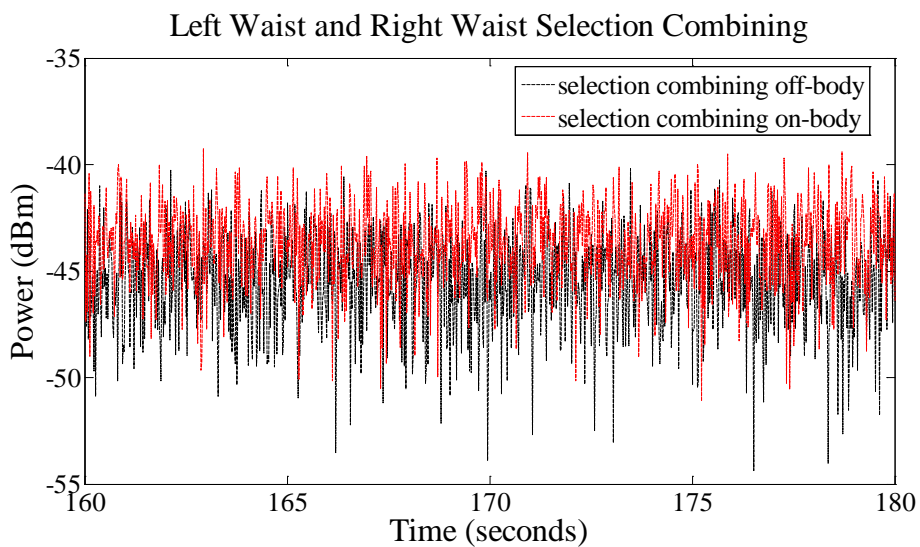
Figure 5-45: LW and RW selection combining

5.17 Tabular summary of the average received and Selection Combining power

In this section, the average of the power received on/off-body is presented along with the average power after selection combining. The variation in power from each environment is shown clearly with the tabular format presented.

For table 5-4 and 5-5 the images used to represent the off-body and on-body are shown in table 5-3.
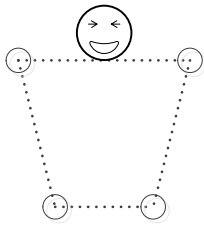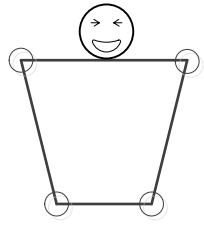
Off-body system with the four possible antenna positions.	
On-body system with the four possible antenna positions.	

Table 5-3: Description of the images used in table 5-4 and 5-5

Table 5-4 is a compilation of the average power received in the antennas for each channel with the off-body. So also is the average power, after selection combining has been carried out with the percentage improvement by selection combining when compared to the channel with the highest mean.
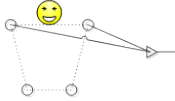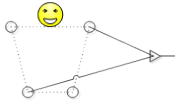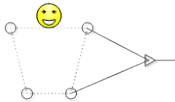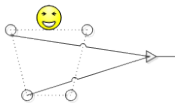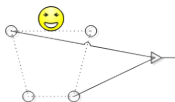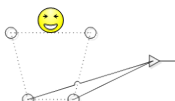
	MIL(x10^-9 W)			SC %	MOC(x10^-9 W)			SC %	MIO(x10^-9 W)			SC %
	Ch1	Ch2	SC		Ch1	Ch2	SC		Ch1	Ch2	SC	
	9.7	14.8	16.4	11	98.1	90.0	112.1	14	21.1	22.9	30.6	34
	8.7	7.3	10.4	20	90.2	37.7	90.7	1	19.3	49.6	50.6	2
	12.5	10.6	14.9	20	97.0	321.4	321.4	0	21.0	25.2	29.7	8
	28.1	63.6	63.7	0	17.8	117.4	117.2	0	73.3	43.5	76.8	5
	14.1	56.9	57.0	0	235.0	130.0	235.0	0	16.0	21.1	23.1	9
	13.3	21.0	22.3	6	257.8	6.6	257.8	0	18.4	27.0	32.6	21

Table 5-4: Average received power in channel 1, channel 2 and the average power after selection combining in the off-body state

Table 5-5 is an average of received power when the antenna is on-body. The average power in channel 1 and channel 2 is stated. Also is the average power after selection combining was carried out.
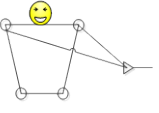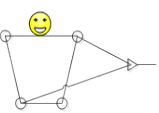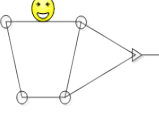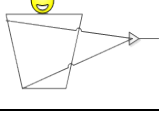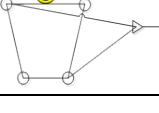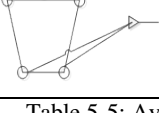
	MIL(x10⁻⁹ W)			SC %	MOC(x10⁻⁹ W)			SC %	MIO(x10⁻⁹ W)			SC %
	Ch1	Ch2	SC		Ch1	Ch2	SC		Ch1	Ch2	SC	
	13.4	45.5	45.6	0	45.8	49.8	60.6	22	40.2	15.4	41.3	3
	8.2	18.3	18.9	0	93.9	20.3	93.9	0	29.6	27.4	38.6	31
	10.5	29.5	29.7	1	107.3	240.3	240.4	0	30.8	14.8	32.3	5
	48.6	96.9	97.0	0	23.8	140.2	140.2	0	57.3	18.8	58.2	2
	37.9	81.6	81.7	0	213.7	119.6	238.7	12	23.0	11.3	25.6	11
	37.9	36.8	43.6	15	225.5	25.0	225.5	0	30.1	38.9	47.0	21

Table 5-5: Average received power in channel 1, channel 2 and the average power after selection combining in the on-body state

5.18 Discussion of Results by Linear Comparison

Tables 5-4 and 5-5 provide the results in nW for all scenarios. Table 5-4 is the off-body and Table 5-5 is the on-body. The icons in the left column are useful for quickly identifying the scenario. A solid torso indicating on-body and a dotted torso indicating off-body. As stated in Section 5.9 the position of the antennas in space for on and off the body were as far as possible identical and therefore the only differences were due to the human.

5.19 Discussion of off-body Selection Combining

Of the 18 combinations measured for SC 12 showed a positive effect. As was anticipated the worst scenario was the corridor where only one alignment; MOC LS & RS showed benefits for SC. It is reasonable to assume that this was as a result of the relative low scattering environment of the corridor.

Overall the best off-body environment was seen to be the office with a mean % benefit of 13% for the six scenarios with the best being 34% and the worst being 2%.

5.20 Discussion of On-body Selection Combining

Of the 18 combinations measured 10 had a positive effect which is slightly worse than the off-body case. The best scenario was again seen in the office where all results showed benefits for SC of between 2% and 31%, which was similar to the off-body case. The office was the richest of the three scenarios for scatters. It can reasonably be concluded that environments rich in scatterers may ameliorate the effects of LOS due to blocking by the body. In other words for on-body SC it is the environment that is significant for beneficial SC.

5.21 Comparisons between On- and Off-body scenarios

	MIL			MOC			MIO		
	off-body SC	on-body SC	improvement %	off-body SC	on-body SC	improvement %	off-body SC	on-body SC	improvement %
Left shoulder and right shoulder	✓		11		✓	22	✓		34
Left shoulder and right waist	✓		20	✓		1		✓	31
Left shoulder and left waist	✓		20				✓		8
Right shoulder and right waist							✓		5
Right shoulder and left waist				✓		12	✓		11
Left waist and right waist		✓	15						

Table 5-6: Table showing the SC with the best improvement

From table 5-6, for the off-body scenarios there were 8 cases where SC was better and for on-body there were only 4 cases. It is therefore reasonable to conclude that off-body SC is generally better. This would seem to be either due to changes caused by the body to the scattering environment or LOS. Note also that the best recorded SC was with LS and RS in the MIO. The positions with no marks and improvement percentage indicates even effects on the SC on-body and off-body.

5.22 Comparison of the probability density function (pdf) results in the environments for each antenna alignment

The pdf results shown here are a comparison of the off/on-body measurements taken in each alignment in the three environments. The pdf makes it simple to compare the

means and variance of two or more functions and it's particularly good when the distribution is symmetrical. The results shown in this section is processed from data taken between 160 seconds and 180 seconds.
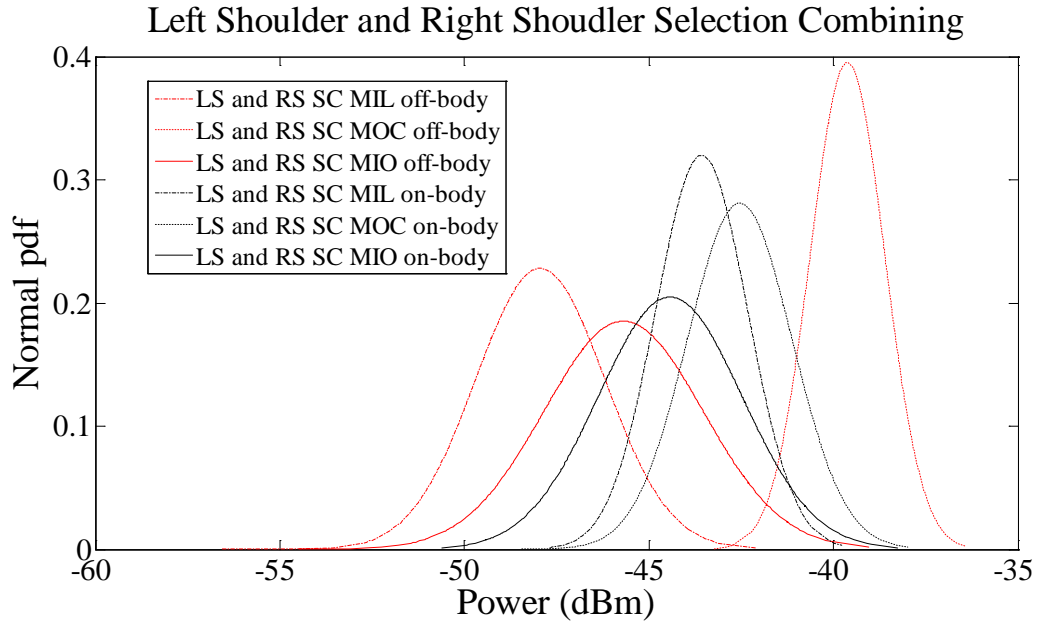
Figure 5-46: pdf of left shoulder and right shoulder selection combining on/off-body in all experimental environments
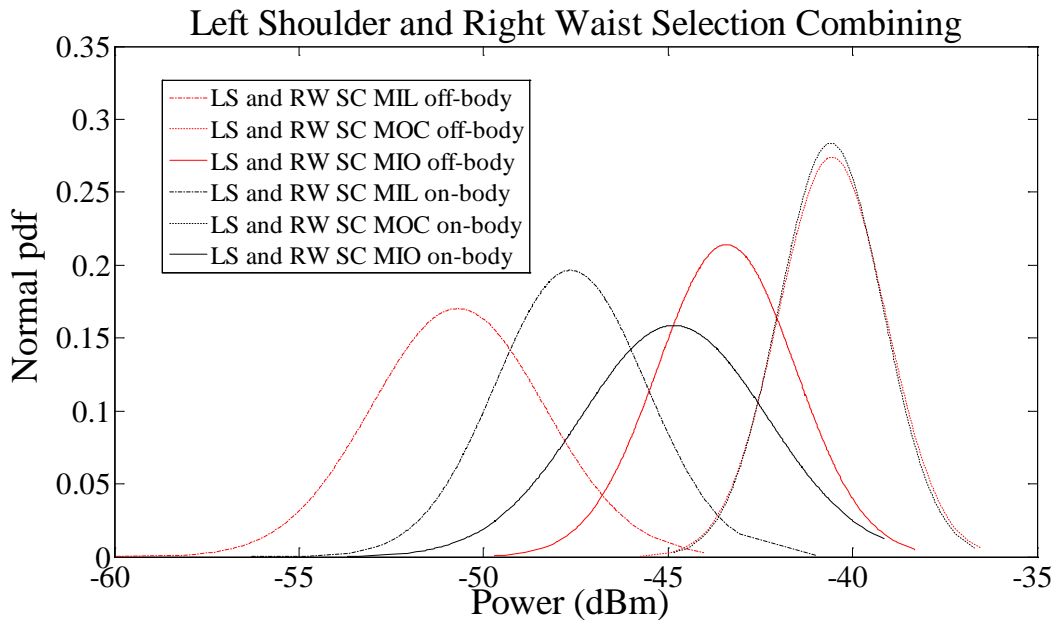
Figure 5-47: pdf of left shoulder and right waist selection combining on/off-body in all experimental environments

Left Shoulder and Left Waist Selection Combining
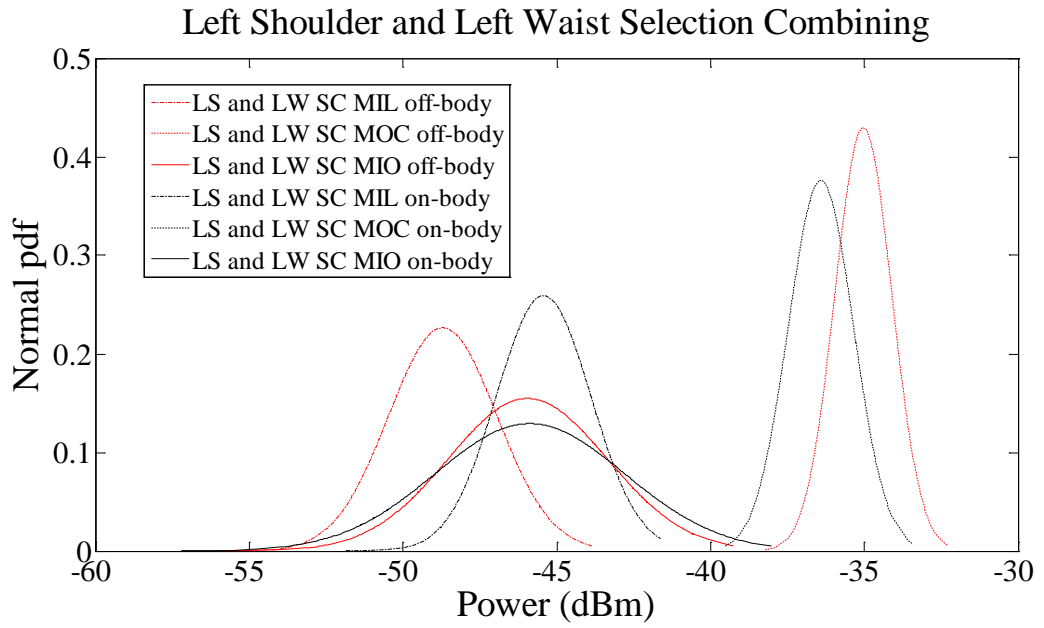
Figure 5-48: pdf of left shoulder and left waist selection combining on/off-body in all experimental environments

Right Shoulder and Right Waist Selection Combining
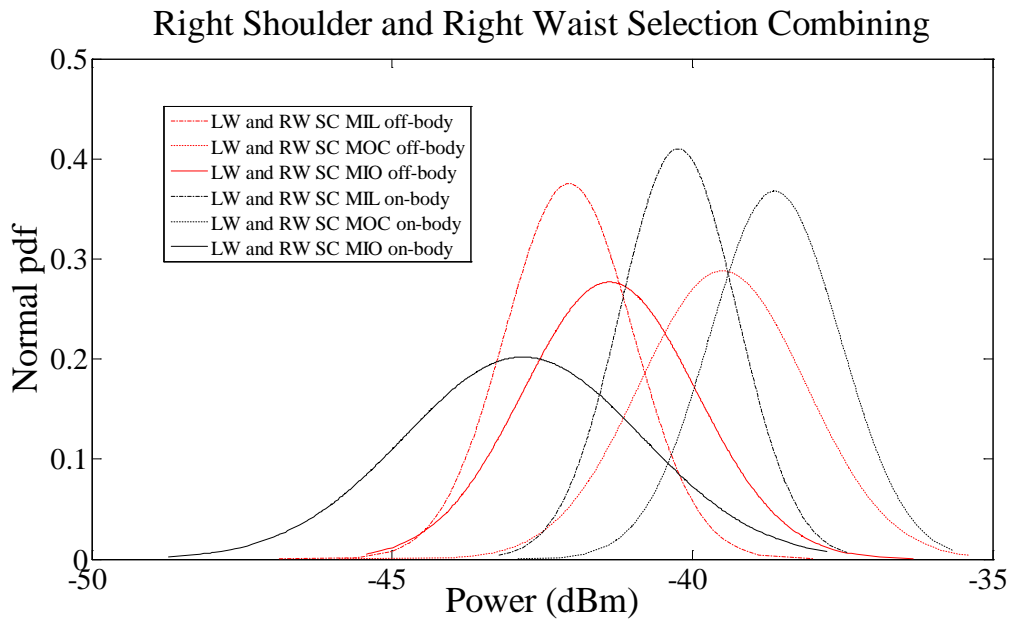
Figure 5-49: pdf of right shoulder and right waist selection combining on/off-body in all experimental environments
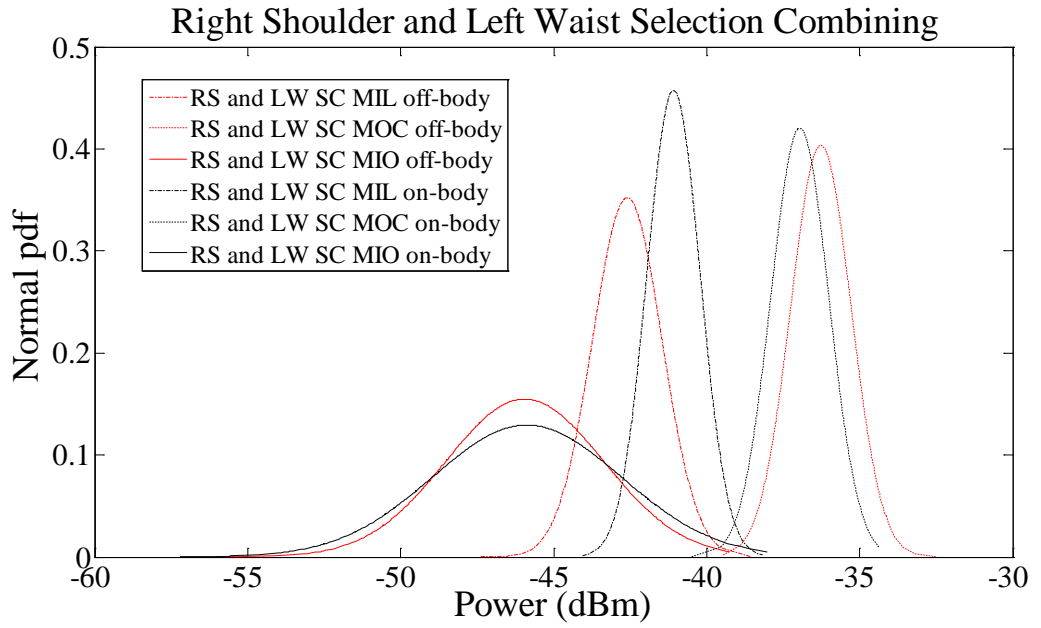
Figure 5-50: pdf of right shoulder and left waist selection combining on/off-body in all experimental environments
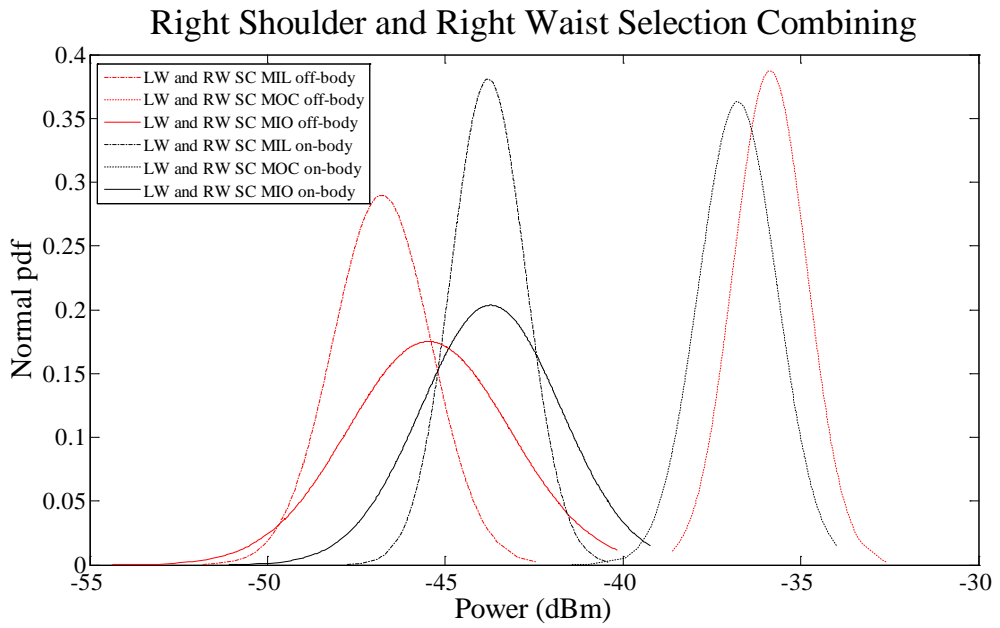
Figure 5-51: pdf of left waist and left waist selection combining on/off-body in all experimental environments

5.23 Comparison of the cumulative distribution function (cdf) results in the environments for each antenna alignment

The cdf of the power received between 160 seconds and 180 seconds in the three environments will be compared for all six alignments off/on-body. In received power measurement, the cdf is good for comparison of gain. The graphs below show the results taken in all the environments.

Left Shoulder and Right Shoudler Selection Combining
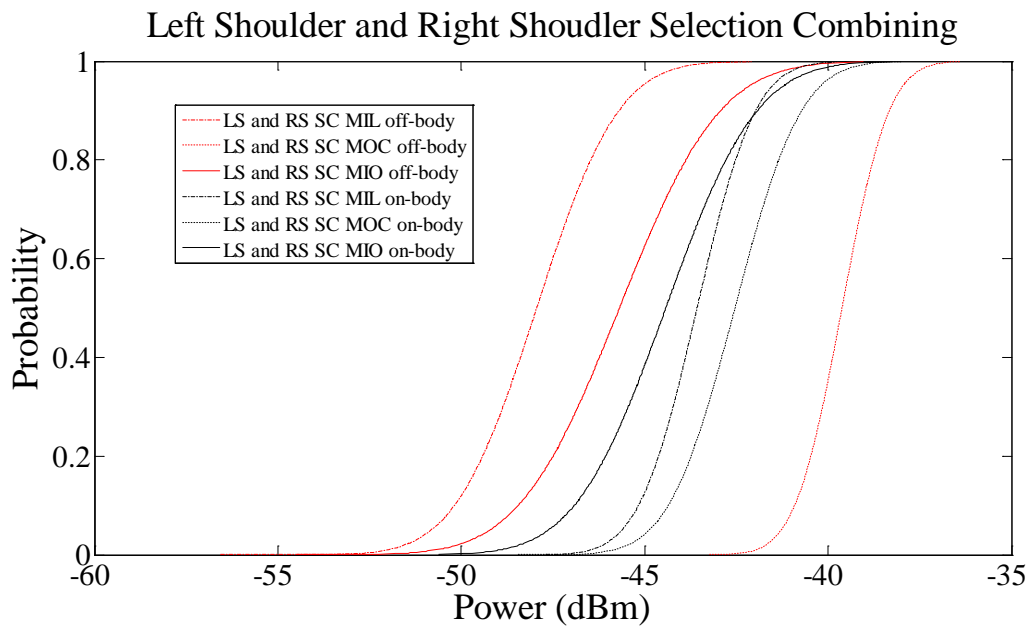
Figure 5-52: cdf of left shoulder and right shoulder selection combining on/off-body in all experimental environments

Left Shoulder and Right Waist Selection Combining
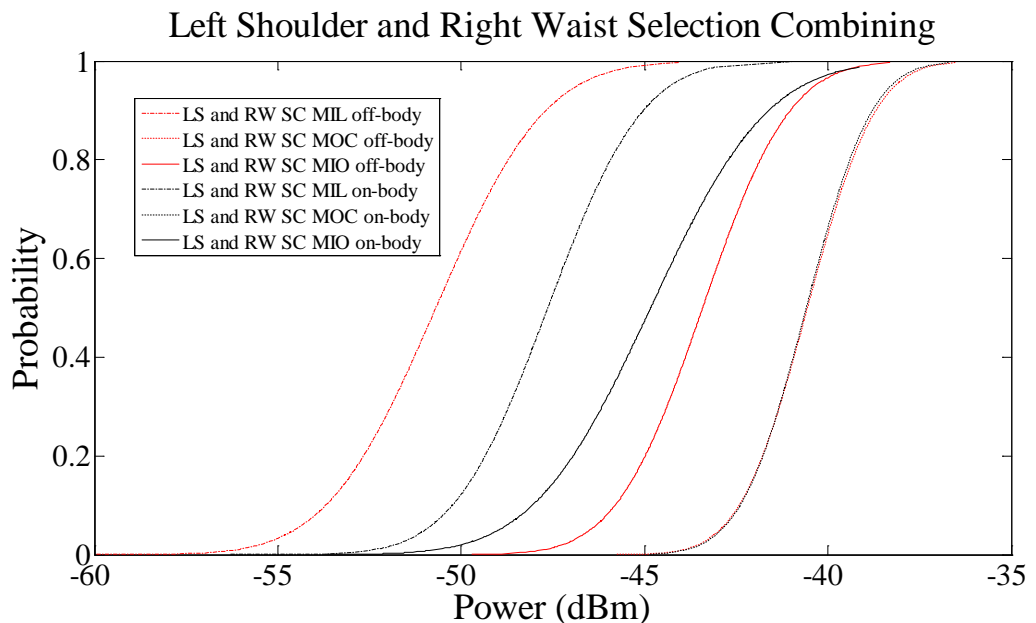
Figure 5-53: cdf of left shoulder and right waist selection combining on/off-body in all experimental environments
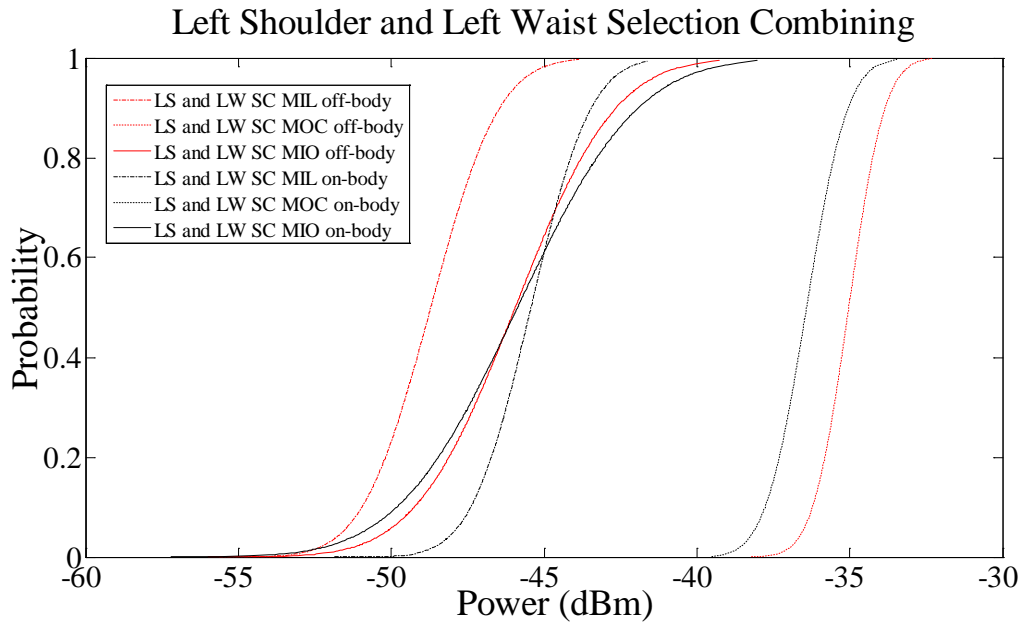
Figure 5-54: cdf of left shoulder and left waist selection combining on/off-body in all experimental environments
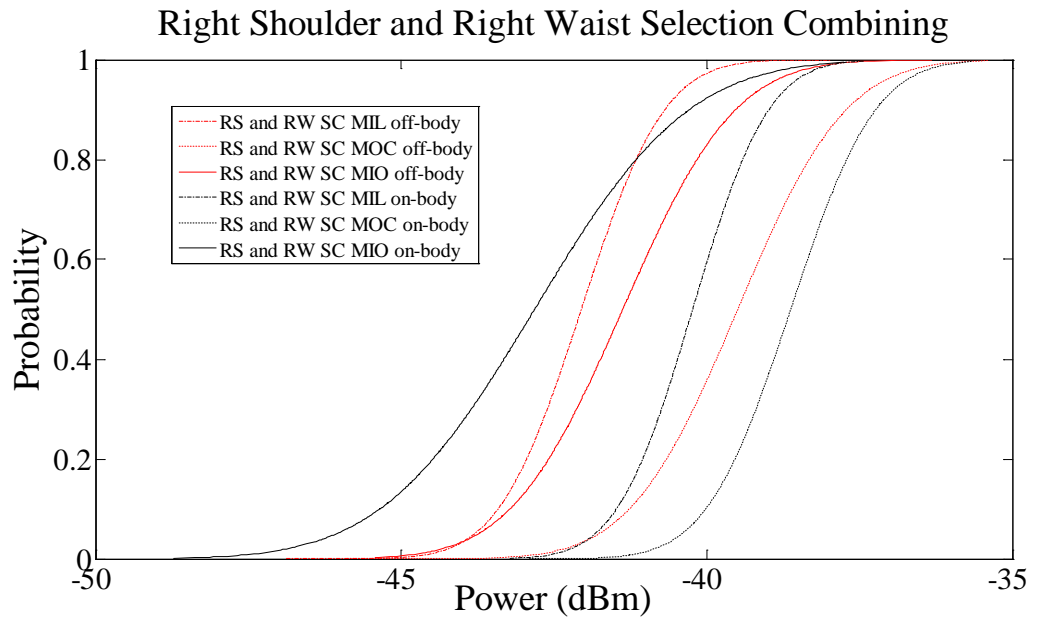
Figure 5-55: cdf of right shoulder and right waist selection combining on/off-body in all experimental environments

Right Shoulder and Left Waist Selection Combining
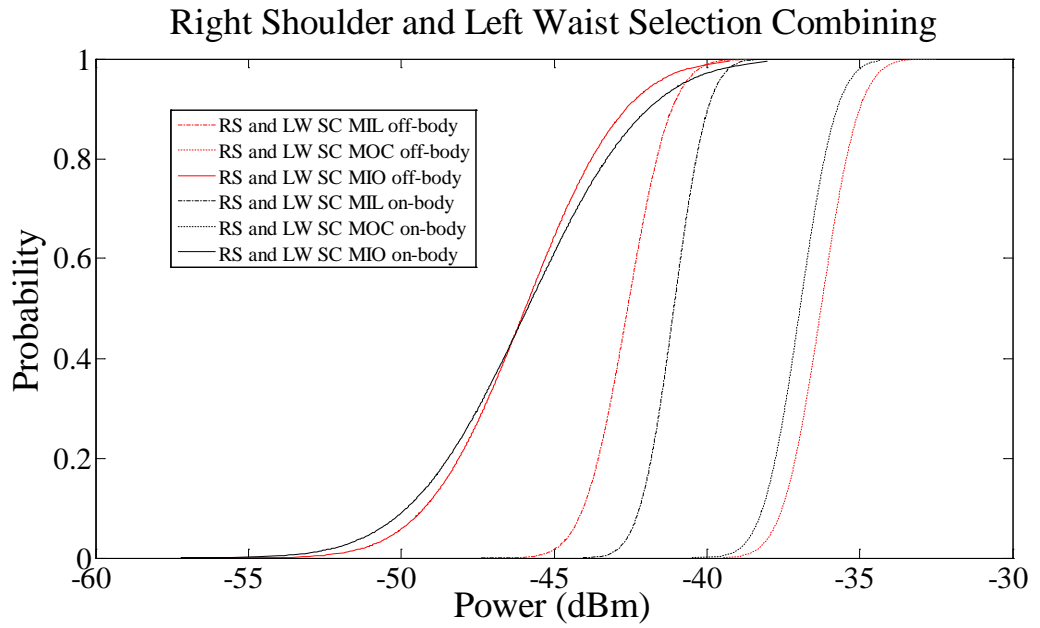
Figure 5-56: cdf of right shoulder and left waist selection combining on/off-body in all experimental environments

Left Waist and Right Waist Selection Combining
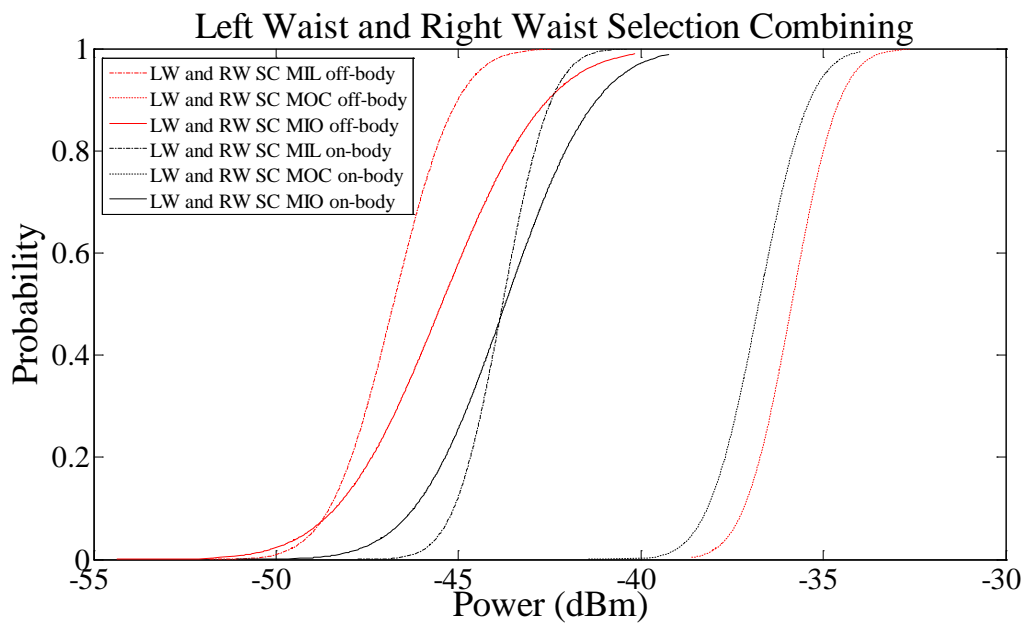
Figure 5-57: cdf of left waist and right waist selection combining on/off-body in all experimental environments

5.24 Result Conclusion

In this experiment the monopole antennas were built to work on the body at 2.4GHz. Antenna contact with human body was taken into emphasis when building the antenna. However, when antennas are receiving signals in various environments multipath and scattering affect the signal strength. This has an influence on the overall performance of the system. With the design of the monopole antenna on a circular ground plane, the effect from edges of antennas on rectangular ground plane is eliminated.

To reduce the effect of mutual coupling, it is recommended to space antennas by at least 0.6λ [72]. In this experiment the antenna location from each other is over the required minimum in all six alignments. It can be concluded that the antennas operated independently of each other in each alignment. Figure 5-19 shows the antenna spacing on the body. The spacing between the antenna positions on the rig and body is presented in the tables 5-7 and 5-8.

Alignment	Distance between antennas (cm)	Distance between antennas (λ)
Left shoulder to right shoulder	52	4.16
Left waist to right waist	37	2.96
Right shoulder to left waist	59	4.72
Left shoulder to left waist	42	3.36
Left shoulder to right waist	59	4.72
Right shoulder to right waist	42	3.36

Table 5-7: Spacing between antennas on the support rig

Alignment	Distance between antennas (cm)	Distance between antennas (λ)
Left shoulder to right shoulder	50	4.00
Left waist to right waist	34.5	2.76
Right shoulder to left waist	56	4.48
Left shoulder to left waist	41	3.28
Left shoulder to right waist	56	4.48
Right shoulder to right waist	41	3.28

Table 5-8: Spacing between antennas on the body

In the off-body measurements, the single channel with the best result is for the antenna connected to the left waist from the measurements on the corridor (MOC). The best single channel result for the on-body measurement is also from the MOC on the left waist (LW). The LS&LW alignment for the on/off-body had the maximum average power for the selection combining. The worst case scenario according to average power for the single channel measurement for the off-body measurement was taken from the MIL on the right waist. For the on-body, the left shoulder position gives the least average received power in the MIL. For the selection combining, the MIL had the least average power for the on/off-body measurement. From the measurements taken in all three environments, based on the average power selection combining is best on/off-body for MOC and is worst on/off-body for MIL. The performance of the system can be concluded to be influenced by the environment regardless of the on/off-body system.

5.25 Conclusion

In this chapter, the antennas were built with the proximity to the human body being a factor. In the building process the antenna was tested on and off the body. The antennas were initially built to resonate at 2.4GHz in free space. When in close proximity with the human body, the antennas were detuned. To prevent this detuning, the antennas were simulated with the human body present. This process made the antenna shorter in length. This proves that the performance of antenna is affected by the human body and also when building antennas for communication in the body region, the human body is a

factor to be considered. To combat the difficulty of antennas working better in a particular orientation, the antenna was built with a circular ground plane. This ground plane gives it the advantage of receiving equal power in any orientation unlike antennas with rectangular ground plane whose edges affect the received power. The ground plane helped make the antenna more robust to working in any environment.

The selection combining with multiple antennas on/off-body carried out in different environment showed that the body affects the signal power received during transmission. In this experiment, the only environment with the consistency in its results is the corridor (i.e. measurements labelled MOC). In this environment, the results showed the detuning effect of the body on the received power in the system. The other environments (i.e. the laboratory and the office) showed a fluctuating result. The off body was not significantly better than the on-body. Hence we can conclude the environment had a huge factor on the received power. The power change in the MIL and MIO was based on the position of the antenna on the body. This work shows that the working condition and environment affects the performance of a communication system. Also a particular alignment of multiple antennas cannot be indicated to be better that the other because the environment is a factor that influences the signal strength. But it also shows that a system with multiple receiving antennas is more efficient than one with a single antenna.

Reference

[1]   E. Reusens, W. Joseph, B. Latré, B. Braem, G. Vermeeren, E. Tanghe, L. Martens, I. Moerman, and C. Blondia, "Characterization of on-body communication channel and energy efficient topology design for wireless body area networks.," *IEEE transactions on information technology in biomedicine : a publication of the IEEE Engineering in Medicine and Biology Society*, vol. 13, no. 6, pp. 933–45, Nov. 2009.

[2]   L. Yue, "Analysis of generalized selection combining techniques," *Vehicular Technology Conference Proceedings, 2000. VTC 2000 …*, pp. 1191–1195, 2000.

[3]   Y. Guo, "Modem/Radio IC Architectures for ISM band Wireless Applications," *IEEE Transactions on Consumer Electronics*, vol. 39, no. 2, pp. 100–106, 1993.

[4] P. Henry and H. Luo, "WiFi: what's next?," *Communications Magazine, IEEE*, no. December, pp. 66–72, 2002.

[5] M. T. Camp, "Development of the Bluetooth version 1.0 specification," *2000 IEEE Emerging Technologies Symposium on Broadband, Wireless Internet Access. Digest of Papers (Cat. No.00EX414)*, p. 7.

[6] IEC62209-2, "Human exposure to radio frequency fields from hand-held and body-mounted wireless communication devices- Human models, instrumentation, and procedures," *International Electrotechnical Commission*, 2010.

[7] P. S. Hall, "Antennas and propagation for body centric communications," *IET Seminar on Antennas and Propagation for Body-Centric Wireless Communications*, pp. 1–4, 2007.

[8] S. L. Cotton and W. G. Scanlon, "Characterization and modeling of on-body spatial diversity within indoor environments at 868 MHz," *IEEE Transactions on Wireless Communications*, vol. 8, no. 1, pp. 176–185, Jan. 2009.

[9] N. Rais, P. Soh, and F. Malek, "A review of wearable antenna," *Antennas and Propagation Conference, LAPC 2009.*, no. November, pp. 225–228, 2009.

[10] a. a. Serra, P. Nepa, G. Manara, and P. S. Hall, "Diversity Measurements for On-Body Communication Systems," *Antennas and Wireless Propagation Letters*, vol. 6, no. 11, pp. 361–363, 2007.

[11] A. A. Serra, P. Nepa, G. Manara, and P. S. Hall, "Experimental investigation of diversity techniques for on-body communication systems," *IET Seminar on Antennas and Propagation for Body-Centric Wireless Communications*, pp. 63–66, 2007.

[12] P. Hall and Y. Hao, "Antennas and propagation for on-body communication systems," *IEEE Antennas and Propagation Magazine*, vol. 49, no. 3, pp. 41–58, 2007.

[13] A. Sani, S. Member, Y. Zhao, Y. Hao, and S. Member, "An Efficient FDTD Algorithm Based on the Equivalence Principle for Analyzing Onbody Antenna Performance," vol. 57, no. 4, pp. 1006–1014, 2009.

[14] I. Khan, P. S. Hall, A. A. Serra, A. R. Guraliuc, and P. Nepa, "Diversity Performance Analysis for On-Body Communication Channels at 2 . 45 GHz," vol. 57, no. 4, pp. 956–963, 2009.

[15] S. Bashir and A. Chauraya, "A flexible fabric metasurface for on body communication applications," *… , 2009. LAPC 2009. …*, no. November, pp. 725–728, 2009.

[16] M. Gallo, P. S. Hall, M. Bozzettil, I. Bari, and V. Orabona, "Use of Animation software in the simulation of On-body Communication Channels," vol. 2, no. 6037, p. 705, Sep. 1976.

[17] N. Chavannes and R. Tay, "Suitability of FDTD-based TCAD tools RF design of mobile phones," *IEEE Antennas and Propagation Magazine*, vol. 45, no. 6, 2003.

[18] W. Scanlon, G. Crumley, and N. E. Evans, "Body-obstructed fading characteristics of an in-ward 2.45 GHz biomedical telecommand link," *Antennas and Propagation Society International Symposium*, pp. 380–383, 1999.

[19] W. Whittow, C. J. Panagamuwa, R. M. Edwards, and J. C. Vardaxoglou, "Specific absorption rates in the human head due to circular metallic earrings at 1800MHz," *Loughborough Antenna & Propagation Conference*, no. April, pp. 277–280, 2007.

[20] W. G. Whittow, C. J. Panagamuwa, R. M. Edwards, and J. C. Vardaxoglou, "On the effects of straight metallic jewellery on the specific absorption rates resulting from face-illuminating radio communication devices at popular cellular frequencies.," *Physics in medicine and biology*, vol. 53, no. 5, pp. 1167–82, Mar. 2008.

[21] M. Khattak, R. Edwards, and O. Ojerinde, "A study of perturbations in linear and circular polarized antennas in close proximity to the human body and dielectric liquid filled rectangular and a cylindrical phantom," in *Loughborough Antenna & Propagation Conference*, 2010, no. November, pp. 409–412.

[22] SPEAG, *OTA Phantoms User Manual*. 2011.

[23] W. G. Scanlon, G. a. Conway, and S. L. Cotton, "Antennas and propagation considerations for robust wireless communications in medical body area networks," *IET Seminar on Antennas and Propagation for Body-Centric Wireless Communications*, pp. 37–37, 2007.

[24] M. R. Kamarudin, Y. I. Nechayev, and P. S. Hall, "Performance of Antennas in the On-Body Environment," *2005 IEEE Antennas and Propagation Society International Symposium*, vol. 3A, pp. 475–478, 2005.

[25] W. G. Scanlon and S. L. Cotton, "Understanding On-Body Fading Channels at 2 .45GHz using measurement based on user state and environment," in *Loughborough Antenna & Propagation Conference*, 2008, no. March, pp. 10–13.

[26] S. Cotton and W. Scanlon, "Characterization of the on-body channel in an outdoor environment at 2.45 GHz," *Antennas and Propagation, 2009. …*, pp. 722–725, 2009.

[27] S. Cotton and W. Scanlon, "A Statistical Analysis of Indoor Multipath Fading for a Narrowband Wireless Body Area Network," *2006 IEEE 17th International*

Symposium on Personal, Indoor and Mobile Radio Communications, pp. 1–5, Sep. 2006.

[28]   P. Hall, Y. Hao, and S. Cotton, "Progress in antennas and propagation for body area networks," *Signals Systems and Electronics ISSSE 2010 International Symposium on*, vol. 1, 2010.

[29]   G. A. Conway, W. G. Scanlon, and S. L. Cotton, "The performance of on-body wearable antennas in a repeatable multipath environment," *2008 IEEE Antennas and Propagation Society International Symposium*, pp. 1–4, Jul. 2008.

[30]   S. Park and S. Jayaraman, "Enhancing the quality of life through wearable technology," *Engineering in Medicine and Biology Magazine*, no. June, pp. 41–48, 2003.

[31]   W. Scanlon, "Antenna-body interaction effects in a 418 MHz radio telemeter for infant use," *Engineering in Medicine and Biology Society*, pp. 278–279, 1996.

[32]   R. Edwards and M. Khattak, "Understanding Body-centric antennas," *Antennas and Propagation Conference LAPC 2010 Loughborough*, no. November, pp. 629–632, 2010.

[33]   D. Gesbert, M. Shafi, P. J. Smith, and a. Naguib, "From theory to practice: an overview of MIMO space-time coded wireless systems," *IEEE Journal on Selected Areas in Communications*, vol. 21, no. 3, pp. 281–302, Apr. 2003.

[34]   A. Molisch and M. Win, "MIMO systems with antenna selection," *Microwave Magazine, IEEE*, no. March, pp. 46–56, 2004.

[35]   W. Jakes, *Microwave mobile communication*. New York: Wiley, 1974.

[36]   Cisco, "No Title," *http://www.cisco.com/c/en/us/support/docs/wireless-mobility/wireless-lan-wlan/27147-multipath.html*, 2008. .

[37]   J. G. Proakis, *Digital Communications*, 5th ed. New York: McGraw-Hill, 2008.

[38]   W. Lee, *Mobile Communications Design Fundamentals*, First. 1986.

[39]   J. D. Gibson, *The Mobile Communications Handbook*, Second. CRC Press, 1999.

[40]   P. Hall, "Progress in radiowave propagation studies of on-body communications channels," *Antennas and Propagation Conference, 2008. LAPC*, no. March, pp. 6–9, 2008.

[41]   P. S. Hall, "Diversity in On-Body Communications Channels," *2008 International Workshop on Antenna Technology: Small Antennas and Novel Metamaterials*, vol. 3, pp. 5–9, Mar. 2008.

[42]   M. K. Simon and M.-S. Alouini, *Digital Communications over Fading Channels*, 2nd ed. Hoboken: Wiley, 2005.

[43]   G. L. Stuber, *Principles of Mobile Communications*, 2nd ed. Norwel, MA: Kluwer, 2000.

[44]   X. Wang and N. C. Beaulieu, "The impact of noise on switching rates in dual selection combining diversity," *2009 Canadian Conference on Electrical and Computer Engineering*, pp. 293–297, May 2009.

[45]   N. Nowshin, a K. M. Arifuzzman, M. A. Hossain, and M. Tarique, "Performance comparison of Selection Combining diversity receivers for different modulation schemes in OFDM system," *2010 13th International Conference on Computer and Information Technology (ICCIT)*, no. Iccit, pp. 579–584, Dec. 2010.

[46]   N. Sezgin, "A performance analysis of selective diversity combining in indoor mobile radio communication environment," *Global Telecommunications Conference, IEEE, 1994. GLOBECOM'94.*, no. 1, pp. 58–61, 1994.

[47]   K. Dietze, C. B. Dietrich, and W. L. Stutzman, "Analysis of a two-branch maximal ratio and selection diversity system with unequal SNRs and correlated inputs for a Rayleigh fading channel," *IEEE Transactions on Wireless Communications*, vol. 1, no. 2, pp. 274–281, Apr. 2002.

[48]   M. Win and J. Winters, "Analysis of hybrid selection/maximal-ratio combining in Rayleigh fading," *ICC'99. 1999 IEEE International*, pp. 6–10, 1999.

[49]   M. Win and J. Winters, "Virtual branch analysis of symbol error probability for hybrid selection/maximal-ratio combining in Rayleigh fading," *Communications, IEEE Transactions on*, vol. 49, no. 11, pp. 1926–1934, 2001.

[50]   X. Cai and G. B. Giannakis, "Performance Analysis of Combined Transmit Selection Diversity and Receive Generalized Selection Combining in Rayleigh Fading Channels," *IEEE Transactions on Wireless Communications*, vol. 3, no. 6, pp. 1980–1983, Nov. 2004.

[51]   M.-S. Alouini and M. K. Simon, "An MGF-based performance analysis of generalized selection combining over Rayleigh fading channels," *IEEE Transactions on Communications*, vol. 48, no. 3, pp. 401–415, Mar. 2000.

[52]   L. B. Milstein, "Average SNR of a generalized diversity selection combining scheme," *IEEE Communications Letters*, vol. 3, no. 3, pp. 57–59, Mar. 1999.

[53]   L. B. Milstein, "SNR of generalized diversity selection combining with nonidentical Rayleigh fading statistics," *IEEE Transactions on Communications*, vol. 48, no. 8, pp. 1266–1271, 2000.

[54]   V. Papamichael and C. Soras, "Generalised selection combining diversity performance of multi-element antenna systems via a stochastic electromagnetic-

circuit methodology," *IET Microwaves, Antennas & Propagation*, vol. 4, no. 7, p. 837, 2010.

[55] Y. Roy, J.-Y. Chouinard, and S. A. Mahmoud, "Selection diversity combining with multiple antennas for MM-wave indoor wireless channels," *Selected Areas in Communications, IEEE*, vol. 14, no. 4, pp. 674–682, 1996.

[56] C. Stefanovic, B. Jaksic, and P. Spalevic, "Performance Analysis of Selection Combining Over Correlated Nakagami-m Fading Channels with Constant Correlation Model for Desired Signal and Cochannel Interference," *Radioengineering*, pp. 1176–1181, 2013.

[57] I. Petrovic, Z. Nikolic, and M. Stefanovic, "Selection diversity receiver over correlated rayleigh fading channels in the presence of multiple interferers," *Revue Roumaine Science Technology*, pp. 61–69, 2011.

[58] P. Spalevic, N. Sekulovic, and G. Zachos, "Performance analysis of system with triple selection combining over correlated Weibull fading channel in the presence of cochannel interference," *Facta universitatis - series: Electronics and Energetics*, vol. 23, no. 1, pp. 87–96, 2010.

[59] S. Cotton and W. Scanlon, "Spatial diversity and correlation for off-body communications in indoor environments at 868 MHz," *Vehicular Technology Conference, IEEE*, pp. 372–376, 2007.

[60] H.-R. Chuang, "Human operator coupling effects on radiation characteristics of a portable communication dipole antenna," *IEEE Transactions on Antennas and Propagation*, vol. 42, no. 4, pp. 556–560, Apr. 1994.

[61] S. L. Cotton and W. G. Scanlon, "Measurements, Modeling and Simulation of the Off-Body Radio Channel for the Implementation of Bodyworn Antenna Diversity at 868 MHz," *IEEE Transactions on Antennas and Propagation*, vol. 57, no. 12, pp. 3951–3961, Dec. 2009.

[62] L. Vallozzi and P. Van Torre, "Wireless communication for firefighters using dual-polarized textile antennas integrated in their garment," *IEEE Transactions on Antennas and Propagation*, vol. 58, no. 4, pp. 1357–1368, 2010.

[63] A. Lea, P. Hui, J. Ollikainen, and R. G. Vaughan, "Propagation between on-body antennas," *... and Propagation, IEEE ...*, vol. 57, no. 11, pp. 3619–3627, 2009.

[64] Nordic Semiconductor, "λ/4 printed monopole antenna for 2.45GHz," no. January, pp. 2–7, 2005.

[65] "http://www.empire.de/." .

[66] C. A. Balanis, *Antenna Theory*, 3rd ed. Hoboken, New Jersey: John Wileys & Sons, 2005.

[67] K. A. Norton, "The Propagation of Radio Waves over the Surface of the Earth and in the Upper Atmosphere," *Proceedings of the Institute of Radio Engineers*, vol. 24, no. 10, pp. 1367–1387, 1936.

[68] J. Wait, "The ancient and modern history of EM ground-wave propagation," *Antennas and Propagation Magazine, IEEE*, vol. 40, no. 5, 1998.

[69] P. Hall and Y. Hao, "Antennas and propagation for body centric communications," *Antennas and Propagation, 2006. EuCAP …*, 2006.

[70] C. Oestges and B. Clerckx, *MIMO Wireless Communication*, First. London: Elsevier Ltd, 2007.

[71] B. Mandelbrot, "How long is the coast of britain? Statistical self-similarity and fractional dimension.," *Science (New York, N.Y.)*, vol. 156, no. 3775, pp. 636–8, May 1967.

[72] W. Zhang and P. S. Hall, "Mutual coupling investigation of two wideband dipole antennas on EBG ground plane," *2007 International workshop on Antenna Technology: Small and Smart Antennas Metamaterials and Applications*, pp. 35–38, Mar. 2007.

6   Conclusion and Future Work

6.1   Summary and Conclusions

This work has investigated various user body interactions with antenna systems. This has included mobile phone radiation coupling to the wires making up hands-free kits and how this impacts on the Specific Absorption Rate inside the body; the influence of the hand holding a mobile phone on its ability to transmit; and the behaviour of an on-body SIMO system.

An introduction to on-body system is given in chapter 1. In his chapter, a background of on-body system was introduced. The method of investigation of the antenna system in the thesis was stated.

In chapter 2, the process of measuring mobile phone SAR was discussed. The types of measuring systems presently available were introduced, followed by the DASY4 used at the School of Electronic, Electrical and Systems Engineering at Loughborough University. The chapter also introduced the front of face phantom developed by the School. The ingredients for making tissue simulating liquid are listed with the quantity needed for manufacturing the tissue simulating liquid for the experiments carried out in Chapter 3.

The effect of a hands free kit (HFK) of a smart phone on the SAR inside the head was investigated in chapter 3. Previous work in this area had looked at the effects on SAR in the head when the phone was mounted at the waist and the HFK extended from that location to the ear. One article in particular by the consumer magazine *Which?* raised a great deal of concern among the general public when it reported that the HFK can increase the SAR in the head. This was in a climate where there was a great deal of misunderstanding and distrust of the mobile phone industry over the radiation absorption in the head. Since that controversial study, a number of academic studies have shown that the SAR does not increase in the head. The research presented in this thesis gains its novelty by considering smartphones (SP) that are held in front of the face. With more advanced multimedia capabilities and larger screens, SPs are more likely to be held in front of the face during a call compared to their 2G counterparts from decades ago. When held in this new in front of face location, the routing and

placement of the HFK relative to the SP is very different from those considered in earlier studies. Furthermore, as the distance from the phone to the ear is shorter, anecdotal evidence suggest that phone users sometimes keep the HFK *tied up in a squashed loop* so as to reduce the length of the cable. This introduces the possibility of a wire loop positioned close to the SP's antenna and hence increasing the coupling to the cable. As a result, if there are larger currents on the HFK wire, radiation into the head may increase and thus resulting in a higher than expected SAR. Chapter 3 tested this hypothesis through a series of experiments. They were carried out in the GSM 1800 band with the DASY4 system. As expected, the measured results showed that when the phone was held in front of the face, and the cable was allowed to drop down from the head to the waist and back up to ear, the SAR in the head was negligible. However, when the SP was held in front of the face with the connecting HFK *tied up into a squashed loop* and the other end fixed to the side of the phantom head, there was a dramatic of 2000% in the side-of-head SAR compared to when the SP is used in front of the face without the HFK. In absolute values, the measured 1g SAR with the HFK was about *half* that observed when the SP was positioned at the side of the head in the standard *talk position*. The study has therefore demonstrated a significant amount of coupling and re-radiation is possible when the HFK is tied up in a squashed loop. Inductance depends on the number of coils, configuration of coil and the material filling the coils of an inductor. The distribution of energy in the HFK is similar to that of a coil. Although 1g and 10g SAR limits were not exceeded, that cannot be assured for other HFKs and mobile phones. Furthermore, when the SP is used at the side of the head in the normal talk position, the head is in effect shielded from the mobile phone by the ear and the skull. This is not the case when the HFK is used; the HFK speaker is pushed into the ear canal when in use thus bypassing the ear and the skull and so might be more problematic in terms of effective SAR. This effective SAR cannot be measured accurately with the current DASY4 configuration and will need a new fixture to encompass the earpiece with a very thin shell. From this we could surmise that the measured SAR with the earpiece attached to the side of the head phantom is artificially low. This could be part of possible future work.

Chapter 4 investigated the effect the hand has on the transmit power of a mobile phone. It is known that the hand influences the antenna resonant frequency by increasing the dielectric loading. Also, due to the lossy nature of tissue, the transmitted power can

also be absorbed in the hand (causing heating). In all, this results in a reduction of the received power at the base station and may cause dropped calls. Here, in a volunteer based study participants were asked to hold a test mobile phone in a specific manner while its transmitted power was measured at a fixed location. Influence of the hand size, had grip location, left and right hand; and finger jewellery was investigated. The location of the index finger above the antenna had the largest influence on the received power. It was found that metallic rings on the fingers have very little effect on the received power. There was no observable difference in the results for left and right hand use. However, if the antenna is located more towards one side of the phone, one can expect to see a larger difference. The measurements also seem to confirm the suitability of the CTIA phantom for over the air measurements. However, it would be beneficial to use several different hand phantoms with varying grip styles when conducting such measurements. The work presented in this chapter is from 33 participants. The maximum margin of error was ±0.81 from measurement with the left finger in position 1 when wearing a ring. The test accuracy can be increased with more participants in the experiment. This will give a wider range of result with different hand sizes. With the finger in the antenna region, it was observed that the finger had an effect on the received power. Since antenna positioning in mobile phones are not standardized. It can be concluded that if the antenna is placed in another region of the phone covered by the hand, the received power by the mobile phone will be affected. Also with metallic accessories worn on the fingers, in a case where the metallic accessory is in the antenna region this is bound to affect the operating frequency of the antenna hence affecting the received power in the mobile phone. Chapter 5 investigated the behaviour of an on-body SIMO antenna system. Two receiver antennas were positioned on different parts of the body and a transmit antenna located off-body. Monopole antennas were built as the receivers to work on the body. From the testing of the antennas, it was observed that even with a large ground plane, the body has a significant impact on the antenna performance. From initial simulation designs, the monopole antennas were tuned to perform better on the body. In this work, the multiple antennas were used on-body in six different orientations. Selection combining was the diversity scheme used to improve the signal to noise ratio in this system. On-body and off-body measurements were taken in these six orientations in three different environments. From the results, it was concluded the environment where the system functions plays a huge factor on the received power. An environment with more scattering and multipath will produce a

system with more selection combining operation. The use of selection combining on/off-body is a technique for isolating the human effect on an antenna system. This result has given rise to the implementation of a factor the propagation channel when measuring systems including a body.

6.2 Future work

From the work done on HFK and a Smart phone, the test can be extended to more Smart phones and their corresponding HFKs. With the recent acquisition of the iSAR kit, SAR measurement is faster and multiple phones and scenarios can be tested. The work can be extended from GSM 1800 to other frequency bands.

The study of the effect of the hand on the phone transmit power can be extended to other types of phones. Mobile phones and smart phones with antennas in different positions in the phone can be used for the experiment.

The work with multiple antennas using the selection combining diversity scheme can be extended to other diversity schemes. In the future, the antenna should be designed to be more compact and less conspicuous. They can also be placed normal and parallel to the surface of the body. There are ongoing projects with wearable antennas in the Loughborough University Communications Division. This can be used for testing on-body antennas.

The system can be changed from a 1-by-2 SIMO to a MIMO system in the future. This will help understand how far the on-body can be pushed before coupling and the body starts affecting the system.

A conference paper for LAPC 2014 will be written from the results of the multiple antenna system off-body and on-body study. This work in chapter 5 will also be used to write a journal paper for the IEEE Transactions on Antennas and Propagation.

Appendix I

Connector Specification
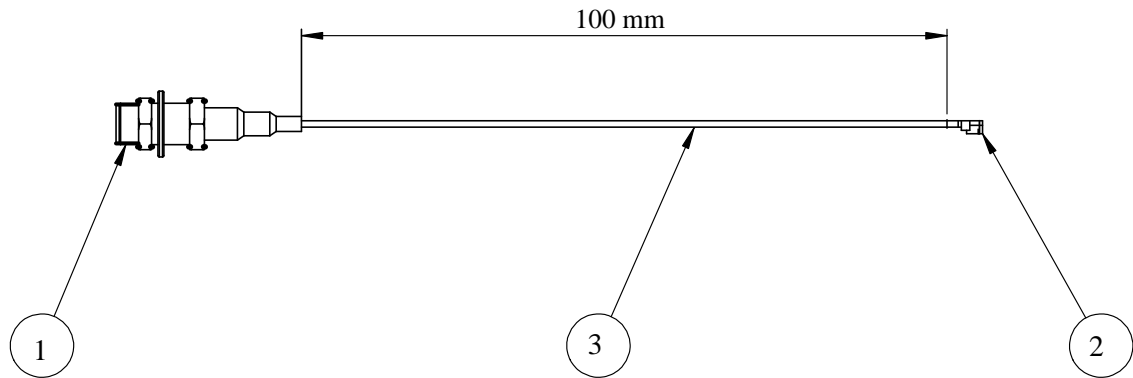
Figure I-1: U.FL-SMT PCB receptacle connector

ITEM NO.	PART NUMBER	DESCRIPTION	QTY.
1	C485G	SMA female Bulkhead Gold	1
2	U.FL	U.FL connector	1
3	010_113	Coax. cable	1

Table I-1: Description of the Connector part of the monopole antenna

RG316 cables Specifications

Details & Specifications	
Description	SMA Plug to SMA Plug, 3 metres, RG316
Fixing Method	Crimp
Jacket	FEP (2.5mm)
Dielectric	PTFE
Bending Radius (static)	13mm
Bending Radius (flexing)	30mm
Weight	58 gms
Impedance	50 ohms
Max. Frequency	3 GHz
Temperature Range	-55 to +200 degrees C
Working Voltage	1200 Volts RMS

Table I-2: Specification for the cables for connecting antenna to SDA

Appendix II

Procedure of making call from Base Station Simulator (BSS):

1. Connect the supplied power cord to the **AGILENT 8922M/S TEST SET** and power up the instrument or select Preset Button.

2. Use the key "SHIFT" and "**CELL CONFIGURE**" and set the following fields.

3. SET "**PAGING IMSI**" — **8010123456043**.

4. SET "**IMSI ATTACH AND DETACH**" – **ON**.

5. Press "**CELL CNTL**"

6. SET "**OPERATING MODE**"

7. SELECT "**CONFIG**" Under "**TO SCREEN**".

8. SET "**RF LEVEL OFFSET dB**" = **ON**

9. SET "**RF IN/OUT**" = **-40**

10. Press "**CELL CONTROL**"

11. SET "**AMPLITUDE**" = **-70dBm**

12. SET **MOBILE PHONE** "**TX LEVEL**" = **5 @ GSM 900**; **1@ GSM 1800**

13. Insert the **TEST SIM CARD** in the Mobile phone.

14. Power ON the mobile phone.

15. After a few moments it should register with the test-set and 'camp' on the 8922s Network. (Most mobile phones display **001-01** when the mobile phone has camped.

Once these parameters given above are changed, we can make call from BSS as follows:

1. Press **ORIGINATE CALL**

2. Accept the call from the test set.

3. The connection status field changes from **ATTACHED** to **SET-UP REQEST** and then to **CONNECTED** when the call is established.

Appendix III

Code for processing and plotting selection combining on/off-body in all six alignments

```
% Performance of Selection Combining
clear all
off = load('\\hs1.lboro.ac.uk\eloao\selection combining\SC MIL\waisttowaist_onbody.txt');
% loads code data for the off body
% on = load('\\hs1.lboro.ac.uk\eloao\selection combining\MIL\Selection combining
average\shouldertoshoulder_offbody.txt'); % loads data for the on-body
plot(off(8000:9000,1),off(8000:9000,2),'--k') % plots the off body data for antenna 1
hold on
plot(off(8000:9000,1),off(8000:9000,3),'--r') % plots the off body data for antenna 2
hold on
plot(off(8000:9000,1),off(8000:9000,4)) % plots the selection combined data of both antenna

title('Left Waist and Right Waist On-body Selection Combining','FontSize',30,'FontName','Times
New Roman')
ylabel('Power (dBm)','FontSize',30,'FontName','Times New Roman')
xlabel('Time (seconds)','FontSize',30,'FontName','Times New Roman')
hleg1 = legend('channel 1','channel 2','selection combining');
```

Code to compare the on-body and off-body selection combining and plot the graph

```
% this is to compare the SC for the onand off-body for each aligment in all the locations
clear all
off = load('\\hs1.lboro.ac.uk\eloao\selection combining\SC
MIL\leftshouldertoleftwaist_offbody.txt'); % loads the selection combining data for off body
```

```
on  = load('\\hs1.lboro.ac.uk\eloao\selection combining\SC
MIL\leftshouldertoleftwaist_onbody.txt'); % loads the selection combining data for on body
plot(off(8000:9000,1),off(8000:9000,4),'--k') % plots a section of the off body selection
combining
hold on
plot(on(8000:9000,1),on(8000:9000,4),'--r') % plots a section of the on body selection combining
title('Left Shoulder and Left Waist Selection Combining','FontSize',30,'FontName','Times New
Roman')
ylabel('Power (dBm)','FontSize',30,'FontName','Times New Roman')
xlabel('Time (seconds)','FontSize',30,'FontName','Times New Roman')
hleg1 = legend('selection combining off-body','selection combining on-body');
```

Code to compare the probability density function of the on/off-body and their selection combining

```
clear all
a = load('\\hs1.lboro.ac.uk\eloao\selection combining\MIL
pdf\rightshouldertorightwaist_offbody.txt'); % load data
b = load('\\hs1.lboro.ac.uk\eloao\selection combining\MOC
pdf\rightshouldertorightwaist_offbody.txt'); % load data
c = load('\\hs1.lboro.ac.uk\eloao\selection combining\MIO
pdf\rightshouldertorightwaist_offbody.txt'); % load data
aa = load('\\hs1.lboro.ac.uk\eloao\selection combining\MIL
pdf\rightshouldertorightwaist_onbody.txt'); % load data
bb = load('\\hs1.lboro.ac.uk\eloao\selection combining\MOC
pdf\rightshouldertorightwaist_onbody.txt'); % load data
cc = load('\\hs1.lboro.ac.uk\eloao\selection combining\MIO
pdf\rightshouldertorightwaist_onbody.txt'); % load data

e = pdf('Normal',a(:,3),mean(a(:,3)), std(a(:,3))); % perform pdf on loaded data
f = pdf('Normal',b(:,3),mean(b(:,3)), std(b(:,3))); % perform pdf on loaded data
```

```
g = pdf('Normal',c(:,3),mean(c(:,3)), std(c(:,3))); % perform pdf on loaded data
plot(a(:,3),e,'-.r'); % plot pdf
hold all
plot(b(:,3),f,':r'); % plot pdf
hold all
plot(c(:,3),g,'r') % plot pdf
p = pdf('Normal',aa(:,3),mean(aa(:,3)), std(aa(:,3))); % perform pdf on loaded data
q = pdf('Normal',bb(:,3),mean(bb(:,3)), std(bb(:,3))); % perform pdf on loaded data
r = pdf('Normal',cc(:,3),mean(cc(:,3)), std(cc(:,3))); % perform pdf on loaded data
plot(aa(:,3),p,'-.k'); % plot pdf
hold all
plot(bb(:,3),q,':k'); % plot pdf
hold all
plot(cc(:,3),r,'k') % plot pdf
title('Right Shoulder and Right Waist Selection Combining','FontSize',30,'FontName','Times New
Roman')
ylabel('Normal pdf')
xlabel('Power (dBm)')
hleg1 = legend('LW and RW SC MIL off-body','LW and RW SC MOC off-body',...
                'LW and RW SC MIO off-body','LW and RW SC MIL on-body',...
                    'LW and RW SC MOC on-body','LW and RW SC MIO on-body');
```

Code to compare the cumulative distribution function of the on/off-body and their selection combining

```
clear all
a = load('\\hs1.lboro.ac.uk\eloao\selection combining\MIL
pdf\leftwaisttorightwaist_offbody.txt'); % load data
b = load('\\hs1.lboro.ac.uk\eloao\selection combining\MOC
pdf\leftwaisttorightwaist_offbody.txt'); % load data
c = load('\\hs1.lboro.ac.uk\eloao\selection combining\MIO
pdf\leftwaisttorightwaist_offbody.txt'); % load data
```

```
aa = load('\\hs1.lboro.ac.uk\eloao\selection combining\MIL
pdf\leftwaisttorightwaist_onbody.txt'); % load data
bb = load('\\hs1.lboro.ac.uk\eloao\selection combining\MOC
pdf\leftwaisttorightwaist_onbody.txt'); % load data
cc = load('\\hs1.lboro.ac.uk\eloao\selection combining\MIO
pdf\leftwaisttorightwaist_onbody.txt'); % load data
e = cdf('Normal',a(:,3),mean(a(:,3)), std(a(:,3))); % perform cdf on loaded data
f = cdf('Normal',b(:,3),mean(b(:,3)), std(b(:,3))); % perform cdf on loaded data
g = cdf('Normal',c(:,3),mean(c(:,3)), std(c(:,3))); % perform cdf on loaded data
plot(a(:,3),e,'-.r'); % plot cdf
hold all
plot(b(:,3),f,':r'); % plot cdf
hold all
plot(c(:,3),g,'r') % plot cdf
p = cdf('Normal',aa(:,3),mean(aa(:,3)), std(aa(:,3))); % perform cdf on loaded data
q = cdf('Normal',bb(:,3),mean(bb(:,3)), std(bb(:,3))); % perform cdf on loaded data
r = cdf('Normal',cc(:,3),mean(cc(:,3)), std(cc(:,3))); % perform cdf on loaded data
plot(aa(:,3),p,'-.k'); % plot cdf
hold all
plot(bb(:,3),q,':k'); % plot cdf
hold all
plot(cc(:,3),r,'k') % plot cdf
title('Left Waist and Right Waist Selection Combining','FontSize',30,'FontName','Times New
Roman')
ylabel('Probability')
xlabel('Power (dBm)')
hleg1 = legend('LW and RW SC MIL off-body','LW and RW SC MOC off-body',...
               'LW and RW SC MIO off-body','LW and RW SC MIL on-body',...
                  'LW and RW SC MOC on-body','LW and RW SC MIO on-body');
```

Appendix IV

Normal Distribution

This is also known as normal or Gaussian probability density function (pdf). It is a smooth version of a histogram. Normal distribution is symmetrical around the mean and is similar to a bell-shaped curve. The mean, mode and median of the distribution are equal. Normal distribution is denser at the centre and less dense at the tail end. It is defined by the mean and standard deviation of the data. The probability density function is written as:

$$f(x) = \frac{1}{\sigma\sqrt{2\pi}}\exp\left[-\frac{(x-\mu)^2}{2\sigma^2}\right], -\infty < x < \infty$$

IV.1

Where σ is the standard deviation and μ is the mean.

The probability has a maximum value when the mean is equal to one of the random data.

$$f(x = \mu) = \frac{1}{\sigma\sqrt{2\pi}}$$

IV.2

Cumulative distribution function (cdf) provides the probability that the distributed variable will assume any value up to a certain point. cdf is equal to the sum of the probabilities calculated by probability density function at all points. The cdf values are shown on the y-axis and it range from 0 to 1 which corresponds to 0% to 100%. cdf is given as

$$F(x) = \frac{1}{\sigma\sqrt{2\pi}}\int_{-\infty}^{x}\exp\left[-\frac{(x-\mu)^2}{2\sigma^2}\right] dx$$

IV.3

Appendix V

The MIMO system can be generalized mathematically. In a single channel system which can be referred to as a single input single output (SISO) system, the received signal can be written as

$$r = hs + n$$

<div align="right">V.1</div>

Where r is the received signal, h is the channel, s is the transmitted signal and n is the noise. In a MIMO system, there are transmitters, multiple channels, signals and receivers. This can be defined in matrix form. The diagram below is a schematic of the mathematical representative.
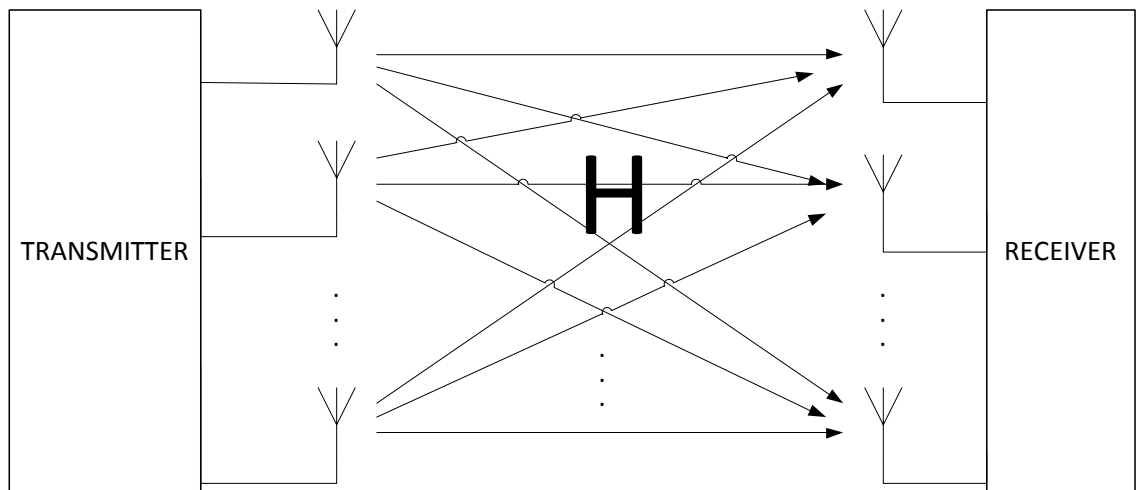
Figure V-1: MIMO system with multiple antennas at the receiver and transmitter

The channel between the transmit antenna and receive antennas can be denoted by the matrix H.

$$H = \begin{bmatrix} h_{11} & h_{12} & ... & h_{1N} \\ h_{21} & h_{22} & ... & h_{2N} \\ \vdots & \vdots & \ddots & \vdots \\ h_{M1} & h_{M2} & ... & h_{MN} \end{bmatrix}$$

<div align="right">V.2</div>

M denotes the number of antennas on the transmitter and N denotes the number of antennas on the receiver.

The noise in the system is mostly assumed as Additive White Gaussian Noise (AWGN). It is written in matrix form as

$$N = \begin{bmatrix} n_1 \\ n_2 \\ \vdots \\ n_M \end{bmatrix}$$

V.3

The signal sent is shown as

$$S = \begin{bmatrix} s_1 \\ s_2 \\ \vdots \\ s_M \end{bmatrix}$$

V.4

The signals at the receiving end of the channel in the MIMO system are

V.5

$$R = HS + N$$

The channel between the transmit antenna and receive antenna can be denoted by

V.6

$$h_1, h_2, \dots, h_M$$

This can be further broken down to

$$
\begin{aligned}
r_1 &= h_1 s_1 + n_1 \\
r_2 &= h_2 s_2 + n_2 \\
&\vdots \\
r_M &= h_M s_M + n_M
\end{aligned}
$$

V.7

Where $r_1, r_2, \dots, r_M$ represent the received signal and $n_1, n_2, \dots, n_M$ represent the noise and interference. $s_{1,2,\dots,M}$ can be the same signal sent over multiple channel but coded orthogonally. It can also be a signal broken down into smaller packets and sent in parallel to the receiver.